Modulational Instability in Nonlinear Electrical Transmission Lines and Suppression of Waves Mixing

Presented by

Eric Tala Tebue

Department of Physics, Faculty of Science,

University of Yaounde I, P.O. Box. 812, Cameroon

Registration Number: **03S315**

and

Submitted in Partial Fulfillment of the Requirements for the Degree of Doctor of Philosophy

at

the University of Yaoundé I

Under the Supervision of

Timoléon Crépin Kofané, ***Professor***

and

Aurélien Kenfack Jiotsa, ***Associate Professor***

23rd April 2015

"All truths are easy to understand once they are discovered; remains to us to discover them."

Galilée

Dedications

↬ *To my Father KAMGUEM and my Mother MATUEAM;*

↬ *To my Wife DJOUFACK Sorelle Joss Martiale;*

↬ *To my Junior Brother KAMGUE TEBUE Collince.*

Acknowledgments

- I first of all thank the Almighty God, for all the strength and mercy he has been giving to me.

- Many thanks to my supervisor, Pr. Kofané Timoléon Crépin, for his time and patience. Certainly, this work would not have been lighter without Pr. Kofane's sense of humour and passion for all things integrable. Thank you Pr. Kofané for sharing with me, the exciting nonlinear research area of soliton theory. The opportunity to undertake research in this area has given me the honor of enriching my experience.

- I am also very grateful to Pr. Kenfack Jiotsa Aurélien, for his constant encouragement and supervision in the preparation of this thesis. This work would not have been possible without the many long hours he spent discussing linear and nonlinear equation in physics. His sympathetic attitude and encouragements have enabled me to broaden my knowledge and improve my research skill and capability.

- I would like to thank each member of jury who has accepted to evaluate the present work.

- I would like to thank all those who dedicated their time to teach me a part of what they knew, from primary school to University, with a particular emphasis on the teaching staff of the Departments of Physics of the University of Yaounde I, the Higher Teachers' Training College and the National Advanced School of Engineering; I am particularly grateful to Pr. Woafo Paul, Pr. Tchawoua Clement, Pr. Essimbi Zobo Bernard, Pr. Beguide Bonoma, Pr. Owono Owono Luc Calvin, Dr Gnokam Edmond, Dr Mbouga Jean Marie, Dr. Nana Nbendjo Blaise, Dr. Noubissié Samuel, Pr. Tonyé Emmanuel and Dr. Bossou Olivier .

- I am equally indebted to Pr. Emmanuel KENGNE of the University of Ottawa Canada, for providing me with relevant documentation in the course of this research.

- I express my gratitude to Dr. Kenmogne Fabien, Dr. Fabien II Ndzana, Djoufack Zacharie, Lontsi Agostiny Marrios and Tatchou Temfack Hervé for many fruitful discussions on different aspects of nonlinear physics. I can not forget their senses of availability and help.

- Particular thanks to my mother-in-law Djoufack Hélène and to Lekeumo Simplice for their encouragements;

- I thank all my classmates of ENS of Yaounde I for all their advice;

- Fruitful discussions with my present PhD mates are also to be appreciated; Souleymanou Abbagari, Djob Roger, Tsobgni Christophe Dechance, Kuika Durdovic, Bastos Bazlna, Gompe Joel, Njassap Thierry, Nkano Larose, Tikeng Manfouo Arnaud, Togueu Motcheyo, Tsopnang Patrice, Fogang Ferdinand, Kamdoum Hervé, Nbonsou Hervé, Momo Gervais.

- I sincerely thank my classmates of ENSP, precisely Tapoko Fopah Narcisse, Tanga Jean Pierre, Djingue Jean Pierre, Happi Jean Paul, Taiwe Paul, Ngankou Otis, Besong Ako, Bondjomi Idriss, Diamard Rachelle for their permanent encouragements;

- I also give special thanks to Kuate Léopold, Kammogne Thomas, Tchinda Timothé, Djilé Martin, Nguetsop's familly, Kenfack Stéphane, Kouta Achille, Yimélé Serge, Feudjio Edmond, Kaptchouang Christ, Momo Armel, Labo désiré and Kotap Tik.

- I am grateful to my colleagues of Government High School of Zamengoé for their multiple encouragements during the development of this work.

- My profound gratitude goes to my whole family (uncles, nieces, nephews, cousins), especially to Pola Tebue Brice, Mogue Tebue Carine, Kuate Tebue Kévin, and to my family-in-law, precisely to Ngoudjou Cabrel, Lakene Raïssa and Metago Helsa.

- With the completion of this thesis, I am again at a crossroad in my life. I look back with a sense of accomplishment and pride mixed with a sense of closure and renaissance. I think of people who came into my life, some by design and some

by accident, people who shaped and influenced who I am today. For better or for worse, it has been an experience.

Contents

List of Figures

List of Tables

Abstract

This thesis seeks to study the dynamics of modulated waves in some nonlinear electrical lines described by nonlinear partial differential equations. Using the Tanuiti reductive method, the rotating wave approximation and the semi-discrete approximation, it is shown that the amplitude equations which derive from the partial differential equations governing these nonlinear lines are reduced to nonlinear Schrodinger equation and to the complex Ginzburg-Landau equation. The analysis of Stuart and Diprima on the linear stability allows to evaluate the modulational instability criteria of a plane wave submitted to a low hit. The accuracy of these analytical studies is confirmed by the numerical simulations of the propagation equations of different networks.

More precisely, it comes from this work that the second-neighbor couplings add new maxima of gain; increase the group velocity, and the magnitude of the wave. Therefore, the network becomes more stable to small external perturbations. Concerning the suppression of waves mixing, the entire network used in this work needs only the half of the total number of additive linear inductors compared to that found in the literature; the overall bandwidth is wider; the new coupling type allows the suppression of some mixing of modes without excluding very low frequencies. It also points out that the nonlinear coupling adds the domains of modulational instability of each line. Finally, we derive the two-dimensional NLS equation governing the propagation of slowly modulated waves in the network; we find the exact transverse solution of this NLS equation and the analytical criteria of stability of this solution.

Keywords: Solitons, Modulational instability, Transmission gain, Second neighbors, Suppression of mixing frequencies, Nonlinear coupling, Transverse solution, Criteria of stability.

Résumé

Dans ce travail, nous étudions la dynamique des ondes modulées dans quelques lignes électriques non linéaires décrites par des équations aux dérivées partielles non linéaires. En utilisant la méthode de TANUITI, l'approximation des ondes rotatives et l'approximation des milieux semi-discrets, nous montrons que les équations d'amplitude dérivant des équations aux dérivées partielles gouvernant ces lignes électriques sont reduites aux équations non linéaires de Schrödinger et de Ginzburg-Landau. L'analyse de la stabilité linéaire de Stuart et Diprima permet d'évaluer le critère d'instabilité modulationnelle ceci dans le but d'observer la propagation au cours du temps d'une onde plane soumise à une faible perturbation. L'exactitude de ces études analytiques est confirmée par une simulation numérique des équations de propagation des différents réseaux.

Plus pécisément, il ressort de ce travail que le couplage des seconds voisins augmentent le gain de transmission, la vitesse de groupe et par conséquent, le système devient plus stable aux petites perturbations extérieures. Concernant la suppression du mixage de fréquences, le modèle utilisé ici a seulement besoin de la moitié d'inductances comparé à celui retrouvé dans la littérature; la bande passante est également plus grande et la suppression ce fait sans exclure les basses fréauences. Il ressort aussi de ce travail que le couplage non linéaire augmente les domaines d'instabilité modulationnelle. Finalement, nous dérivons une équation de Schrödinger en dimension 2, nous trouvons la solution de cette équation et nous déterminons son critère de stabilité.

Mots clés: Solitons, Instabilité modulationnelle, Gain de transmission, Second voisins, Suppression du mixage de fréquences, Couplage non linéaire, Solution transversale, Critère de stabilité.

List of Abbreviations

CDCGL: Coupled Discret Complex Ginzburg-Landau;

CNLS: Coupled Nonlinear Schrödinger;

GL: Ginzburg-Landau;

KdV: Korteweg and de Vries;

KP: Kadomtsev-Petviashvili;

MI: Modulational Instability;

NETL: Nonlinear Electrical Transmission Line;

NGL: Nonlinear **GL**;

NLS: Nonlinear Schrödinger;

NLSEs: NLS Equations;

PDE: Partial Differential Equation;

RF: Radio Frequency;

RWA: Rotating Wave Approximation;

sG: sine-Gordon;

ZK: Zakharov-Kuznetsov;

General Introduction

Since the first observation of a soliton by John Scott Russell in 1834, this type of solitary wave with exceptional stability has fascinated scientists; primarily because of their spectacular experimental properties and their undeniable elegances, but also due to their mathematical properties. The mathematical aspect was preferred in most of the references relating to the literature on solitons. In fact, it leads to beautiful theoretical developments such as the inverse scattering transform method that solves a nonlinear equation by a complex series of steps which are all linear. Beyond the mathematical aspects, the physics of soliton is also interesting and relevant to modern research. Thus, many experiments on the Bose-Einstein condensation have been done from the nonlinear Schrödinger equation which is one of the major equations of the theory of solitons. The field of solitons in general and the field of Telecommunications using solitons in particular have witnessed significant developments since the word soliton was coined. Most of this growth occurred over the last decade or so, during which many new kinds of solitons **[1, 2]** have been identified. A soliton can be viewed as a result of an instability that leads to a self-induced modulation of the steady state produced by the interaction between nonlinear and dispersive effects. To illustrate the above assumptions, some fundamental properties of nonlinear systems have been confirmed experimentally: the generation of solitary waves, the interaction between solitons (see **[3–10]**) and the recurrence phenomenon (see **[10–12]**). Marquié *et al.* **[13, 14]** have presented a careful and quantitative experimental analysis about modulational instability and the generation of either envelope or hole solitons, depending on an appropriate choice of the carrier wave frequency. Modulational instability has been studied in diverse fields and in nonlinear electrical transmission lines in particular **[15–19]**.

The single LC transmission line adequately describes a great variety of physical phenomena in certain parameter regimes. To cite just an example, the single electrical transmission line gives a good description of nonlinear deep water waves. In fact, distributed electrical transmission lines that consist of a large number of identical sections

have been used to experimentally study the propagation of solitons obeying the Korteweg de Vries (KdV) equation. This equation was originally derived in order to model the shallow-water wave experiments of John Scott Russel in the 19th century. The results obtained on studies concerning KdV equation could then be transposed and will be very useful for either the investigation of nonlinear transmission lines or of other similar physical problems, such as nonlinear waves in the plasma. The KdV equation has been found nearly in all branches of physics, especially for shallow-water waves, nonlinear lattice, plasma physics **[20–22]**. Recently, many researchers have studied the transverse perturbations to the one-dimensional KdV equation **[24]**. The typical ones are the Zakharov-Kuznetsov (ZK) equation and the Kadomtsev-Petviashvili (KP) equation **[23]**. The ZK equation has also been found in many branches of physics, for example in plasma physics **[25]**.

The single electrical transmission line as model fails when considering nonlinear waves in the long gravity wave region **[26, 27]**. More importantly, there are many physical phenomena which can be investigated by the use of more than a single electrical transmission line **[28]**. Similarly, if the single electrical line shares many phenomena with certain optical fibres, it can not model the birefringent fibre which allows two modes of propagation **[29]**. So, Kakutani and co-workers **[27, 30]** have investigated theoretically and experimentally the Korteweg-de Vries solitons on a coupled LC transmission line consisting of two nonlinear LC ladder lines connected by identical intermediary capacitors and have shown that the network admits two different modes (a fast-mode and a slow-mode), in each direction of wave propagation. These two modes of propagation can combine during the transmission. This causes qualitatively different phenomena compared with the ordinary process of propagation, such as the annihilation. Modes mixing effect is then undesirable for the nonlinear modulated waves propagation. Separating these two modes will lead to avoid their simultaneous generation in each line. On the other hand, what would happen if we couple two transmission lines with second-neighbors ? What would happen if we couple two identical lines with a nonlinear capacitance ?

The answers to these questions will be the focus of our development. At the same time, we will study the transverse stability in a network. The present work is organized as follows:

- In chapter 1, we make a literature review on the soliton, nonlinear electrical transmission lines and modulational instability;

- The second chapter is devoted to methodology. We present the mathematical

(the Tanuiti reductive method, the rotating wave approximation) and numerical methods (the fourth order Runge-Kutta algorithm and other) used to attain our aims;

- The last chapter presents results and discussions. This chapter is divided into five sections:

• In section one, we study the effect of nonlinear coupling on modulational instability in nonlinear transmission lines;

• In section two, we study the effect of second-neighbor inductive coupling on the modulational instability in a coupled line of transmission;

• In section three and four, the suppression of modulated waves mixing in coupled nonlinear LC transmission lines is presented;

• The last section is based on the transverse stability in the discrete inductance-capacitance electrical network.

Finally, we end this work with a general conclusion in which we present our main results. Some recommendations are also made in relation to these results.

Chapter 1

Literature Review: Generalities on Soliton, Nonlinear Electrical Lines and Modulational Instability

Introduction

Considerable interest is being directed to wave motion in nonlinear equations because of its particular properties in nonlinear physical models. It is well known that most of the phenomena that arise in mathematical physics and engineering can be described by nonlinear equations, namely, by spatio-temporal partial differential equations (PDE). Generally, the solutions of these PDEs are solitons. This chapter will bring out the origin of soliton and the different kinds of soliton, general informations on the nonlinear electrical transmission lines and modulational instability.

1.1 Origin of the soliton concept

Over one hundred and seventy nine years ago, while conducting experiments to determine the most efficient design for canal boats, a young engineer named John Scott Russell (1808-1882) made a remarkable scientific discovery. As he described it in his Report on Waves **[31]**: "*I was observing the motion of a boat which was rapidly drawn along a narrow channel by a pair of horses, when the boat suddenly stopped - not so the mass of water in the channel which it had put in motion; it accumulated round the prow*

of the vessel in a state of violent agitation, then suddenly leaving it behind, rolled forward with great velocity, assuming the form of a large solitary elevation, a rounded, smooth and well-defined heap of water, which continued its course along the channel apparently without change of form or diminution of speed. I followed it on horseback, and overtook it still rolling on at a rate of some eight or nine miles an hour, preserving its original figure some thirty feet long and a foot to a foot and a half in height. Its height gradually diminished, and after a chase of one or two miles I lost it in the windings of the channel. Such, in the month of August 1834, was my first chance interview with that singular and beautiful phenomenon which I have called "the Wave of Translation". This event took place on the Union Canal at Hermiston, very close to the Riccarton campus of Heriot-Watt University, Edinburgh. The soliton is a wave that has an energy localized in space and that is extremely stable in the presence of disturbances. It generally moves without changing its form or its characteristics. In the field of hydrodynamics for example, tsunamis, rogue waves are well known manifestations of solitons. Solitons are caused by an association of nonlinear and dispersive effects in the propagating medium. The term dispersive effect refers to a property of certain systems where the speed of the waves varies according to the frequency. Solitons arise as the solutions of a widespread class of weakly nonlinear dispersive partial differential equations describing physical systems. Helmholtz **[32]** measured the propagation velocity of nerve pulses in 1850. In 1902, Lehmann **[33]** found the formation of localized anode spots in long gas-discharge tubes. Nevertheless, the term "soliton" was originally developed in a different context. These observations initiated the theoretical work of Rayleigh **[34]** and Boussinesq **[35]** around 1870, which finally led to the approximate description of such waves by Korteweg and de Vries (KdV) in 1895; this description is known today as the conservative KdV equation **[36]**. The KdV equation is one of the prototypes of the theory of solitons because it has remarkable mathematical properties. Its study allows to understand the basic ideas of the concept of soliton, but its derivation through hydrodynamic equations in shallow water is a little tedious. Figure 1.1 shows a device similar to that used by John Scott Russell to study experimentally the solitary wave. The waves are generated by a piston placed at the beginning of a channel. J. S Russell was able to verify the following properties:

• An initial excitation, according to its amplitude and its form, produced one, two, or many solitary waves;

• These waves propagate at a speed greater than the speed of the linear waves $c_0 =$

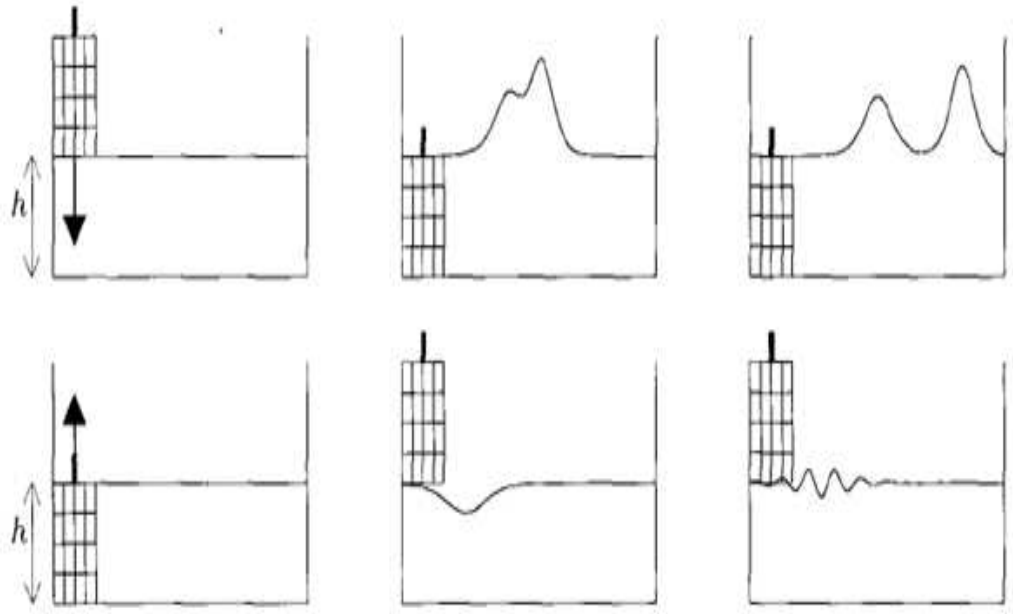

Figure 1.1: *Schematic evolution of a perturbation of the water surface in a reservoir created by the movement of a piston in the down or up direction* ***[37]***.

$\sqrt{hg}$, where g denotes the gravity and h the depth of water. This velocity is given by $v = c_0(1 + \eta A)$, where η represents the height of the liquid surface above the level of balance and A is the amplitude of the initial pertubation.

On this background the term "soliton" was coined by Zabusky and Kruskal **[38]** in 1965. These authors investigated certain well localised solitary solutions of the KdV equation and named these objects solitons. Among other things they demonstrated that solitons exist in 1-dimensional space. Gardner *et al.* **[39]** introduced the inverse scattering technique for solving the KdV equation and proved that this equation is completely integrable. In 1972, Zakharov and Shabat **[40]** found another integrable equation and finally it turned out that the inverse scattering technique can be applied successfully to a whole class of equations (e.g. the nonlinear Schrödinger and sine-Gordon equations). From 1965 up to about 1975, a common agreement was reached: to reserve the term soliton to pulse-like solitary solutions of conservative nonlinear partial differential equations that can be solved by using the inverse scattering technique. At a conference dedicated to the solitons and for their applications, which took place in Edinburgh in 1982, several scientists tried to recreate a solitary wave in the famous canal dear to J. S. Russell. It

was a failure as a result of technical problems. This experiment will be possible in 1995, at the Heriot-Watt University, those researchers have simulated the observations made by J. S. Russell. Figure 1.2 shows it. On this figure, we can see an example of the solitary wave.

Figure 1.2: *Simulation of the observation of J. S. Russell (Heriot-Watt University, 1995)* ***[41]***.

1.1.1 The different classes of soliton

There are two types of solitons, namely:

- The non-topological soliton;
- and the topological soliton.

1.1.1.1 The non-topological solitons

A soliton is non-topological when the propagation medium remains in the same state before and after the wave has passed. These solitons are those observed in hydrodynamics (although some are also observed in solid mechanics). The non-topological soliton in a hydrodynamic environment can be described by the KdV equation. Writing the Euler equations for a fluid which is incompressible and assumed inviscid, the boundary conditions at the bottom and to the surface, and assuming that the flow is irrotational, we can obtain the KdV equation, valid in the case of weak nonlinearities (see ref. **[37]**):

$$\frac{1}{c_0}\frac{\partial \eta}{\partial t} + \frac{\partial \eta}{\partial x} + \frac{3\eta}{2h}\frac{\partial \eta}{\partial x} + \frac{h^2}{6}\frac{\partial^3 \eta}{\partial x^3} = 0 \tag{1.1}$$

where $c_0 = \sqrt{gh}$ is the speed of propagation of linear waves in the limits of great wavelengths, h the depth and η the height of the liquid surface above the level of balance. Setting $X = x - c_0 t$ and $T = t$, it is possible to strike out the second term of eq.(1.1); we then have:

$$\frac{1}{c_0}\frac{\partial \eta}{\partial T} + \frac{3\eta}{2h}\frac{\partial \eta}{\partial X} + \frac{h^2}{6}\frac{\partial^3 \eta}{\partial X^3} = 0 \tag{1.2}$$

Introducing well chosen dimensionless variables, we obtain eq.(1.2) in its standard form as follows:

$$\frac{\partial \rho}{\partial \tau} + 6\rho\frac{\partial \rho}{\partial \xi} + \frac{\partial^3 \rho}{\partial \xi^3} = 0 \tag{1.3}$$

where $\rho = \eta/h$, $\xi = X/X_0$ and $\tau = T/T_0$; X_0 and T_0 are constants.

The KdV equation has among others the following spatially localized solutions

$$\rho = A sech^2[\sqrt{\frac{A}{2}}(\xi - 2A\tau)] \qquad (A > 0), \tag{1.4}$$

where A is the amplitude. Returning to original variables in the landmark laboratory, the solution can be written as follows:

$$\eta = \eta_0 sech^2[\frac{1}{2h}\sqrt{\frac{3\eta_0}{h}}(x - c_0[1 + \frac{\eta_0}{2h}]t)] \tag{1.5}$$

Plotting this equation, we can easily observe that the width of soliton $L = \sqrt{2/A}$ vary with the amplitude A. The width L decreases when the amplitude A increases and tend to the infinity when the amplitude tends to zero. This is presented on figure 1.3.

1.1.1.2 The topological solitons

A soliton is topological when the propagation medium is in different states before and after the passing of the wave. The soliton can be described in this state by the sine-Gordon (sG) equation. This sG equation derives from a chain of pendulum of mass m and length l.

$$\frac{\partial^2 \theta}{\partial t^2} - c_0^2\frac{\partial^2 \theta}{\partial x^2} + \omega_0^2 \sin(\theta) = 0 \tag{1.6}$$

where $\omega_0^2 = \frac{mgl}{I}$ is the frequency, $c_0^2 = \frac{Ca^2}{I}$ is the velocity and g is the gravity; I is the moment of inertia, C is the constant of torsion of the spring and a is the distance between

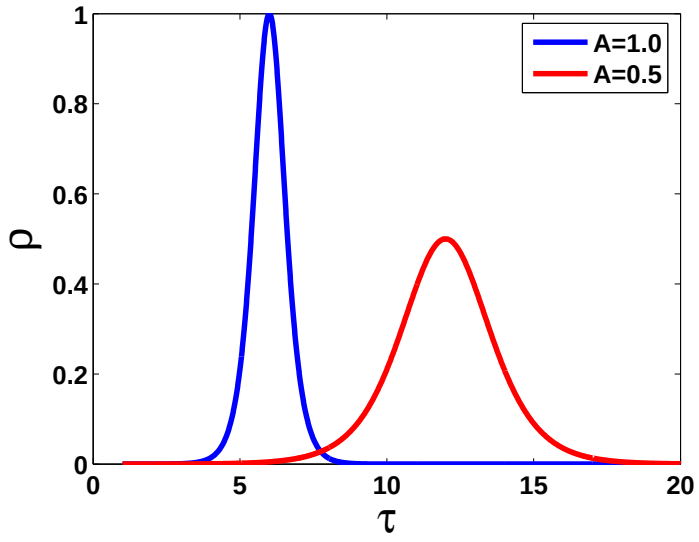

Figure 1.3: *Comparison between two solitons; for the curve in blue, $A = 1.0$ and for the red curve, $A = 0.5$. The width of soliton decreases when A increases and inversely.*

the pendulum. As the KdV equation, this equation is completely integrable and admits exact soliton solutions. A solution of this equation is (see **[37]**):

$$\theta(x,t)_{\pm} = 4\arctan[\exp(\pm\frac{x-ct}{L})] \tag{1.7}$$

where $L = \frac{c_0}{\omega_0}\sqrt{1-\frac{c^2}{c_0^2}}$ measures the spatial extension of the solution. Figure 1.4 shows the evolution of Eq.(1.7).

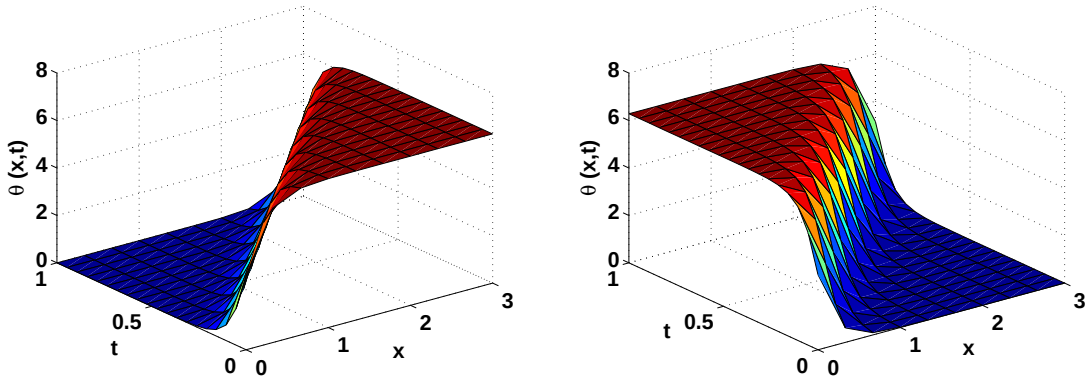

Figure 1.4: *Schematic representation of the solution of the sine-Gordon equation. The left figure corresponds to kink soliton, while the right figure represents the antikink soliton.*

1.1.2 Collision of two solitons

In addition to maintaining their shape, solitons possess other important properties **[42–44]**. First, a taller soliton travels faster than a shorter one. Due to this amplitude-dependent speed, as shown in Fig. 1.5, a taller soliton originally placed behind a shorter one catches it up and moves ahead of it after a collision. Another important set of properties is observed in this collision process. During the collision, the two solitons do not linearly superpose. In fact, they only interpenetrate and come out with their original shapes.

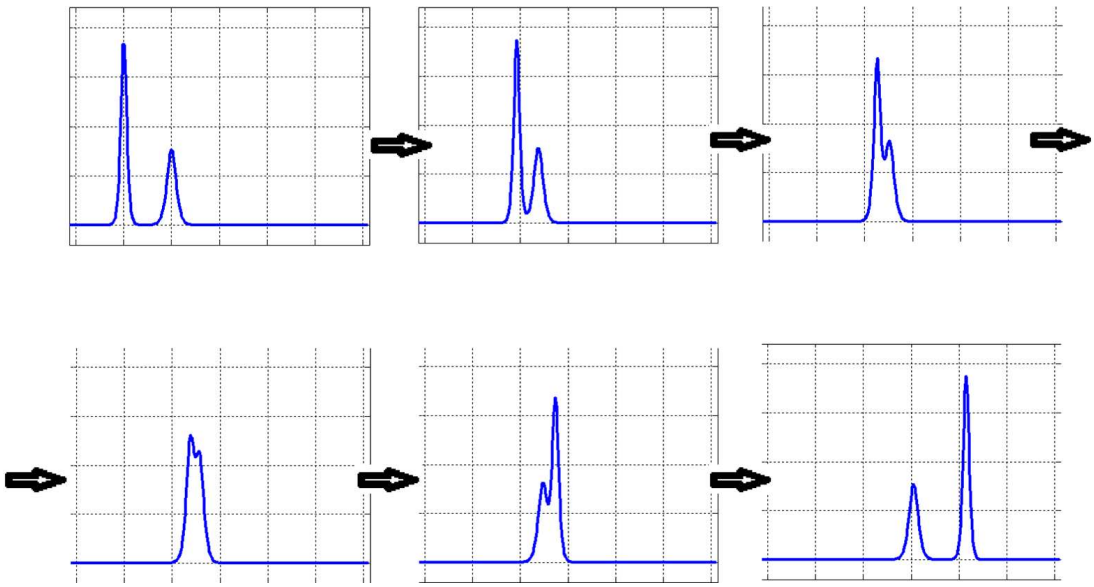

Figure 1.5: *Collision of two solitons with different amplitudes.*

1.1.3 Applications of Solitons

Since the early 1990s, the applications of solitons keep growing.

♣ **Telecommunications:**

• In 1991, a team transmits solitons on over 14 000 km using a technique of amplifying signals in an optical fiber.

• In 1998, a team from the Center for Research and Development of France Telecom combines solitons of different wavelengths to achieve a transmission with a rate higher than one terabite per second;

♣ **Chemistry:**

• In 2000, chemists showed that the electrical conductivity of conductive plastics is provided by solitons;

• In 2006, solitons were observed in crystals of aluminum supported by a high temperature due to experiments of scattering with X-rays and neutrons.

♣ **Biology:**

• The pulse that we take at the wrist can be considered as a soliton. This soliton results from the balance between nonlinearity from the hydrodynamics of blood flow and dispersion related to the elasticity of the artery wall.

Currently, one of the main challenges of solitons is in the field of Telecommunications. Solitons are very important in Telecommunications. In a data transmission system, the transmission medium is the physical path between transmitter and receiver. The transmission media that are used to convey information can be classified as guided or unguided. For unguided media, wireless transmission occurs through the atmosphere, outer space or water. The characteristics and quality of a data transmission are determined both by the characteristics of the medium and the characteristics of the signal. In the case of guided media, the medium itself is more important in determining the limitations of transmission. One key property of signals transmitted by antenna is directionality. In general, signals at lower frequencies are omnidirectional; that is, the signal propagates in all directions from the antenna. At higher frequencies, it is possible to focus the signal into a directional beam. A number of design factors relating to the transmission medium and the signal determine the data rate and distance:

• **Bandwidth:** All other factors remaining constant, the greater the bandwidth of a signal, the higher the data rate that can be achieved.

• **Transmission impairments:** Impairments, such as attenuation, limit the distance. For guided media, twisted pair generally suffers more impairment than coaxial cable, which in turn suffers more than optical fiber.

• **Interference:** Interference from competing signals in overlapping frequency bands can distort or wipe out a signal. Interference is of particular concern for unguided media but is also a problem with guided media. For guided media, interference can be caused by emanations from nearby cables. For example, twisted pairs are often bundled together and conductors often carry multiple cables. Interference can also be experienced from unguided transmissions. Proper shielding of a guided medium can minimize this problem.

• **Number of receivers:** A guided medium can be used to construct a point-to-point link or a shared link with multiple attachments. In this latter case, each attachment introduces some attenuation and distortion on the line, limiting distance and/or data rate.

What we can observe is that with guided medium, the transmission is more important than the unguided medium. That is one of reasons for which this work focusses only on the electrical transmission lines. We also use nonlinear electrical lines to model certain phenomena observed in optical fiber like the two modes of propagation with birefringent fiber.

1.2 Generalities on nonlinear electrical transmission lines

Several investigations have been performed to improve the first nonlinear and dissipative transmission line built by Hirota and Suzuki **[11]**; this because electrical transmission lines are very convenient tools to study the fascinating properties of nonlinear waves **[45–49]**. Indeed, it has been shown that the equation governing the physics of nonlinear electrical lines can be reduced to a cubic nonlinear Schrödinger equation or a pair of coupled nonlinear Schrödinger equations, the KdV equation, the complex Ginzburg-Landau equation or the coupled complex Ginzburg-Landau equations **[50, 51]**. Like every nonlinear system, a nonlinear transmission line can exhibit an instability that leads to a self-induced modulation of an input plane wave with the subsequent generation of localized pulses; this phenomenon is known as a Benjamin-Feir modulational instability and it is responsible for many interesting physical effects such as the formation of envelope solitons **[13]**.

The NETL is constructed with a normal transmission line which is periodically loaded with reverse biased diodes. These diodes are extremely nonlinear and are used to introduce nonlinearities in the basic linear transmission lines. The capacity of this kind of diode changes with the applied voltageas shown in Fig. 1.6.

A NETL has been explored as frequency multipliers with high frequencies in **[52–54]**, focusing primarily on high harmonic content. NETLs have three fundamental and quantifiable characteristics. These are nonlinearity, dispersion and dissipation.

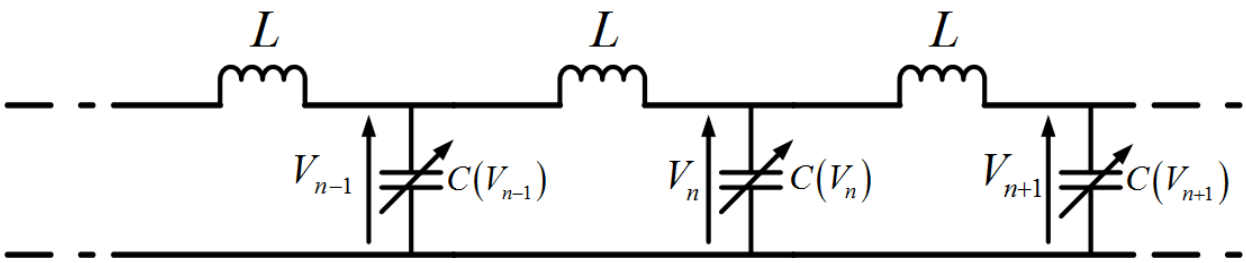

Figure 1.6: *Single nonlinear transmission line. Three unit cells are reproduced.*

1.2.1 Dispersion

The dispersion of the NETL results from the structural periodicity of the NETL. NETLs are characterized by a dispersion relation which is the relation between the angular frequency shift ω and wave number k. Let us consider as example the unit cell of Fig. 1.6 from where Kirchhoff's law in weak amplitude regime leads to the following linear traveling wave equation:

$$\frac{d^2V_n}{dt^2} + \frac{1}{LC_0}(2V_n - V_{n-1} - V_{n+1}) = 0 \tag{1.8}$$

where L and C_0 are the linear inductance and shunt capacitance at dc bias voltage respectively. This equation can be solved as follows

$$V_n(t) = V_0 \exp\big[i(kn - \omega t)\big], \tag{1.9}$$

where $V_n(t)$ and V_0 are the voltage at node n and initial voltage respectively. k and ω are linked through the following relation

$$\omega^2 = \frac{4}{LC_0}\sin^2(\frac{k}{2}) \tag{1.10}$$

known as the linear dispersion relation describing low-pass filter character of the network in the linear regime with upper cut-off frequency:

$$\omega_0 = \frac{2}{\sqrt{LC_0}} \tag{1.11}$$

At the cut-off frequency, the wave number k is equal to π. Since the phase velocity $v_p = \omega/k$ is a function of wave number k, the wave will spread out, or disperse itself during the propagation. The shape of the wave packet is determined by the dispersion

coefficient, defined as $P = \partial^2\omega/\partial k^2$ and the propagation velocity of the wave is the group velocity given by $v_g = \partial\omega/\partial k$.

1.2.2 Nonlinearity

The nonlinearity of the NETL comes from the nonlinear diodes because their capacitance varies with applied voltage. With the nonlinearity alone, the transmission equation will be given as follows:

$$\frac{d^2V_n}{dt^2} + g(V_n, V_n^2, ...) = 0. \tag{1.12}$$

Thus, $g(V_n, V_n^2, ...)$ is the nonlinear function of voltage V_n. A traveling wave $V_n(t) = V(n - ct)$, solution of Eq. 1.12 must have an amplitude V_0 proportional to the velocity c. Different points of a wave profile will hence propagate at different velocities, with points of higher amplitude overtaking points of lower amplitude leading to steepening of the wave form.

1.2.3 Dissipation

There are two main sources of dissipations in the NETLs. These are diode series resistance and metallic losses which arise from the geometry and finite conductivity of the coplanar waveguide. Another source of loss is radiation. Radiation loss is theoretically studied by Rutledge **[55]**, but this loss mechanism is much less significant in the NETLs than the other two.

1.2.4 Dispersion and nonlinearity effect on the input signals

The theory of soliton stores the information on some famous equations: the KdV equation, the nonlinear Schrödinger equation, the sine-Gordon equation, the Boussinesq equation, and others. This theory provides a fascinating glimpse into studying the nonlinear processes in which the combination of dispersion and nonlinearity together lead to the appearance of solitons. **When loss is present solitons cannot maintain their shape, but they still maintain spatial localization of energy in a pulse shape through a unique damping process [56]**. In the presence of a nonlinear capacitor given by $C(V) = C_0(1-\alpha V)$, the instantaneous capacitance is smaller for higher voltages. Therefore, the points with higher amplitudes will propagate with faster velocity than the

points with low amplitudes due to nonlinearity, as shown in the upper row of Fig. 1.7. Now, if we take into account the dispersion, the wave will spread out, as shown in the lower half of Fig. 1.7.

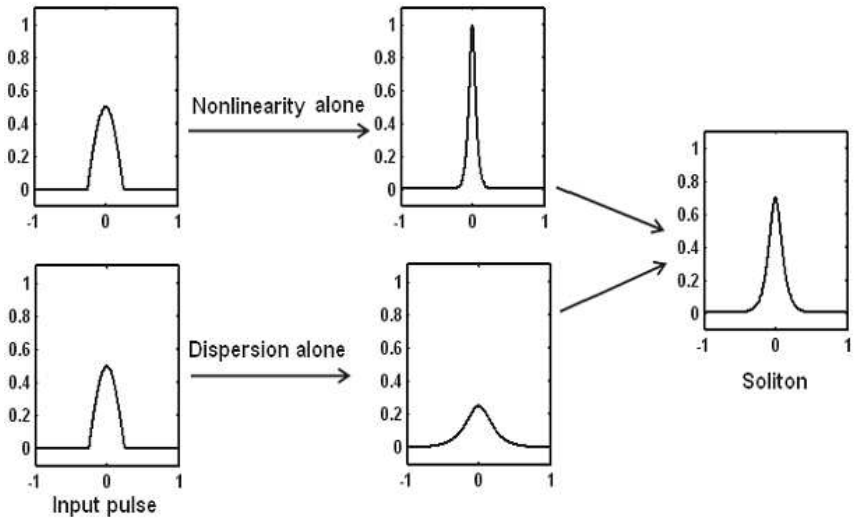

Figure 1.7: *Dispersion and nonlinear effects in the NETL.*

1.2.5 Generalities on diodes

A diode is a two-terminal device, having two active electrodes, between which it allows the transfer of current in one direction only. Basically, diodes are used for the purpose of rectifying waveforms, and can be used within power supplies or within radio detectors. They can also be used in circuits where one way effect of diode is required. Most diodes are made from semiconductors such as silicon; however, germanium is also used sometimes. Several types of diodes are available for use in electronics design. But in this work, we will focus only on Schottky and Varicap diodes.

1.2.5.1 Schottky diode

These diodes feature lower forward voltage drop as compared to the ordinary silicon PN junction diodes. The voltage drop may be situated between 0.15 and 0.4 volt at low current, as compared to the 0.6 volt for a silicon diode. In order to achieve this performance, these diodes are constructed differently from normal diodes, with metal to semiconductor contact. Schottky diodes are used in radio frequency (RF) applications,

rectifier applications and clamping diodes. The advantages of NETLs explored for use in pulse sharpening require extremely fast diode meeting those requirements. Its unique properties enable it to be used in a number of applications where other diodes would not be able to provide the same level of performance.

1.2.5.2 Varicap diode

This type of diode is used in many radio frequency (RF) applications. The diode has a reverse bias placed upon it and this varies the width of the depletion layer according to the voltage placed across the diode. In this configuration the varactor or varicap diode acts like a capacitor with the depletion region being the insulating dielectric and the capacitor plates formed by the extent of the conduction regions. The capacitance can be modified by changing the bias on the diode as this will vary the width of the depletion region which accordingly will change the capacitance.

1.3 Generalities on the modulational instability

Modulation instability (MI) is a universal process that is inherent to most nonlinear wave systems in nature. Because of MI, small amplitude perturbations that originate from noise on top of a homogeneous wave front grow rapidly under the combined effect of nonlinearity and dispersion **[57, 58]**. In the fields of nonlinear optics and fluid dynamics, modulational instability or sideband instability is a phenomenon whereby deviations from a periodic waveform are reinforced by nonlinearity, leading to the generation of spectral-sidebands and the eventual breakup of the waveform into a train of pulses **[57, 59, 61]**. The phenomenon was first discovered and modeled for periodic surface gravity waves (Stokes waves) on deep water by T. Brooke Benjamin and Jim E. Feir, in 1967 **[62]**. Therefore, it is also known as the Benjamin-Feir instability. It is a possible mechanism for the generation of rogue waves **[63, 64]**. Modulation instability only happens under certain circumstances. The most important condition is anomalous group velocity dispersion, whereby pulses with shorter wavelengths travel with higher group velocity than pulses with longer wavelength **[60, 61]**. There is also a threshold power, below which no instability will be seen **[61]**. The instability is strongly dependent on the frequency of the perturbation. At certain frequencies, a perturbation will have little effect, while at other frequencies, a perturbation will grow exponentially. Random perturbations will generally

contain a broad range of frequency content, and so will cause the generation of spectral sidebands which reflect the underlying gain spectrum. The tendency of a perturbing signal to grow makes modulation instability a form of amplification. Recent theoretical and experimental work have proved that MI can also occur with partially spatially incoherent light **[65–67]**. The implication of this result is that MI can appear in almost any weakly correlated nonlinear wave system. Figure 1.8 illustrates the modulational instability phenomenon in incoherent waves.

Figure 1.8: *Photograph of progressive wave trains illustrating the incoherent wave breaking into incoherent signals due to instability* ***[68]****.*

Conclusion

In this chapter, we provided the background of the soliton theory and their applications; we also point out some generalities about nonlinear electrical transmission lines and on the modulational instability. The pioneer experimental soliton work of J. S. was also presented. It appears that the combination of dispersion and nonlinearity together lead to the appearance of solitons. When dispersions and nonlinearities are in the same order of magnitude, solitary wave will propagate through the network in stable manner. The nonlinear components studied in this chapter which are usually used to introduce nonlinearity in the standard NETL are nonlinear diodes. In the next chapter, we will present the mathematical and numerical way used to obtain our results.

Chapter 2

Methodology of investigations: The Analytical and Numerical Methods

Introduction

In order to accomplish our aims, we combine the analytical and numerical methods. Generally, from the Kirchhoff's law, it is easy to show that the network is governed by a discrete ordinary differential equations which is difficult to solve and where solutions need to be approximated. There are many analytical methods which are used to obtain these approximated solutions. These analytical methods lead to the discrete nonlinear Schrödinger equation, the complex Ginzburg-Landau equation and many others. The numerical methods are used to consolidate the analytical results. In the first part of this chapter, we will give the generalities on the analytical methods used; the second part will be devoted to the numerical methods.

2.1 Analytical methods

There is a vast body of literature concerned with finding approximations to wave equations. Nowadays, there are a number of sophisticated methods at our disposal for determining approximate equations. We will use in this work the reductive method of Tanuiti and the rotating wave approximation.

2.1.1 The Tanuiti reductive method

The reductive method is based on the multiple-scale approximation in order to obtain the Nonlinear Schrödinger (NLS) equation, the well-known Ginzburg-Landau (GL) equation or the extension of the nonlinear Schrödinger equation. Following this method, the voltage $V_n(t)$ is expanded in power series as follows **[69–71]**:

$$V_n(t) = \sum_{l,m} \varepsilon^l A_{l,m} \exp(im\theta(n,t)) + cc \tag{2.1}$$

where cc denotes the complex conjugate, $A_{l,m}$ is the envelope of waves while $\exp(im\theta(n,t))$ is the carrier. The parameter l in Eq. (2.1) is the perturbation range, while m is the order of frequency which can be created from the fundamental frequency. It has been proved that Eq. (2.1) contains only three important terms which can be different to zero, leading this equation to:

$$V_n(t) = \epsilon^r A_{11}(x,t)e^{i\theta} + \epsilon^{2r}[A_{20}(x,t) + A_{22}(x,t)e^{2i\theta}] + c.c. \tag{2.2}$$

The parameter r in Eq. (2.2) accounts for the nonlinear partial differential equation that one expects to obtain. If we neglect the dissipative effects and if $r = 1$, this form of expansion leads to the usual NLS equation **[72]**. If $r = 1/2$ and if we take into account the dissipative effects like resistances, we obtain the GL equation **[73]**. While for $r = 0$, the extension of the nonlinear Schrödinger equation **[69]** can be obtained. The parameter A_{11} proportional to $e^{i\theta}$ is the first harmonic term which usually is the input wave. A_{20} is the the dc term which is usually introduced by the direct current in the network while terms proportional to $e^{mi\theta}$,$m = 2, .., M$ respectively, are the second, third, ..., M^{th} harmonic terms, which characterized the ability of the network to generate harmonics. θ is the linear phase, given in term of the angular frequency and wave number k by

$$\theta = kn - \omega t \tag{2.3}$$

which characterize the fast local oscillation. To take care of the slow variation in amplitude, we use the slow variables x and τ given by

$$\begin{cases} x = \varepsilon^r(n - v_g t) \\ \tau = \varepsilon^{2r} t \end{cases} \tag{2.4}$$

The constant v_g is the wave velocity associated to the wave packet given by

$$v_g = \frac{d\omega}{dk}. \tag{2.5}$$

For $r = 0$, the dispersion relation and the group velocity are obtained by assuming a sinusoidal wave in which V_n is proportional to $e^{i\theta}$ and by neglecting the terms of power greater than 1. For $r = 1$, the dispersion relation is obtained from equation $e^{i\theta}$ proportional to ε, and v_g from equation $e^{i\theta}$ proportional to ε^2. The evaluation of the potential at cells $n \pm 1$ is given by Eq. (2.6)

$$V_{n\pm1}(t) = \varepsilon^r A_{11}(x\pm\varepsilon^r,\tau)e^{i\theta}e^{\pm ik}+\varepsilon^{2r}A_{20}(x\pm\varepsilon^r,\tau)+\varepsilon^{2r}A_{22}(x\pm\varepsilon^r,\tau)e^{2i\theta}e^{\pm2ik}+...+cc \tag{2.6}$$

$A_j(x\pm\varepsilon^r,\tau)$ is expanded by means of Taylor series expansion method, where all derivatives of $A_j(x,\tau)$ are taken at the expansion point (x,τ). Thus, $A_j(x \pm \varepsilon^r,\tau)$ can be Taylor expanded as:

$$A_j(x \pm \varepsilon^r,\tau) = A_j(x,\tau) \pm \varepsilon^r \frac{\partial A_j(x,\tau)}{\partial x} + \frac{\varepsilon^{2r}}{2}\frac{\partial^2 A_j(x,\tau)}{\partial x^2} \pm ... \tag{2.7}$$

The dispersion relation generally proved that the angular frequency ω belong to interval $]\omega_0;\omega_c[$, where ω_0 is the gap frequency and ω_c is the cut-off frequency. For $\omega_0 = 0$, the network is the low-pass filter, while for $\omega_0 \neq 0$, the network is the band-pass filter, which in this case is characterized by the absence of A_{20} in Eq. (2.2) due to the band-pass filter character of the network which eliminates all the *dc* terms.

2.1.2 The rotating wave approximation

The rotating wave approximation is an approximation used in atom optics, magnetic resonance and in nonlinear electrical lines. The rotating wave approximation (RWA) **[74]** was used frequently in papers that appeared in the late eighties and early nineties, for instance (see **[75–79]**). Since the solutions are time periodic, they can be expressed as a Fourier series,

$$V_n(t) = \sum_{p=-\infty}^{p=+\infty} \epsilon^r \psi_{np}(T)e^{ip\omega t} + c.c. \tag{2.8}$$

where ψ_{np} are coefficients to be determined, and $\omega = 2\pi/T$, T being the period of the motion. The previous ansatz is substituted into the discrete ordinary differential equation obtained from Kirchhoff's laws, and one equates coefficients of terms with the same

frequency $p\omega$, $p = 0, \pm 1, \pm 2, ...$ in the resulting equation. In the simplest approximation, only terms which are resonant with the fundamental frequency $e^{i\omega t}$ are retained, and terms with $|p| \geq 2$ (namely, $e^{2i\omega t}, e^{3i\omega t}, e^{4i\omega t}, ...$) are neglected. Thus, taking into account these considerations Eq. (2.8) simply takes the form

$$V_n(t) = \epsilon^r \psi_{11}(x,t)e^{i\omega t} + c.c. \tag{2.9}$$

In this thesis, we chose $r = 1$ to obtain the complex Ginzburg-Landau (CGL) equation .

2.2 Numerical methods

Numerical solution of ordinary differential equations is the most important technique in continuous time dynamics. Since most ordinary differential equations are not soluble analytically, numerical integration is the only way to obtain information about the trajectory. Many different methods have been proposed and used in an attempt to solve accurately various types of ordinary differential equations. However there are a handful of methods known and used universally (i.e., Runge-Kutta, Adams-Bashforth and Backward Differentiation Formula methods). All these methods discretize the differential system to produce a discrete system of equation or map. The methods obtain different maps from the same differential equation, but they have the same aim; that the dynamics of the map should correspond closely to the dynamics of the differential equation. In this work, we use the fourth order Runge-Kutta algorithm.

The fourth order Runge-Kutta is a much more locally accurate method. Suppose that we have an equation of the form (with $U(t_0) = U_0$);

$$\frac{dU}{dt} = f(t, U) \tag{2.10}$$

then if we know U^n and set $t = (n-1)h$, the value of U^{n+1} is given by the sequence of operations

$$U^{n+1} = U^n + \frac{1}{6}(k_1 + 2k_2 + 2k_3 + k_4) \tag{2.11}$$

where k_1, k_2, k_3 and k_4 are the coefficients of the fourth order Runge-Kutta given by the system below

$$\begin{cases} k_1 = hf(t, U^n) \\ k_2 = hf(t + \frac{h}{2}, U^n + \frac{k_1}{2}) \\ k_3 = hf(t + \frac{h}{2}, U^n + \frac{k_2}{2}) \\ k_4 = hf(t + h, U^n + k_3) \end{cases} \tag{2.12}$$

h is the normalized integration time step. This method is very widely favoured as:

- It is easy to use and no equations need to be solved at each stage;
- It is highly accurate for moderate h values;
- It is a one step method i.e. U^{n+1} only depends on U^n;
- It is easy to start and easy to code.

In the special case when $f(t, U) = f(t)$, we have

$$U(t) = \int_{t_o}^{t} f(t)dt + U_0 \tag{2.13}$$

and the task of evaluating this integral accurately is called quadrature. To solve any differential equation with the fourth order Runge-Kutta algorithm, we need to put it into the standard form given by Eq. (2.10).

Conclusion

This chapter was devoted to the presentation of analytical and numerical methods used to model the nonlinear evolution equation governing the network under consideration. Using the analytical methods, we have shown that it is possible to solve the discrete ordinary differential equations obtained from the Kirchhoff's law. In the view to consolidate the analytical results, we use the numerical methods to proof that the results obtained are valid. In the next chapter, we will present our results together with discussions.

Chapter 3

Results and Discussions: Description of the Models, Basic Properties and Derivation of the Nonlinear Schrödinger and the Ginzburg-Landau Equations

Introduction

In the previous chapters, we have given the generalities on the soliton, nonlinear electrical transmission lines and on modulational instability. We have also pointed out the different methods used to reach our goals. The mathematical methods were based on the Tanuiti reductive method and on the rotating wave approximation method. To confirm the analytical methods and to plot the different curves, we have used the fourth order Runge-Kutta algorithm. This chapter presents our results. There are a lot of work on coupled nonlinear electrical lines and in this thesis, we focus on the effect of nonlinear coupling on modulational instability in a NETLs, the effect of second-neighbor inductive coupling on the modulational instability in a coupled lines of transmission; we also look how to suppress mixing waves in a coupled NETLs and finally, we study the transverse stability.

3.1 Effect of nonlinear coupling on modulational instability in coupled nonlinear transmission lines

3.1.1 Model and equations

The model of our study consists of nonlinear network with two identical coupled nonlinear LC transmission lines. Each line contains a finite number of cells which consist of three elements: a linear inductor of inductance L_s in the series branch, a linear inductor of inductance L_p and a nonlinear capacitor of capacitance $C(V_n)$ in the shunt branch. The two lines are connected by an intermediary nonlinear capacitor $C(\delta V_n)$ since we want to catch the effect of nonlinear coupling, with $\delta V_n = V_{jn} - V_{3-jn}$; where j can take the values 1 or 2, 1 for the first line and 2 for the second line. The network is depicted in figure 3.1.

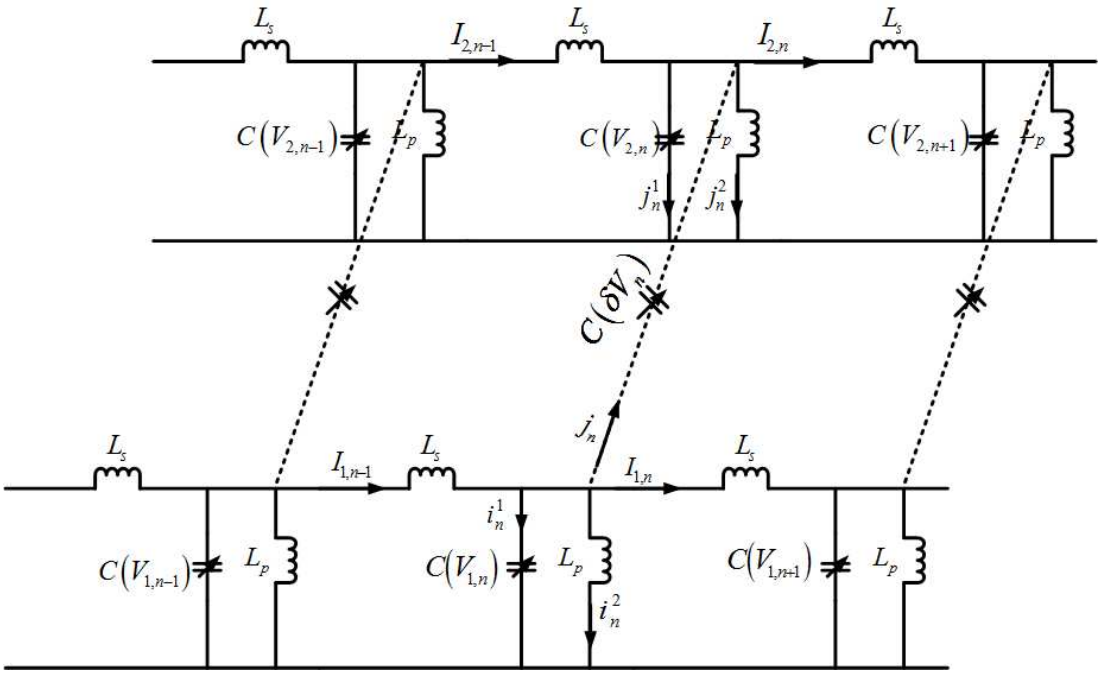

Figure 3.1: *Network of two identical nonlinear transmission lines coupled by a nonlinear capacitance. Three unit cells are reproduced for each line.*

The nonlinear charges in the shunt and in the coupling branch, are voltage dependent and are given by:

$$\begin{cases} Q_{1,n} = C_{01}(V_{j,n} - \eta_1 V_{j,n}^2 + \delta_1 V_{j,n}^3) \\ Q_{2,n} = C_{02}\Big[(V_{j,n} - V_{3-j,n}) - \eta_2(V_{j,n} - V_{3-j,n})^2 + \delta_2(V_{j,n} - V_{3-j,n})^3\Big] \end{cases} \tag{3.1}$$

Hence, due to the presence of the term in η_2, the capacitance $C(\delta V_n)$ depends on the way current is directed in the coupling branch and to write the Kirchhoff's law for the model, we must assume one way for the current in this branch.

Thus, if we assume that the current j_n in the n^{th} coupling branch goes from $V_{j,n}$ to $V_{3-j,n}$, it follows that for this branch,

$$\begin{cases} V_{j,n} - V_{3-j,n} = \int \frac{j_n}{C(V_{j,n} - V_{3-j,n})} dt \\ j_n = \frac{dQ_{2,n}}{dt} \end{cases} \tag{3.2}$$

With these equations and using the Kirchhoff's law in the two coupled lines, one can obtain the following equation (**see Appendix A**):

$$\begin{cases} \frac{d^2Q_{1,n}}{dt^2} = \frac{1}{L_s}(V_{1,n+1} + V_{1,n-1} - 2V_{1,n}) - \frac{1}{L_p}V_{1,n} - \frac{d^2Q_{2,n}}{dt^2} \\ \frac{d^2Q_{1,n}}{dt^2} = \frac{1}{L_s}(V_{2,n+1} + V_{2,n-1} - 2V_{2,n}) - \frac{1}{L_p}V_{2,n} + \frac{d^2Q_{2,n}}{dt^2} \end{cases} \tag{3.3}$$

Inserting expressions (3.1) and (3.5.4) yields the following set of two coupled equations governing waves propagation in the network:

$$\begin{aligned} (V_{j,n} - \eta_1 V_{j,n}^2 + \delta_1 V_{j,n}^3)_{tt} &= u_0^2(V_{j,n+1} + V_{j,n-1} - 2V_{j,n}) - \omega_0^2 V_{j,n} \\ &\quad -a[(V_{j,n} - V_{3-j,n}) - (-1)^{3-j}\eta_2(V_{j,n} - V_{3-j,n})^2 \\ &\quad +\delta_2(V_{j,n} - V_{3-j,n})^3]_{tt}. \end{aligned} \tag{3.4}$$

In Eq. (3.4), the subscript tt represents the second derivative about the time; the characteristic frequencies of each line, u_0 and ω_0, and the coupling coefficients a are given by:

$$\begin{cases} u_0^2 = \frac{1}{L_s C_{01}} \\ \omega_0^2 = \frac{1}{L_p C_{01}} \\ a = \frac{C_{02}}{C_{01}} \end{cases} \tag{3.5}$$

Due to the presence of the term $\eta_2(V_{j,n} - V_{3-j,n})^2$ in equation (3.4), the equation in $V_{3-j,n}$ is different to that in $V_{j,n}$ and the following remark can be done: waves propagating in the two lines are not governed by the same equation at the same moment. The equation governing waves propagation in each line depends on which direction the current in the coupling branch is flowing. But since the current might be alternative, the way it is directed may change alternatively and the equation governing waves propagation in each line also changes alternatively between the two equations of the set (3.4) obtained for $j = 1$ and $j = 2$.

3.1.2 Derivation of the coupled NETLs governing waves propagation in the model

To describe modulated waves in the network, we consider waves with a slow variation of envelope in time and space with respect to a given carrier with angular frequency ω and wave vector k. Then, in order to use the reductive perturbation method in the semi-discrete limit, we introduce the slow-envelope variables $x = \varepsilon(n - v_g t)$ and $\tau = \varepsilon^2 t$ where ε is a small parameter and v_g is a group velocity. Hence, the solution of equation (3.4) is assumed to have the following general form:

$$V_{j,n}(t) = \varepsilon A_j(x,\tau)e^{i\theta} + \varepsilon^2[\phi_j(x,\tau) + B_j(x,\tau)e^{2i\theta}] + cc \tag{3.6}$$

with $\theta = kn - \omega t$ and "cc" stands for complex conjugate.
Inserting this relation into the equation governing wave propagation, and keeping terms proportional to $(\varepsilon, e^{i\theta})$ yields the following linear dispersion relation:

$$\omega^2 = \Gamma^{(l)}(\omega_0^2 + 4u_0^2 \sin^2(\frac{k}{2})) \tag{3.7}$$

where $\omega_{min} = \omega_0\sqrt{\Gamma^{(l)}}$ and $\omega_{max} = \sqrt{\Gamma^{(l)}(\omega_0^2 + 4u_0^2)}$. Hence, as for the two lines coupled by a linear capacitor **[28]**, the two lines coupled with nonlinear capacitors exhibits two modes of propagation of waves i.e. the slow- and the fast-mode. The superscript l stands for the mode of propagation and

$$\Gamma^{(l)} = \begin{cases} 1 \text{ if } l = 1 \text{ (fast mode)} \\ \frac{1}{1+2a} \text{ if } l = 2 \text{ (slow mode)} \end{cases} \tag{3.8}$$

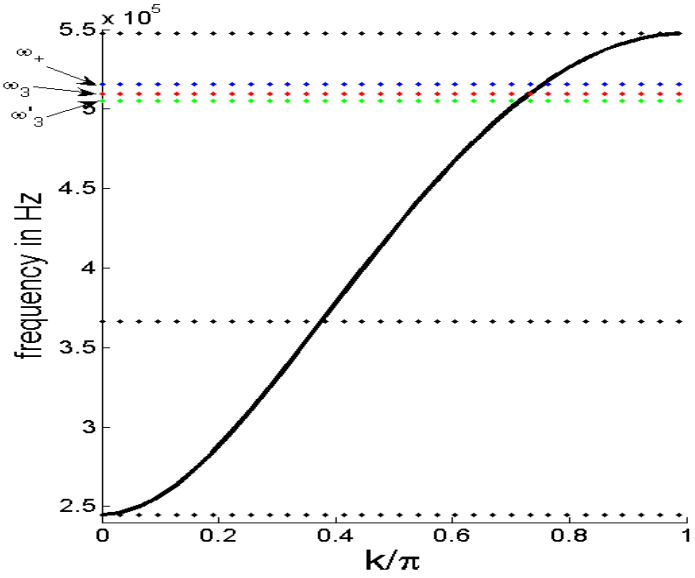

Figure 3.2: *Dispersion relation depicted for the slow-mode with* $Lp = 0.220\ mH$, $Ls = 0.220\ mH$, $C_0 = 320\ pF$ *and* $a = 2.5$. ω_3 *and* $\omega_3^{'}$ *are the roots of the polynomials* $q(\omega)$ *respectively for the first and the second line while* ω_+ *is the solution of the nonlinear coefficient with the linear coupling.*

This dispersion relation is presented in figure 3.2 for the slow mode.

The terms of order ε^2 proportional to $e^{i\theta}$ allow to obtain the following relation:

$$A_j = -(-1)^l A_{3-j} \tag{3.9}$$

Keeping terms of order ε^2 proportional to $e^{2i\theta}$, one also obtains the relation:

$$B_j = -4(\eta_1 b_1^{(l)} + (-1)^{(3-j)}\eta_2 b_2^{(l)})A_j^2 \tag{3.10}$$

$$with \begin{cases} b_1^{(l)} = \frac{1}{-4\omega^2+\omega_0^2+4u_0^2\sin^2 k} \\ b_2^{(l)} = \frac{\lambda^{(l)}}{-4(1+2a)\omega^2+\omega_0^2+4u_0^2\sin^2 k} \\ \lambda^{(l)} = 4(l-1) \end{cases} \tag{3.11}$$

Similarly, the terms of order ε^3 proportional to $e^{i\theta}$ yield the following uncoupled nonlinear Schrödinger equations:

$$\begin{cases} i\frac{\partial A_j}{\partial \tau} + P\frac{\partial^2 A_j}{\partial x^2} + Q|A_j|^2 A_j = 0 \\ i\frac{\partial A_{3-j}}{\partial \tau} + P\frac{\partial^2 A_{3-j}}{\partial x^2} + Q'|A_{3-j}|^2 A_{3-j} = 0 \end{cases} \tag{3.12}$$

where the dispersion and the nonlinear coefficients are respectively given by:

$$\begin{cases} P = -\frac{1}{8\omega^3}(\omega^4 - \omega_{min}^2\omega_{max}^2) \\ Q = 4\eta_1^2\omega\Gamma^{(l)}(\alpha_2 + b_1^{(l)}\omega^2 + \alpha_1 b_2^{(l)}\omega^2) \\ Q' = 4\eta_1^2\omega\Gamma^{(l)}(\alpha_2 + b_1^{(l)}\omega^2 + \alpha_1' b_2^{(l)}\omega^2) \end{cases} \tag{3.13}$$

$$with \begin{cases} {\omega_{min}^{(l)}}^2 = \Gamma^{(l)}\omega_0^2 \\ {\omega_{max}^{(l)}}^2 = \Gamma^{(l)}(\omega_0^2 + 4u_0^2) \\ \alpha_1 = \frac{4a\eta_2^2}{\eta_1^2} + \frac{\eta_2}{\eta_1} \\ \alpha_1' = \frac{4a\eta_2^2}{\eta_1^2} - \frac{\eta_2}{\eta_1} \\ \alpha_2 = \frac{3a\delta_2}{\eta_1^2} + \frac{3\delta_1}{8\eta_1^2} \end{cases} \tag{3.14}$$

Thus, we have deduced two uncoupled nonlinear Schrödinger equations describing the evolution of the the envelope of the nonlinear wave traveling in the two nonlinearly coupled transmission lines. We can then point out that the dispersion coefficient P remains the same as in the case of linear coupling, while the nonlinear coefficient Q is considerably changed by the nonlinear coupling. This is illustrated by additional terms in Q and Q'. In addition, the curves of figure 3.3 show the evolution of nonlinear coefficients as function of wave frequency for both linear and nonlinear coupling. An important remark is that for the fast-mode, Q and Q' are identical. They are different only for the slow-mode and for this reason, further investigations are made just for the slow-mode. We can note from this figure 3.3 that for a very large range of frequency, the system that is defocusing ($Q > 0$) with linear coupling becomes focusing ($Q < 0$) with the nonlinear coupling. Our attention will be focussed only on the slow-mode which is related to the coupling. We recall for memory that the fast-mode remains equal to the case of uncoupled system i.e. a single line.

Using the preceding expressions of dispersion and nonlinear coefficients, one can express the gain of instability for the two coupled lines as function of the wave number γ of the perturbation. For the slowly modulated wave used, this function is given as:

$$\begin{cases} G = 2|P\gamma|\sqrt{2\frac{Q}{P}\Phi_0^2 - \gamma^2} \\ G' = 2|P\gamma|\sqrt{2\frac{Q'}{P}\Phi_0^2 - \gamma^2} \end{cases} \tag{3.15}$$

Note that the modification of the gain due to nonlinear coupling is induced by the modification of the nonlinear coefficient Q.

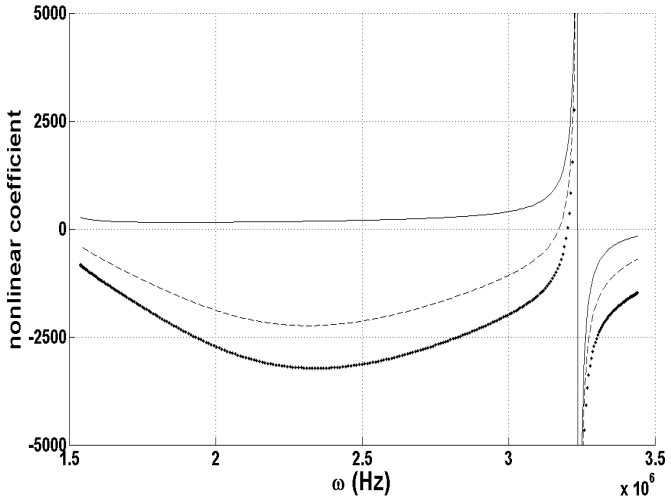

Figure 3.3: *Nonlinear coefficient depicted as function of ω for the slow-mode with the same parameters as in figure 3.2. Solid line is used for the case of linear coupling that is $\eta_2 = \delta_2 = 0$; dashed line (-) and dotted (.) are used for the coefficient Q' and Q respectively in the case of nonlinear coupling that is $\eta_2 = 0.21\ V^{-1}$, $\delta_2 = 0.0197\ V^{-2}$. In the first zone, the nonlinear coefficient corresponding to the linear coupling is positive while in the case with the nonlinear coupling, this coefficient is negative.*

3.1.3 Modulational instability in the model

The NLSEs derived in the preceding section describe the evolution of the amplitude of waves in the two coupled lines; the equations are different from one line to another but are not coupled because each equation depends only on the voltage amplitude of waves moving on the line it describes. Since the equation describing evolution of each line depends on the way the current is directed, one can conclude that the evolution of the amplitude of waves moving in each line is alternatively described by two NLSEs given for cell n on the line j by:

$$\begin{cases} i\frac{\partial A_j}{\partial \tau} + P\frac{\partial^2 A_j}{\partial x^2} + Q|A_j|^2 A_j = 0 \text{ if } V_{j,n} \geq V_{3-j,n} \\ i\frac{\partial A_j}{\partial \tau} + P\frac{\partial^2 A_j}{\partial x^2} + Q'|A_j|^2 A_j = 0 \text{ if } V_{j,n} \leq V_{3-j,n} \end{cases} \tag{3.16}$$

It is well known that the Benjamin-Feir modulational instability, exhibited by a dispersive nonlinear medium, constitute the proof of its capacity to support envelope solitons in certain domains of propagation. From the first equation of set (3.16), it is easy to show that a continuous slowly modulated plane wave should be unstable if $PQ > 0$. This instability leads to the formation of small wave packets or envelope pulse solitons train, solution of the NLS equation (3.16) and whose explicit expression is given by:

$$A^{(l)}(x,\tau) = A_0 sech[\frac{(x - P^{(l)} v_e \tau)}{L_e^{(l)}}] exp[\frac{i v_e (x - P^{(l)} v_c \tau)}{2}] \tag{3.17}$$

where v_e and v_c are respectively the envelope and phase velocities while L_e designates the spatial soliton extension. According to the dispersion relation, the network exhibits the propagation of the fast-mode envelope soliton for the same frequencies as the network with linear coupling (see **[28]**).

For the slow-mode envelope soliton, the sign of the product P with the nonlinear coefficient depends on the direction of the current flow through the coupling branch and then alternates between the sign of PQ and that of PQ'. In order to study this sign, we rewrite the nonlinear coefficient Q in the form:

$$Q = 4\Gamma\omega\eta^2 \frac{q(\omega)}{(4\omega^2 - \omega_0^2 - 4u_0^2 \sin^2(k))(4(1+2a)\omega^2 - \omega_0^2 - 4u_0^2 \sin^2(k))} \tag{3.18}$$

with

$$q(\omega) = \alpha_2 \omega^8 - \lambda_1 \omega^6 + \lambda_2 \omega^4 - \lambda_3 \omega^2 + \lambda_4 \tag{3.19}$$

where for the first NLS equation we have:

$$\begin{cases} \lambda_1 = 4\alpha_2\Gamma\omega_0^2 + \Gamma^2(1 + 4\alpha_1 + 8a\alpha_2)u_0^2 \\ \lambda_2 = 6\alpha_2\Gamma^2\omega_0^4 + \Gamma^2u_0^2\omega_0^2[2\Gamma + 8\alpha_1\Gamma + 2\alpha_2(3 + 8a\Gamma)] + 32\Gamma^4a\alpha_1u_0^4 \\ \lambda_3 = \Gamma^3\omega_0^2[4\alpha_2\omega_0^4 + (\Gamma + 4\alpha_1\Gamma + 8a\Gamma\alpha_2 + 12\alpha_2)u_0^2\omega_0^2 + 3(1 + 4\alpha_1 + 8a\alpha_2)\Gamma u_0^4] \\ \lambda_4 = \alpha_2\Gamma^4\omega_0^4(\omega_0^2 + 3u_0^2)^2 \end{cases} \tag{3.20}$$

and for the second NLS equation, the corresponding coefficients are obtained by substituting α_1 by α_1'.

Due to the complex nature of the polynomial $q(\omega)$, before studying the sign of PQ, we will substitute the characteristic parameters of the network by their values given in section 4, except the coupling constant for which the effect will be analyzed.

In this particular case, since $u_0 = \omega_0$, one can easily obtain for the first NLSE of relation (3.16):

$$q(\omega) = \frac{197}{56}\omega^8 - \frac{3721}{504}\omega_0^2\omega^6 + \frac{737}{162}\omega_0^4\omega^4 - \frac{3721}{4536}\omega_0^6\omega^2 + \frac{197}{4536}\omega_0^8 \tag{3.21}$$

and for the second NLSE:

$$q(\omega) = \frac{197}{56}\omega^8 - \frac{1147}{168}\omega_0^2\omega^6 + \frac{5147}{1512}\omega_0^4\omega^4 - \frac{1147}{1512}\omega_0^6\omega^2 + \frac{197}{4536}\omega_0^8 \tag{3.22}$$

The above expressions show that for each coupling constant a and for each NLSE, several frequency domains for which $PQ > 0$, may exist depending on the numerical values of the following characteristic angular frequencies, $\omega_+, \omega_-, \omega_1, \omega_2, \omega_3, \omega_4, \omega_1', \omega_2', \omega_3', \omega_4'$ given by:

$$\begin{cases} \omega_\pm^2 = \Gamma\omega_0^2\sqrt{[3 - 2\Gamma \pm 2\sqrt{\delta}]} \\ \delta = \Gamma^2 - 3\Gamma + \frac{5}{4} \end{cases} \tag{3.23}$$

and where the sets $(\omega_1, \omega_2, \omega_3, \omega_4)$ and $(\omega_1', \omega_2', \omega_3', \omega_4')$ are the roots of the polynomials $q(\omega)$ for the first and the second NLSEs respectively, and their values could be find numerically for each coupling constant a.

To determine the domain of modulational instability as function of both coupling constant and frequency, we need to introduced a reduced frequency that will be independent of the coupling constant. We use the reduced frequency because ω_{min} and ω_{max} are function of coupling constant a and are evaluated for each new value of the coupling parameter a. This reduced frequency is given as:

$$\omega_{reduced} = \frac{\omega - \omega_{min}}{\omega_{max} - \omega_{min}} \tag{3.24}$$

Using numerical values of the quantity mentioned above, domains of modulational instability are presented in the charts of figure 3.4. This chart presents domains of MI for the two lines. Fig.3.4a results from the linear capacitor (obtained by taking $\eta_2 = 0$ and $\delta_2 = 0$) while Fig.3.4b corresponds to the coupling with the nonlinear capacitor. In the case of nonlinear coupling *i.e.* $\eta_2 = 0.21\ V^{-1}$, $\delta_2 = 0.0197\ V^{-2}$, since waves propagation in each line of the network is alternatively described by two different NLSEs, we may distinguish four kinds of domains while in the linear coupling case, only two kinds of MI domains are encountered.

We have set to the blue color the domain for which none of the two NLSEs predict

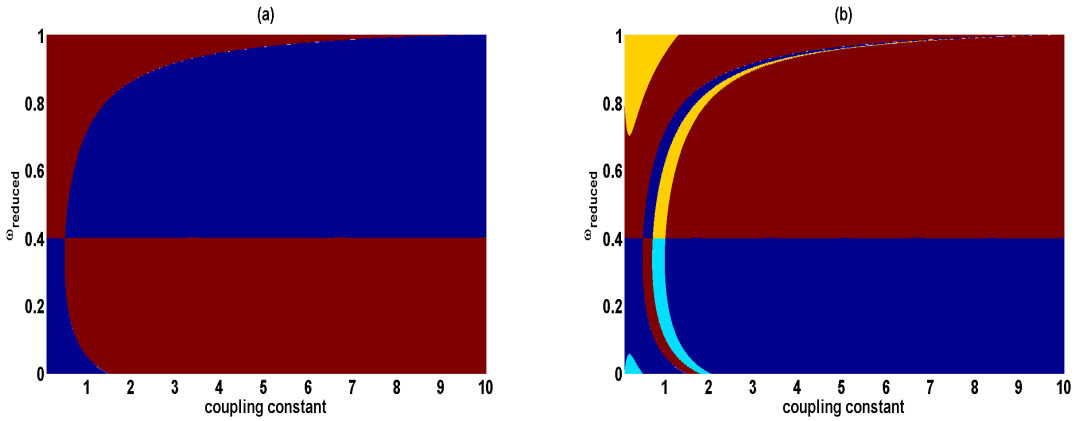

Figure 3.4: *Chart showing the domain of modulational instability as function of coupling constant a and frequency $\omega_{reduced}$ for $L_p = L_s = 0.220\ mH$. Colors have the following meaning: red is associated to the domains for which MI is predicted by the two NLSEs, yellow and cyan denote the regions for which only one of the two NLSEs predicts MI, and blue is dedicated to domains with no MI. These charts are depicted for the same parameters as in figure 3.2. (a) linear coupling i.e. $\eta_2 = 0$, $\delta_2 = 0$; (b) nonlinear coupling for $\eta_2 = 0.21\ V^{-1}$, $\delta_2 = 0.0197\ V^{-2}$.*

MI while the region of MI (i.e. predicted by the two NLSEs) is represented with the red color. Some regions have an unknown status since the MI is predicted by only one of the two NLSEs. These latter regions have been marked by two different colors, cyan and yellow depending on whether the first or the second NLSE predicts MI or not. We remark that: (i) the ratio 2/5 of the allowed bandwidth is a particular threshold as the coupling constant varies with no care of the type of the coupling (linear as well as nonlinear); (ii)

for values of parameter a varying approximately up to 0.5, the MI region is found in the upper 3/5 allowed bandwidth (independently of the type of coupling); above this value, the MI only occurs for frequencies less than the reduced frequency threshold 0.4 for the linear coupling; while the nonlinear coupling induces another critical value of parameter a around 1.0 for which the MI is still found above the reduced frequency threshold; (iii) as the threshold line $\omega_{reduced} = 0.4$ separates the space of parameters (a, ω) into two regions with 3/5 of the entire domain above and only 2/5 below, we can claim that the nonlinear coupling gives more flexibility to select parameters for MI. Moreover, the frequencies belong to the same band both for small and large values of the parameter a.

The coefficients of the nonlinearity δ_2 and η_2 are characteristics to the nonlinear component. During their manufacture, different events such as the assembling of reversed biased diodes as well as their misuse might induce small changes of the exact values of δ_2 and η_2. This suggest that it is important to have a look on the issue of domains of MI when these parameters are tuned around their known values. In this regard, we have analyzed the number of domains of MI in one hand as function of the coupling constant a and of nonlinear coefficient of the reversed biased diode η_2. The results are presented in the chart of figure 3.5. Notice that the stairs visualized are not an artefact due to the size step of parameters a and η_2. In fact, reducing Δa and $\Delta\eta_2$ for a small region still presents the same shape. This highlights the sensitivity of the nonlinear parameter. In other hand, we have analyzed this number of domains of MI as function of the coupling constant a and nonlinear coefficient δ_2. The results are presented in the chart of figure 3.6. It appears from these charts that for $a \in [3.5; 7.5]$ and $\delta_2 \in [0.0247; 0.0297]$, the system is not predictable because a very slow variation of one parameter cause the change of the state of the system. White color on figure 3.6 represents the domains where there is no MI.

3.1.4 Numerical experiments

According to the analytical calculations presented in the preceding sections, it is possible to determine in the spectrum of the coupled NLSEs the frequency range for which the network support the propagation of envelope solitons. In order to verify the validity of this prediction, we present in this section the numerical experiments on the propagation of slowly modulated waves in the network.

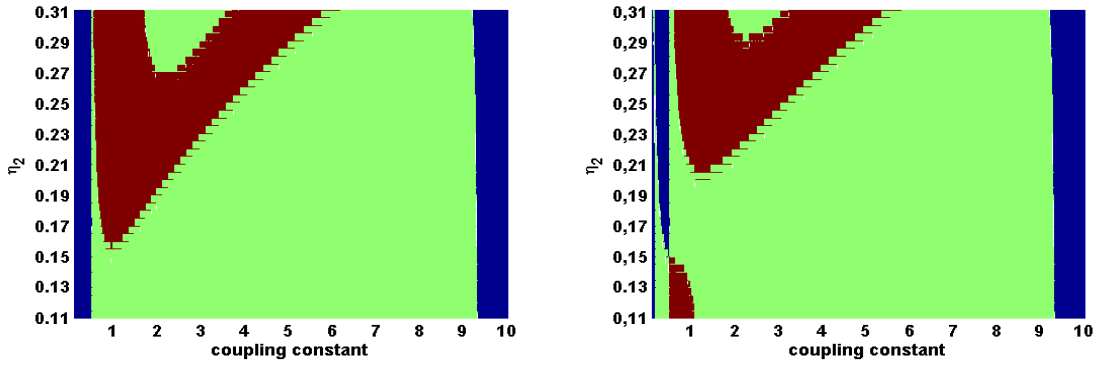

Figure 3.5: *Chart showing the number of domain of modulational instability as function of coupling constant a and nonlinear coefficient of the reversed biased diode η_2 for $L_p = L_s = 0.220$ mH. Where for each couple of values, colors have the following meaning: blue for one domain of modulational instability (MI), green for two domain of MI, red for tree domain of MI. The different charts are plotted for the same parameters as in figure 3.2. η_1 and δ_1 have the same values used before. The left figure corresponds to the NLSE with nonlinear coefficient Q while the right figure stands for the NLSE with nonlinear coefficient Q'.*

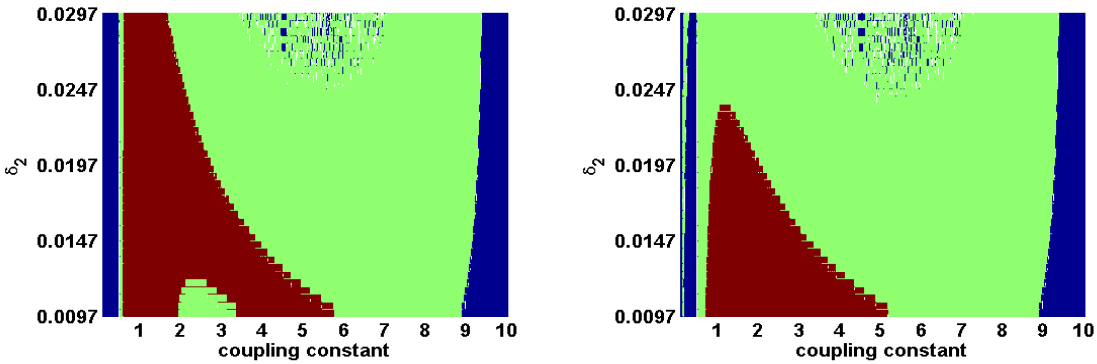

Figure 3.6: *With the same parameters as in 3.2, we show the number of domain of modulational instability as function of coupling constant a and nonlinear coefficient of the reversed biased diode δ_2 for $L_p = L_s = 0.220$ mH. Where for each couple of values, colors have the following meaning: blue for one domain of modulational instability (MI), green for two domain of MI, red for tree domain of MI. The left figure corresponds to the NLSE with nonlinear coefficient Q while the right figure stands for the NLSE with nonlinear coefficient Q'.*

The numerical experiments are carried out on the exact equation (3.4) describing the propagation of waves in the two identical non linearly coupled electrical transmission lines. The parameters of the network are chosen to be $L_s = L_p = 0.220$ mH, $C_0 = C_{01} = C_{02} =$

320 pF and $a = 2.5$ which insure absence of mixing of slow-and fast-mode envelope soliton. The characteristic parameters of the reversed biased diode are $\eta = \eta_1 = \eta_2 = 0.21\ V^{-1}$ and $\delta = \delta_1 = \delta_2 = 0.0197\ V^{-2}$. The corresponding cut-off frequencies are $f_c = 547.57\ kHz$ and $f_0 = 244.88\ kHz$ for the slow-mode of propagation of linear waves. The fourth-order Runge-Kutta scheme is used with normalized integration time step $\Delta t = 2.6533 \times 10^{-3}$ s. Similarly, the number of cells is variable in order to avoid waves reflection at the end of the line. This allows us to run the experiments with sufficiently large time.

The input of each line (cell n=0) is supplied by a slowly modulated signal of the form

$$V_0(t) = V_m[1 + m.cos(2\pi f_m t)]cos(2\pi f_p t) \tag{3.25}$$

where V_m is the amplitude of the unperturbed plane wave (carrier wave) and where $m = 0.01$ and f_m are the rate and the frequency of modulation, respectively.
The frequency of modulation f_m or the wave number of modulation k_m is given by a value that will maximize the modulational gain given by (3.15). This means that we may have:

$$k_m = \frac{V_m}{2}\sqrt{\frac{Q}{P}} \tag{3.26}$$

The experiment is carried out with a frequency $f_p = 515.63\ kHz$ which corresponds to the domain where the two lines predict MI. In this case, according to relation (3.26), there are two different values for the frequency of modulation, i.e. $f_m = 4.56\ kHz$ obtained with Q and $f_m = 5.6\ kHz$ obtained with Q'. We select the minimum of above two values.

Figure 3.7 shows an example of MI developed by the network for a slowly modulated wave with initial amplitude $V_m = 0.6\ V$.

We note in this figure the double modulation of the wave which can be explained by the two NLSEs describing the evolution of a slowly modulated wave in the network, each NLSE giving rise to one frequency of modulation. This could be linked to the so called phenomenon "bi-envelope" soliton.
For comparison and validation of analytical investigations, we recapitulate the numerical results obtained from the direct simulation in the following table:

In the view to consolidate the validity of the previous results, we propagate the solution of the **NLS** equation to proof that the network can support envelope solitons. For this purpose, we take as the input voltage the profile of a modulated soliton given by Eq.(3.17). The results are given on the figure 3.8.

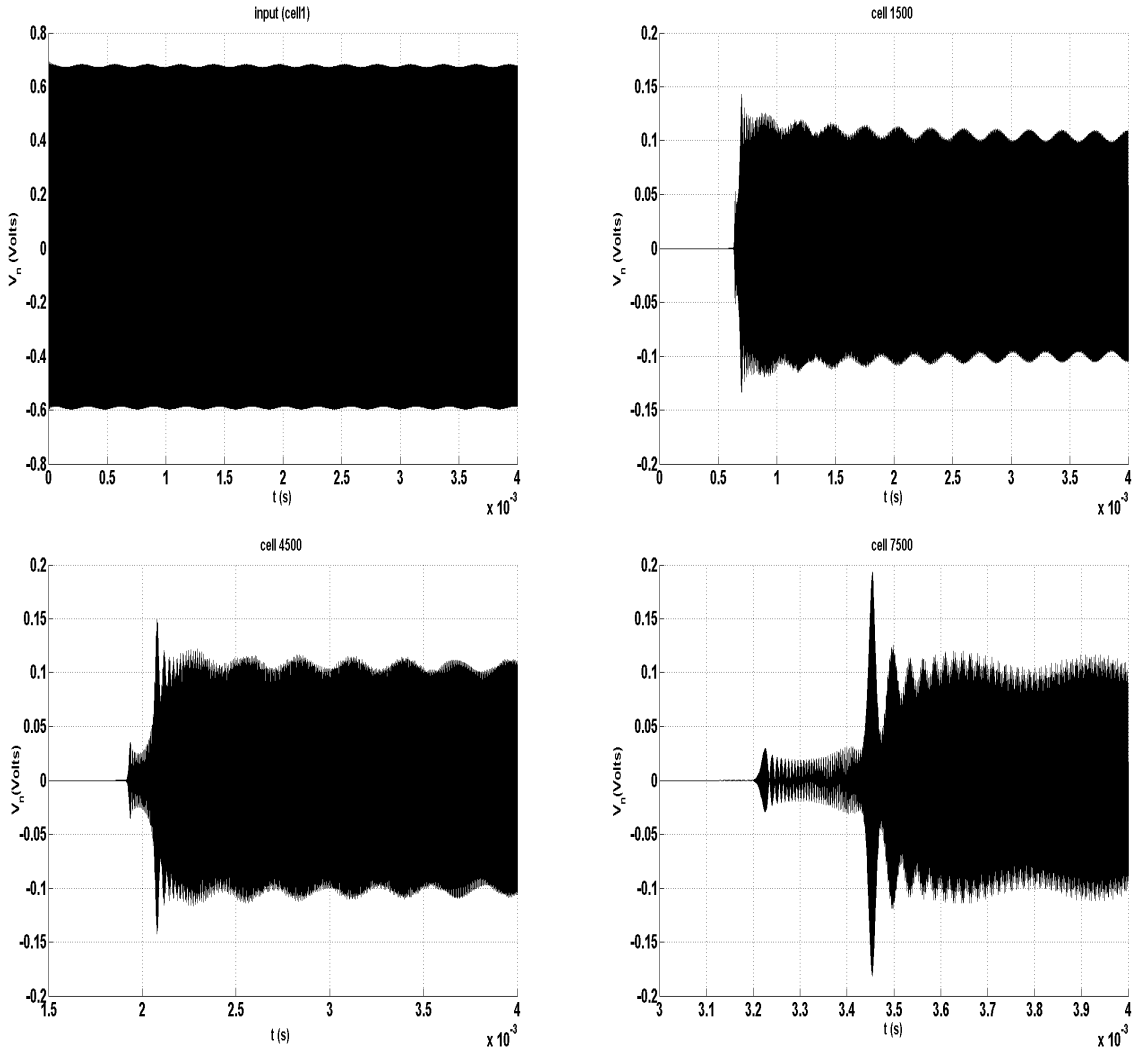

Figure 3.7: *Modulational instability exhibits by the propagation of the slow-mode in the network in the case where the two NLSEs predict the MI plotted with* $L_p = 0.220\ mH$; $L_s = 0.220\ mH$; $C_0 = 320\ pF$; $a = 2.5$.

Given the example above, the initial solution as provided by equation (3.17), for a given amplitude, is readjusting during its propagation. This is remarkable on the above curve since the solitary wave pass through the cell number 7500.

3.1.5 Concluding remarks on nonlinear coupling

The dynamics of modulated waves in a coupled nonlinear LC transmission line is investigated. We studied the effect of nonlinear coupling on nonlinear electrical transmission lines (NETLs). The elements of the network are associated in a way to avoid mixing of frequencies. By using the semi-discrete approximation, we derived the coupled

Domains of **IM** (slow-mode)		
a	Analytical predictions (kHz)	Numerical results (kHz)
8.0	[217.41 - 323.33] ∪ [324.78 - 325.30]	[218.3 - 319.7]
5.0	[270.27 - 394.35] ∪ [397.48 - 404.41]	[272.8 - 388.5]
0.8	[412.00 - 460.30] ∪ [670.88 - 787.22]	[412.8 - 458.2] ∪ [672.0 - 786.3]

Table 3.1: *Frequency values for which there is modulational instability.*

nonlinear Schrödinger (CNLS) equations describing the propagation through the network. Analytical and numerical studies presented a good agreement. We have shown that by coupling NETLs in this way, the propagation of waves in each line can be alternatively described by two nonlinear Shrödinger equations according to the direction of the current flow through the coupling branch. We have also pointed out that the nonlinear coupling adds the domains of modulational instability (MI) of each line. Finally, we have shown that a small variation of the nonlinear elements used in the coupling branch can change significantly the behavior of the network.

One achievement of the present part is the successful derivation of the NLSEs modeling waves propagation in two nonlinear transmission lines coupled with nonlinear capacitance. They alternatively describe the dynamics of the waves propagating through the coupled lines. The fast-mode corresponds to the uncoupled system i.e. for a single line and the two NLSEs are equivalent; while, the slow-mode imposes the use of the two NLSEs. The merit of the introduction of a nonlinear coupling capacitance results in (i) the determination of the threshold line $\omega_{reduced} = 0.4$ independently of the type of coupling; (ii) the creation of a second equation governing waves propagation in the network; (iii) the increasing of the percentage of MI in the slow-mode envelope soliton since the MI region covers the upper 3/5 of the bandwidth instead of 2/5 as in the case of linear coupling and (iv) the frequencies in (a, ω) space allowing MI belong to the same band (above the $\omega_{reduced}$ threshold) both for small and large values of the parameter a.

The study of the effects of the coupling constant has been attained with the derivation of different domains of modulational instability. The comparison with the case of linear coupling has been done. It comes out a rich, complex and very diversified structures according to the variations of the nonlinear coefficients and parameter a. Therefore, the sensitivity of these parameters is highlighted.

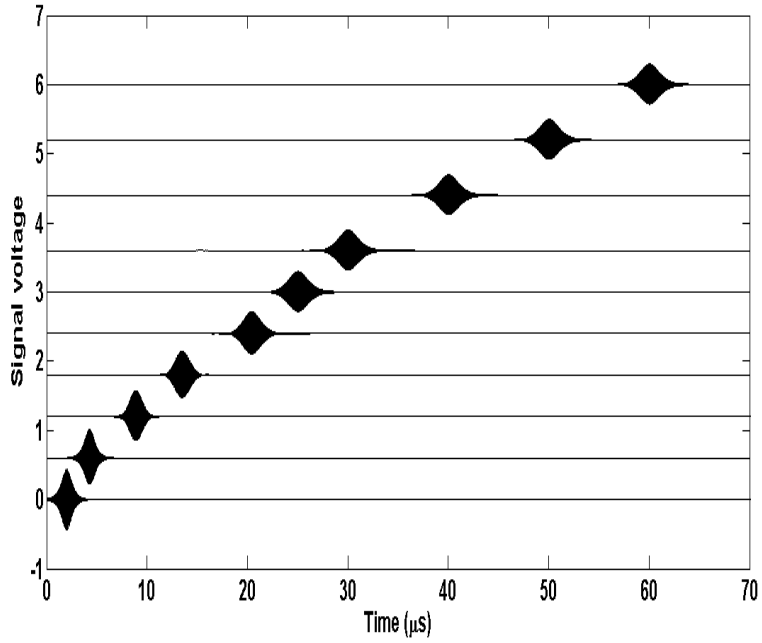

Figure 3.8: *Signal voltage as function of time at different cells obtained for the same parameters as in figure 3.7. From left to right, we have the cells number 1, 300, 800, 1500, 4500, 650, 7500, 10000, 12500 and 15000 respectively.*

3.2 Effect of second-neighbor inductive coupling on the modulational instability in a coupled line of transmission

3.2.1 Model and equations of dynamics

We use a nonlinear network with two identical coupled nonlinear **LC** transmission lines. Each line contains a finite number of cells and each cell contains a linear inductor of inductance L_1 and L_3 in the series branch and a linear inductor of inductance L_2 in parallel with a nonlinear capacitor $C(V_{jn})$ (j=1 for the first line and 2 for the second line). The conductance g_1 describes the dissipation in the inductor L_1 while g_2 accounts for the dissipation of the inductor L_2 in addition to the loss of the nonlinear capacitor $C(V_{jn})$. The second-neighbors are taken into account through the inductance L_3. The two lines are connected by an intermediary linear capacitor C, as shown in Fig. 3.9.

In this network, the nonlinearity is introduced by a varicap diode for which the

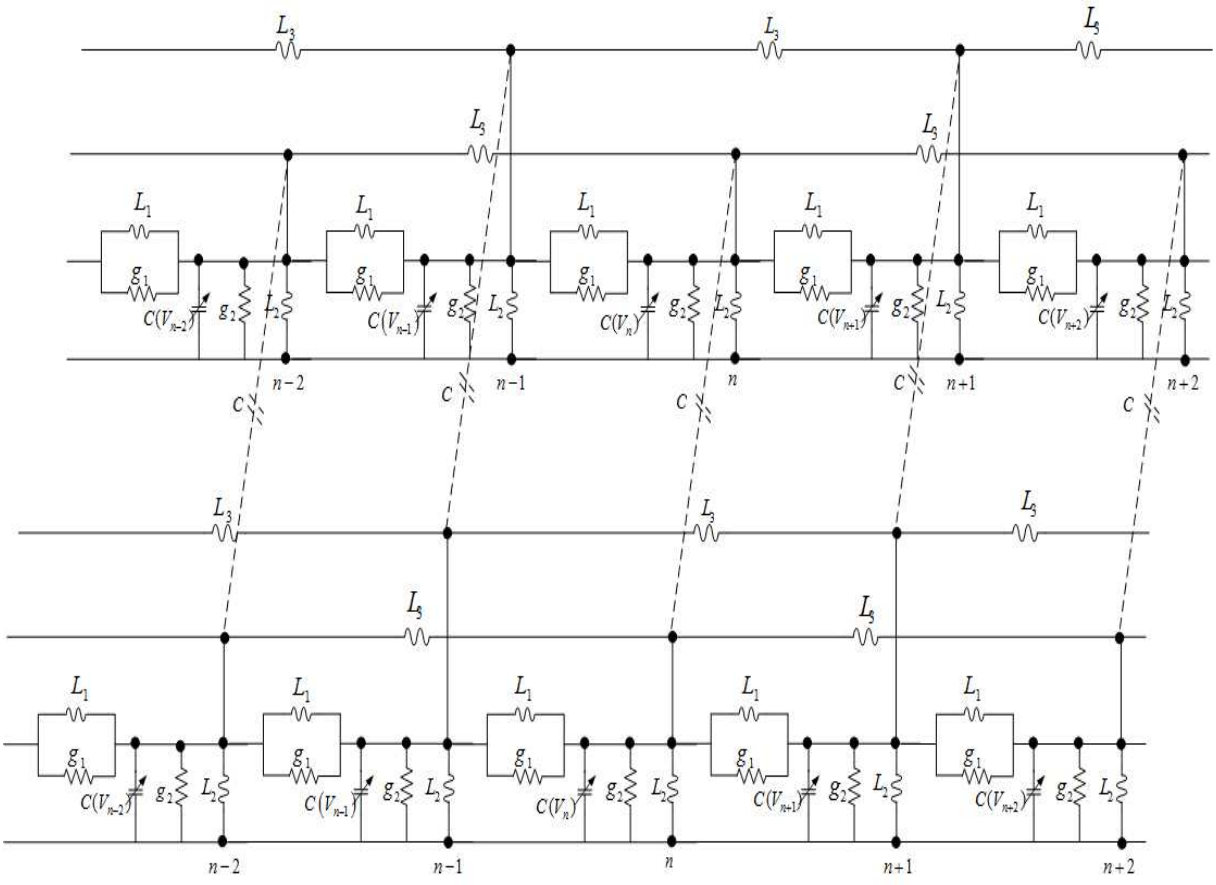

Figure 3.9: *Diagram of nonlinear electrical line*

capacitance varies with the applied voltage V_{jn}. Generally, the electric charge of the varicap diode for the nth cell is given by

$$Q(V_{jn}) = C_0 A \ln(1 + \frac{V_{jn}}{A}) \tag{3.27}$$

where C_0 and A are constant capacitance and voltage at the operating point respectively; the subscript n designates the number of cells in the network. Negative nonlinear resistances are defined with their nonlinear current-voltage characteristics. They are made of operational amplifiers, transistors, or multipliers. The corresponding conductance is given by

$$g_2 = \alpha - \beta V_{jn} \tag{3.28}$$

where α and β are constant and characterize the linear and nonlinear part of the resistance

in parallel.

From the Kirchhoff's laws applied to the circuit of Fig. 3.9, we derive the following system of nonlinear equations for the voltage $V_{jn}(t)$, considering the relation (3.27)

$$\begin{aligned}(A+V_{jn})\frac{d^2V_{jn}}{dt^2}-(\frac{dV_{jn}}{dt})^2 &= \frac{U_0^2}{A}(A+V_{jn})^2(V_{j(n+1)}-2V_{jn}+V_{j(n-1)})\\ &+2\sigma_1\frac{U_0}{A}(A+V_{jn})^2(\frac{d(V_{j(n+1)}-2V_{jn}+V_{j(n-1)})}{dt})\\ &+\frac{\Omega_0^2}{A}(A+V_{jn})^2(V_{j(n+2)}-2V_{jn}+V_{j(n-2)})+\frac{\beta}{C_0A}(A+V_{jn})^2\frac{dV_{jn}^2}{dt}\\ &-2\sigma_2\frac{U_0}{A}(A+V_{jn})^2\frac{dV_{jn}}{dt}-\frac{\omega_0^2}{A}(A+V_{jn})^2V_{jn}\\ &-\frac{a}{A}(A+V_{jn})^2(\frac{d^2V_{jn}}{dt^2}-\frac{d^2V_{(3-j)n}}{dt^2})\end{aligned} \tag{3.29}$$

with $\omega_0^2=\frac{1}{L_2C_0}, U_0^2=\frac{1}{L_1C_0}, a=\frac{C}{C_0}, \Omega_0^2=\frac{1}{L_3C_0}, \frac{g_1}{C_0}=2U_0\sigma_1, \frac{\alpha}{C_0}=2U_0\sigma_2$

The linear properties of the network can be studied by assuming a sinusoidal wave of the form

$$V_{jn}(t)=V_je^{i(kn-\omega t)}+c.c \tag{3.30}$$

where k and ω are respectively the wave number and the angular frequency, and " $c.c$ " stands for a complex conjugated. Using the previous equations (Eq. 3.29 and 3.30) , we obtain the system below:

$$\begin{cases}(-\omega^2(1+a)+4(U_0^2\sin^2\frac{k}{2}+\Omega_0^2\sin^2k)+\omega_0^2)V_1+a\omega^2V_2=0\\ a\omega^2V_1+(-\omega^2(1+a)+4(U_0^2\sin^2\frac{k}{2}+\Omega_0^2\sin^2k)+\omega_0^2)V_2=0\end{cases} \tag{3.31}$$

This system leads to two modes of propagation whose angular frequency ω and wave number k are described by the dispersion relation of a typical band-pass filter. For the slow-mode, we have

$$\omega_1^2=\frac{4U_0^2\sin^2(\frac{k}{2})+\omega_0^2+4\Omega_0^2\sin^2(k)}{1+2a} \tag{3.32}$$

and for the fast-mode, we have

$$\omega_2^2=4U_0^2\sin^2(\frac{k}{2})+\omega_0^2+4\Omega_0^2\sin^2(k) \tag{3.33}$$

The dispersion graph is given below (Fig. 3.10). The second-neighbor coupling can increase the bandwidth of allowed frequencies as shown in Fig.3.10(a) in which a large difference between the cases with and without second-neighbor coupling appears. The later case presents a gap between slow-mode and fast-mode bandwidth while the chosen parameters with second-neighbor coupling shows a crossing domain of slow-mode and fast-mode bandwidth. This cross-over can induce a mixing of frequencies and then a loss of signal during the propagation. An appropriate choice of the **NETL** parameters can suppress the mixing of these bandwidth as presented on Fig.3.10(b) (see also ref. [28])

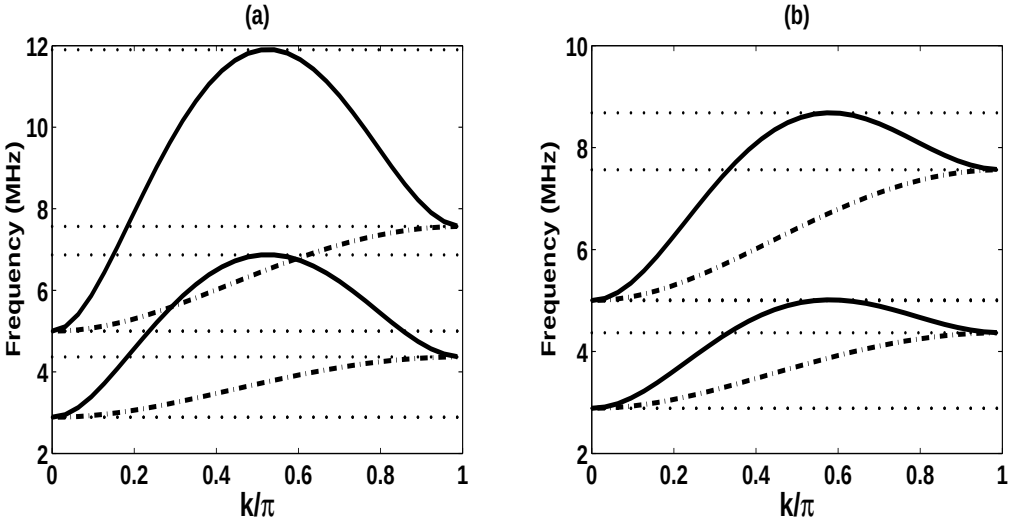

Figure 3.10: *Dispersion graph: (dash dot) slow and fast mode without second-neighbor, (solid line) slow and fast mode with second-neighbor, (dotted) maxima and minima for slow and fast mode, obtained with (a)* $L_2 = L_3 = 0,100mH$*;* $L_1 = 0,310mH$*;*$C_0 = C = 400pF$*, (b)* $L_1 = L_3 = 0,310mH$*;* $L_2 = 0,100mH$*;* $C_0 = C = 400pF$*.*

With these dispersion relations, we can determine the group velocity given by

$$v_{gl} = \frac{\partial \omega_l}{\partial k} = \delta \frac{U_0^2 \sin(k) + 2\Omega_0^2 \sin(2k)}{\omega_l} \tag{3.34}$$

$\delta = \frac{1}{1+2a}$ for the slow-mode and $\delta = 1$ for the fast-mode. $l = 1$ for the slow-mode and 2 for the fast-mode.

This group velocity increases by including second-order couplings as one can see in Fig. 3.11. It is important to note that there is an inversion of the sign of v_{gl}. This negative group velocity occurs on the first brillouin zone $k \in [\arccos(\frac{-U_0^2}{4\Omega_0^2}); \pi]$ when the

condition $U_0 < 2\Omega_0$ is satisfied.

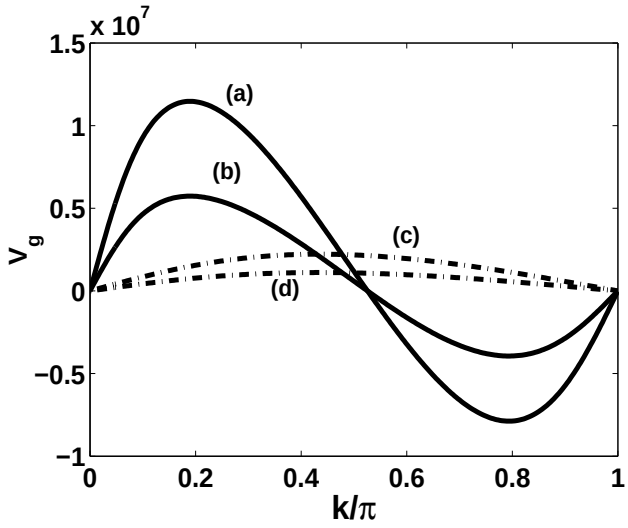

Figure 3.11: *Group velocity obtained with* $L_2 = L_3 = 0,100mH; L_1 = 0,310mH; C_0 = C = 400pF$. *(a)fast-mode with second-neighbor; (b)slow-mode with second-neighbor; (c)fast-mode without second-neighbor; (d)slow-mode without second-neighbor.*

The amplitudes of the signal voltage propagating along the two coupled lines are linearly dependent and satisfy the relation $V_2 = \lambda^l V_1$ with

$$\lambda^l = 1 + \frac{1}{a}(1 - \frac{4U_0^2 \sin^2(\frac{k}{2}) + \omega_0^2 + 4\Omega_0^2 \sin^2(k)}{\omega_l^2}) \tag{3.35}$$

To describe modulated waves in the network, we consider waves with slow temporal variations of the envelope. We look for a solution of Eq. (3.29) in the form

$$V_{jn}(t) = \epsilon\psi_{jn}(T)e^{i\omega t} + \epsilon\psi^*_{jn}(T)e^{-i\omega t} \tag{3.36}$$

where ϵ is a small parameter and $T = \epsilon^2 t$. Inserting this relation into Eq. (3.29) and collecting solutions of order $(\epsilon^n, e^{i\omega t})$ we have:

i) The cofficient ϵ proportional to $e^{i\omega t}$ gives us

$$\begin{aligned}[\omega_0^2 + 2(U_0^2 + \Omega_0^2) - \omega^2(1+a)]\psi_{jn} &= U_0^2(\psi_{j(n+1)} + \psi_{j(n-1)}) + \Omega_0^2(\psi_{j(n+2)} + \psi_{j(n-2)}) \\ &\quad - a\omega^2\psi_{(3-j)n}\end{aligned} \tag{3.37}$$

ii)The cofficient ϵ^2 proportional to $e^{0i\omega t}$ gives us

$$\begin{aligned} 2[\omega_0^2-(1+a)\omega^2]|\psi_{jn}|^2\psi_{jn} &= U_0^2(\psi^*_{j(n+1)}-2\psi^*_{jn}+\psi^*_{j(n-1)})\psi^2_{jn} \\ &+\Omega_0^2(\psi^*_{j(n+2)}-2\psi_{jn}+\psi^*_{j(n-2)})\psi^2_{jn} \\ &+U_0^2(\psi_{j(n+1)}-2\psi_{jn}+\psi_{j(n-1)})|\psi_{jn}|^2 \\ &-a\omega^2(\psi^*_{(3-j)n}\psi^2_n+\psi_{(3-j)n}|\psi_n|^2) \\ &+\Omega_0^2(\psi^*_{j(n+2)}-2\psi_{jn}+\psi^*_{j(n-2)})|\psi_{jn}|^2 \end{aligned} \tag{3.38}$$

iii) By setting $\psi_{jn}=\phi_{jn}e^{i(\frac{\omega_0^2+2(U_0^2+\Omega_0^2)-\omega^2(1+a)}{U_0^2})\tau}$ with $\tau=\frac{U_0^2}{2\omega}T$, the coefficient ϵ^3,proportional to $e^{i\omega t}$ leads to

$$\begin{aligned} i\gamma\phi_{jn}+\Gamma\phi_{(3-j)n} &= i\phi_{jn,\tau}+i\eta\phi_{(3-j)n,\tau}+P_1(\phi_{j(n+1)}-2\phi_{jn}+\phi_{j(n-1)}) \\ &+P_2(\phi_{j(n+2)}-2\phi_{jn}+\phi_{j(n-2)})+Q|\phi_{jn}|^2\phi_{jn} \end{aligned} \tag{3.39}$$

Relation (3.39) is the **CDCGL** equations with second-neighbor corresponding to the two different lines of the network; $P_1=P_{1r}+iP_{1i}$, $P_2=P_{2r}+iP_{2i}$, $Q=Q_r+iQ_i$,$\gamma=\gamma_r+i\gamma_i$, $\Gamma=\Gamma_r+i\Gamma_i$ and η are given in **Appendix B**. Fig. 3.12 represents the variation of some of these coefficients in function of k. The uncoupled form of this equation has been proposed to describe frustrated states in a linear array of vortices [80]. Let us note that the first study of second-order coupling has been done by Efremidis et *al.* through the study of discrete diffraction properties of nonlinear waveguide arrays [81]. Recently, Ndzana et *al.* reported on the derivation of the discrete complex Ginzburg-Landau equation with first and second-neighbor couplings using a nonlinear electrical network [50]. This system possesses a traveling wave solution that can be unstable under linear perturbations.

3.2.2 Analytical study of modulational instability through the coupled cubic complex Ginzburg-Landau equations

In this section, we find the conditions under which a uniform wave train moving along the nonlinear lines will become stable or unstable to a small perturbation. This instability leads to the formation of envelope pulse solitons, plane wave solution of Eq. (3.39). We look for plane wave solutions in the form

$$\phi_{jn}=A_je^{i(\nu n-\varpi\tau)},(j=1,2) \tag{3.40}$$

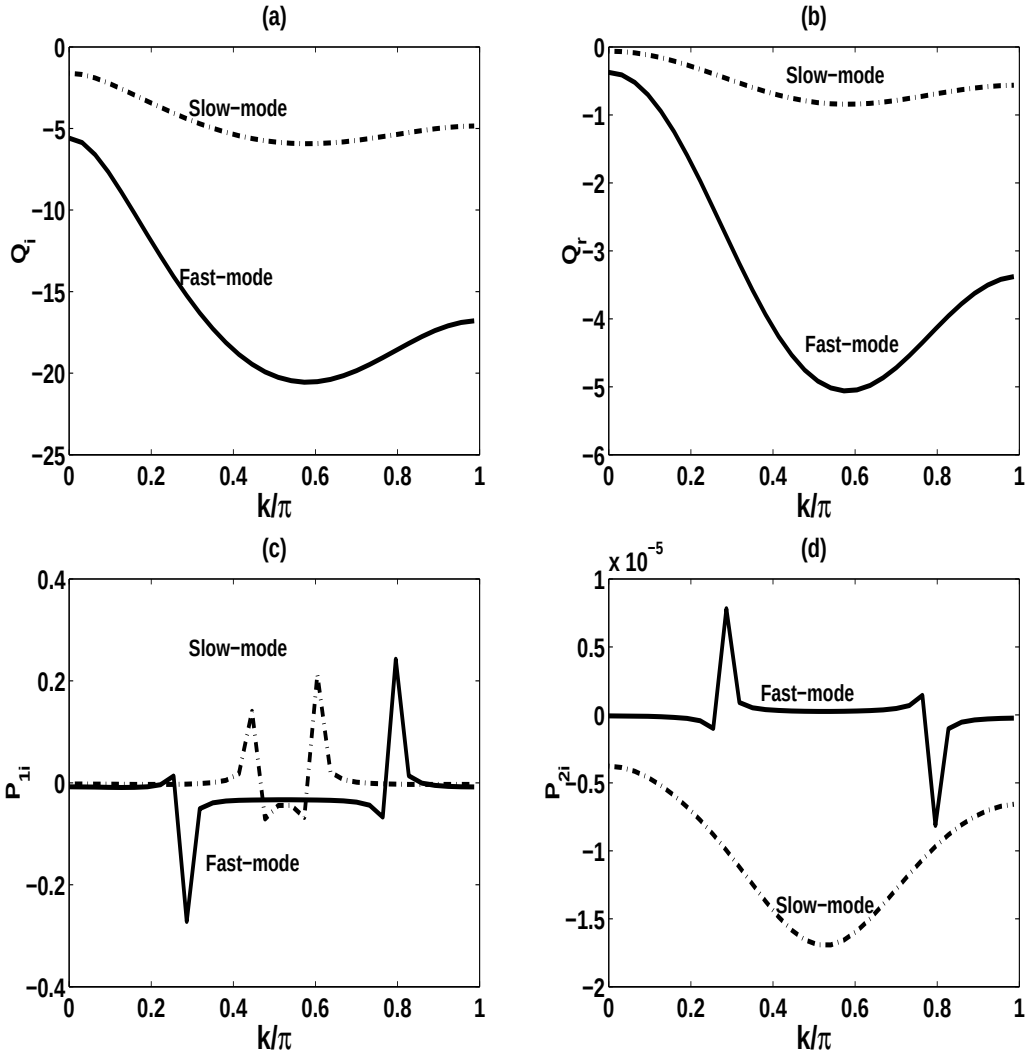

Figure 3.12: *Coefficients of* **CDCGL** *equations as a function of the wave number obtained with* $\sigma_1 = 0,00461$*;* $L_1 = 0.310mH$*;* $L_2 = L_3 = 0.100mH$ $C_0 = 400pF$*;* $\beta = 0,0197V^{-2}$ *and* $\sigma_2 = 0.00015$*. (a) Imaginary part of the nonlinear coefficient; (b) Real part of the nonlinear coefficient; (c) Imaginary part of the dispersion coefficient regarding first-neighbor; (d) Imaginary part of the dispersion coefficient regarding second-neighbor.*

Inserting Eq. (3.40) into Eq. (3.39), we obtain the following expression describing implicitly the characteristics of the continuous-wave solution: the real parts of this relation is

$$\begin{cases} \varpi(A_1 + \eta A_2) = -2(P_{1r}\cos\nu + P_{2r}\cos 2\nu)A_1 - Q_r|A_1|^2A_1 + \Gamma_r A_2 \\ \varpi(\eta A_1 + A_2) = -2(P_{1r}\cos\nu + P_{2r}\cos 2\nu)A_2 - Q_r|A_2|^2A_2 + \Gamma_r A_1 \end{cases} \tag{3.41}$$

and the imaginary parts of this relation is

$$\begin{cases} 2(P_{1i}\cos\nu + P_{2i}\cos 2\nu)A_1 - Q_i|A_1|^2A_1 = \Gamma_i A_2 \\ 2(P_{1i}\cos\nu + P_{2i}\cos 2\nu)A_2 - Q_i|A_2|^2A_2 + \Gamma_i A_1 \end{cases} \tag{3.42}$$

Now, we consider a small perturbation (B_{jn} with $j = 1, 2$)

$$\phi_{jn} = (A_j + B_{jn})e^{i(\nu n - \varpi\tau)} \tag{3.43}$$

B_{jn} is a complex function. Substituting this relation into Eq. (3.39), one obtains a linearized equation for the perturbations. For the first line, we have:

$$\begin{aligned} -i\eta B_{2n,\tau} + B_{2n}(\Gamma - \eta\varpi) &= iB_{1n,\tau} + P_1[(B_{1(n+1)} - 2B_{1n} + B_{1(n-1)})\cos(\nu) \\ &+ i(B_{1(n+1)} - B_{1(n-1)})\sin(\nu)] + P_2[(B_{1(n+2)} - 2B_{1n} \\ &+ B_{1(n-2)})\cos(2\nu) + i(B_{1(n+2)} - B_{1(n-2)})\sin(2\nu)] \\ &+ B_{1n}(\Gamma - \eta\varpi)\frac{A_2}{A_1} + Q|A_1|^2(B_{1n} + B_{1n}^*) \end{aligned} \tag{3.44}$$

and for the second line, we have:

$$\begin{aligned} -i\eta B_{1n,\tau} + B_{1n}(\Gamma - \eta\varpi) &= iB_{2n,\tau} + P_1[(B_{2(n+1)} - 2B_{2n} + B_{2(n-1)})\cos(\nu) \\ &+ i(B_{2(n+1)} - B_{2(n-1)})\sin(\nu)] + P_2[(B_{2(n+2)} - 2B_{2n} \\ &+ B_{2(n-2)})\cos(2\nu) + i(B_{2(n+2)} - B_{2(n-2)})\sin(2\nu)] \\ &+ B_{2n}(\Gamma - \eta\varpi)\frac{A_2}{A_1} + Q|A_1|^2(B_{2n} + B_{2n}^*) \end{aligned} \tag{3.45}$$

We take a general solution in the form

$$B_{nj} = b_j e^{i(Kn + \Omega\tau)} + c_j^* e^{-i(Kn + \Omega^*\tau)} \tag{3.46}$$

where K and Ω are an arbitrary real wave number of the perturbation and the corresponding propagation frequency respectively, which is complex in the general case, b_j and c_j being perturbation's amplitudes. Inserting Eq. (3.46) into Eq. (3.44) and (3.45), we arrive at a set of linear homogeneous equations for b_j and c_j. This set of homogeneous equations which can be written in matrix form as

$$M \times (b_1, c_1, b_2, c_2)^t = 0 \tag{3.47}$$

where M is a 4×4 matrix whose different elements are given in **Appendix B**. We solve the condition of the existence of nontrivial solutions using a Matlab code. Figures 3.13 represents threshold's amplitude on the (K, ν) plane.

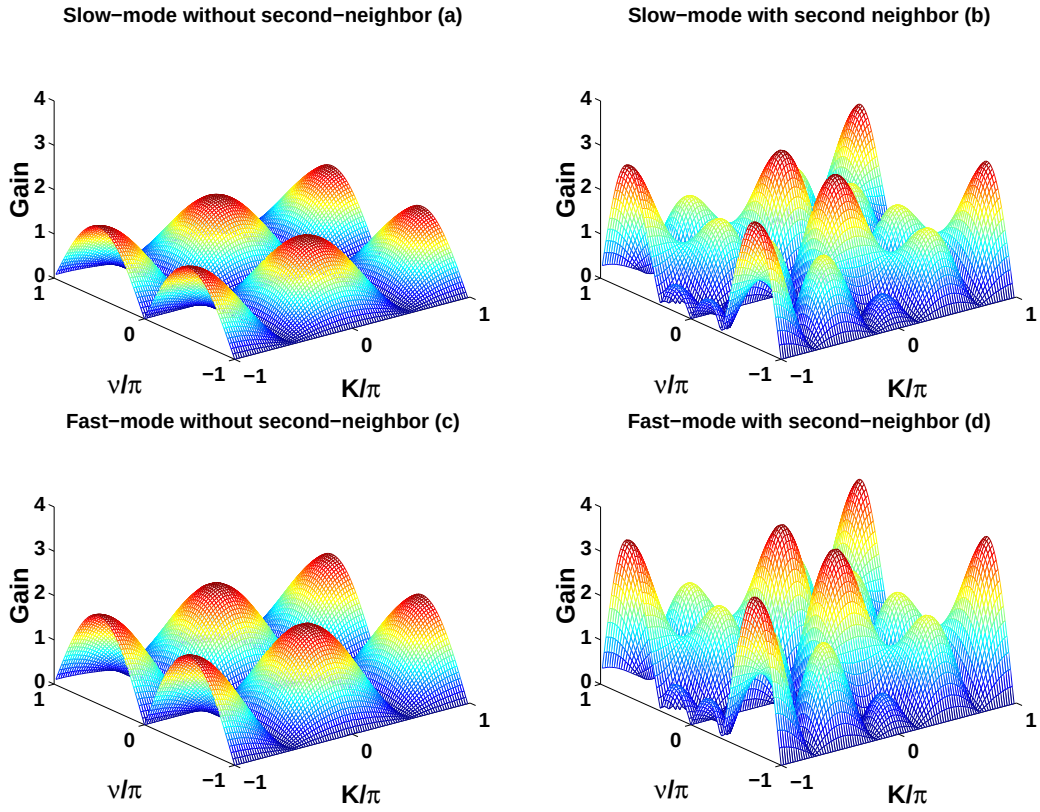

Figure 3.13: *Threshold's amplitude on the* (K, ν) *plane.*

The Fig. 3.13 presents regions of **MI** in the (K, ν) plane for the slow-mode [Fig. 5(a) and Fig. 3.13(d)] and fast-mode [Fig. 3.13(c) and Fig. 3.13(d)] with [Fig. 3.13(b) and Fig. 3.13(d)] and without [Fig. 3.13(a) and Fig. 3.13(c)] second-neighbor. As remark, we note that there is a slight increase of the gain due to the second-neighbor coupling. Moreover, there is a generation of new spot of maxima of gain in the same (K, ν) region comparatively to the case of only first-neighbor.

3.2.3 Numerical experiments

We present in this section the numerical experiments on the propagation of slowly modulated waves in the network, this to check the analytical calculations presented in the previous sections. The numerical experiments are carried out on the equation (3.29)

describing the propagation of waves in the **NETL** of figure 3.9 . The parameters of the network are chosen to be $L_1 = 0.310mH$; $L_2 = L_3 = 0.100mH$ $C_0 = 400pF$; $\beta = 0,0197V^{-2}$. The wave introduced has the form

$$V_{n=0}(t) = V_0[1 + m\cos(2\pi f_m t)][1 + \tanh(\frac{t - T_0}{L_e})]\cos(2\pi f t) \tag{3.48}$$

where V_0 is the amplitude of the wave, L_e indicates a parameter making it possible to control the slope of the excitation, T_0 is a real which shifts the solution of the origin of times, m stands for the modulation rate and f_m is the frequency of modulation. We take the carrier frequency $f = 3121KHz$ for slow-mode and $f = 6100KHz$ for the fast-mode; the initial amplitude is $V_0 = 1.5V$, $L_e = 4\mu s$, $T_0 = 20$, $m = 5\%$ and $f_m = 18KHz$. Compared to dissipations, we take for each line $\sigma_1 = 0.00461$ and $\sigma_2 = 0.0$. The fourth-order Runge-Kutta scheme is used with normalized integration time step $\Delta t = 5 \times 10^{-3}$. Moreover, the number of cells is chosen so that we do not encounter the wave reflection at the end of the lines.

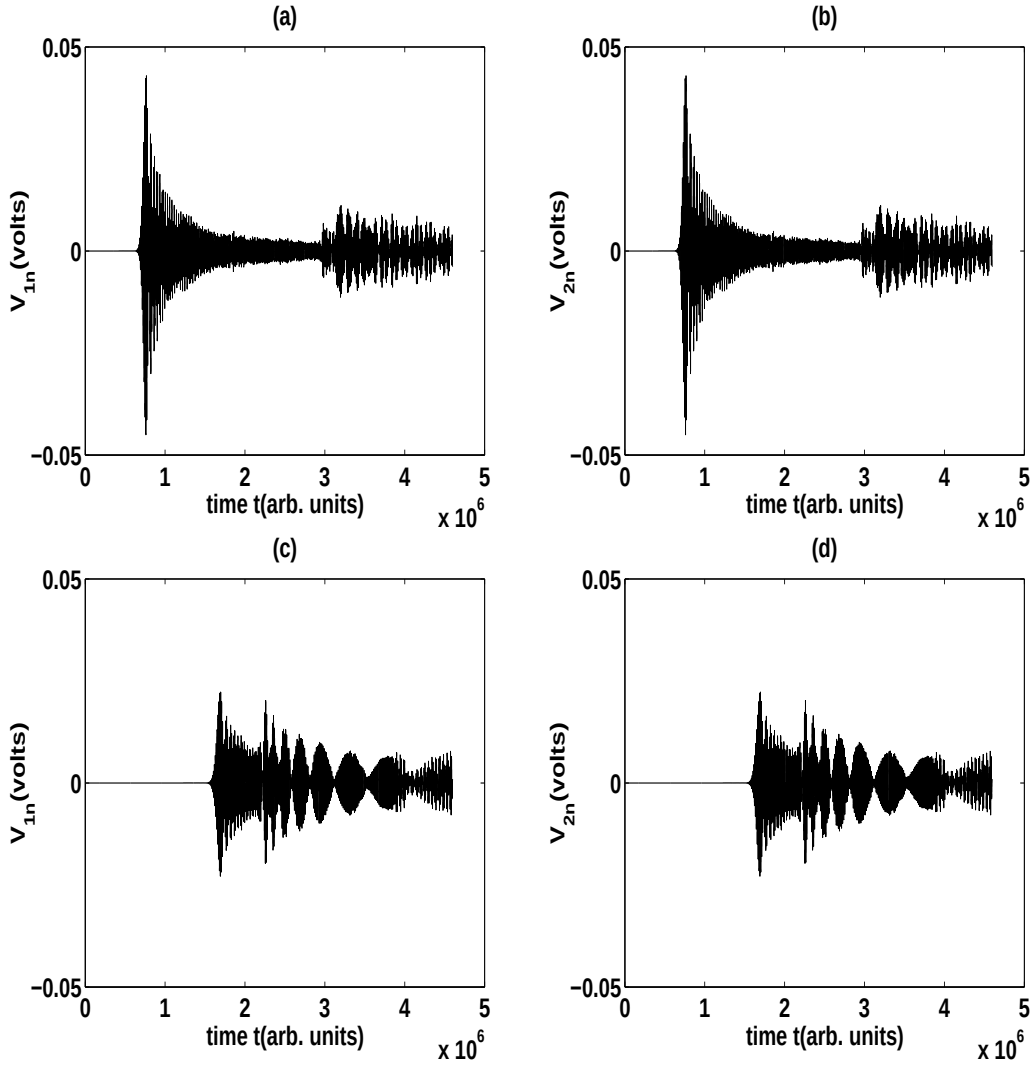

Figure 3.14: *Propagation of waves through the network for the slow-mode in the absence of second-neighbor. (a) and (c) For line 1 respectively in the cells 400 and 500; (b) and (d) For line 2 respectively in the cells 400 and 500. The parameters of the network are:* $L_1 = 0.310mH$*;* $L_2 = 0.100mH$ $C_0 = 400pF$*;* $\beta = 0,0197V^{-2}$.

Figures 3.14, 3.15, 3.16 and 3.17 show us examples of the **MI** exhibited by the network with the two modes of propagation. Signal voltage (in Volts) as a function of time at different cells (400 and 500). We observe a synchronization between the waves through the two lines in the same cells. As time goes on, the wave exhibits a modulation of its amplitude, which lead to the formation of wave packets. The wave introduced at cell n = 0 with a small modulation exhibits some nonlinear distortions of the envelope when time grows. It is a typical example of **MI** phenomenon. Figure 3.14 presents the behavior of waves through the line when the propagation mode is the slow-mode in

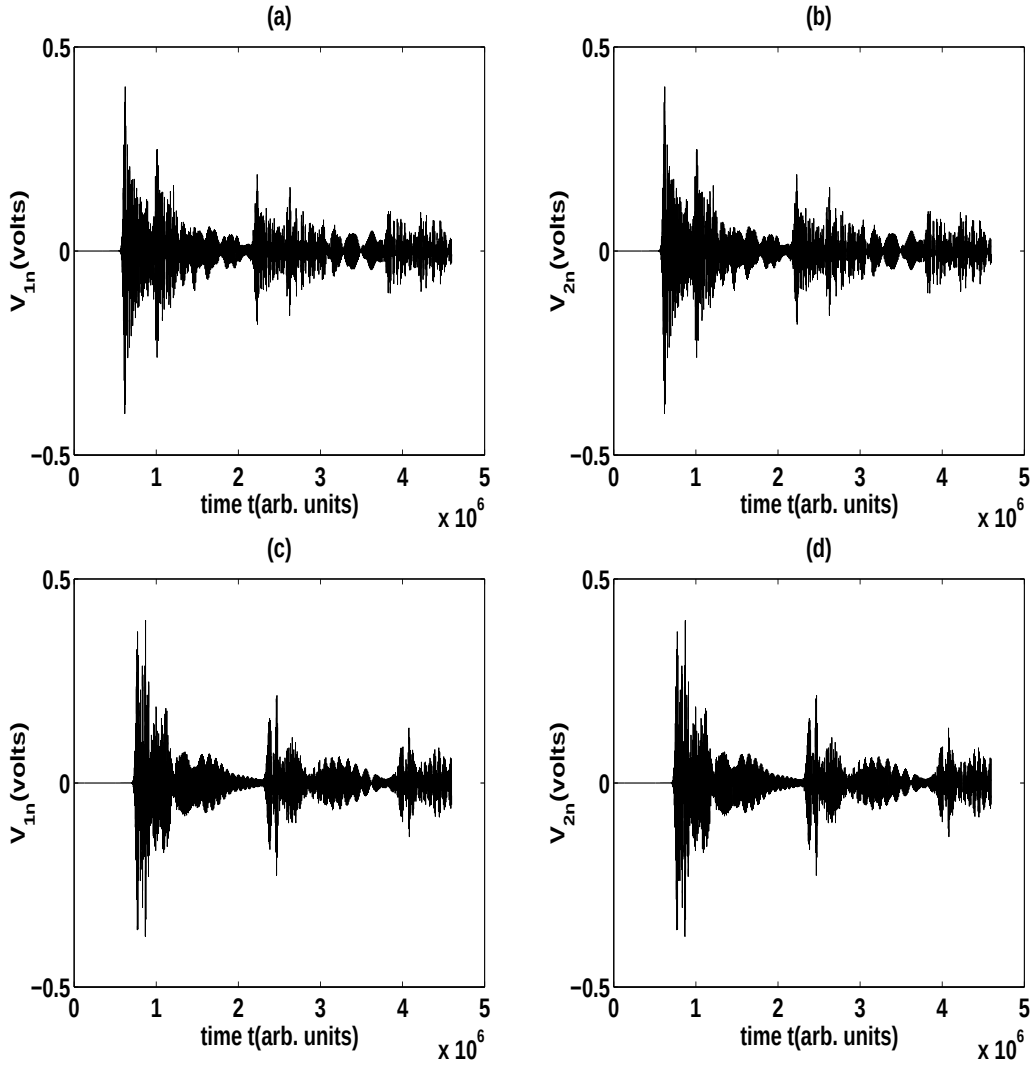

Figure 3.15: *Propagation of waves through the network for the slow-mode in presence of second-neighbor. (a) and (c) For line 1 respectively in the cells 400 and 500; (b) and (d) For line 2 respectively in the cells 400 and 500. The parameters of the network are:* $L_1 = 0.310mH$*;* $L_2 = L_3 = 0.100mH$ $C_0 = 400pF$*;* $\beta = 0,0197V^{-2}$.

the absence of second-neighbor while Figure 3.15 presents the behavior of waves through the line when the propagation mode is the slow-mode in presence of second-neighbor. Figure 3.16 presents the behavior of waves through the line when the propagation mode is the fast-mode in the absence of second-neighbor and Figure 3.17 presents the behavior of waves through the line when the propagation mode is the fast-mode in presence of second-neighbor. Figures [3.14, 3.15, 3.16, 3.17](a) and [3.14, 3.15, 3.16, 3.17](b) account for cell 400, Figures [3.14, 3.15, 3.16, 3.17](c) and [3.14, 3.15, 3.16, 3.17](d) account for cell 400. On the Figures 3.15 and 3.17, we see the contribution of the second-neighbor

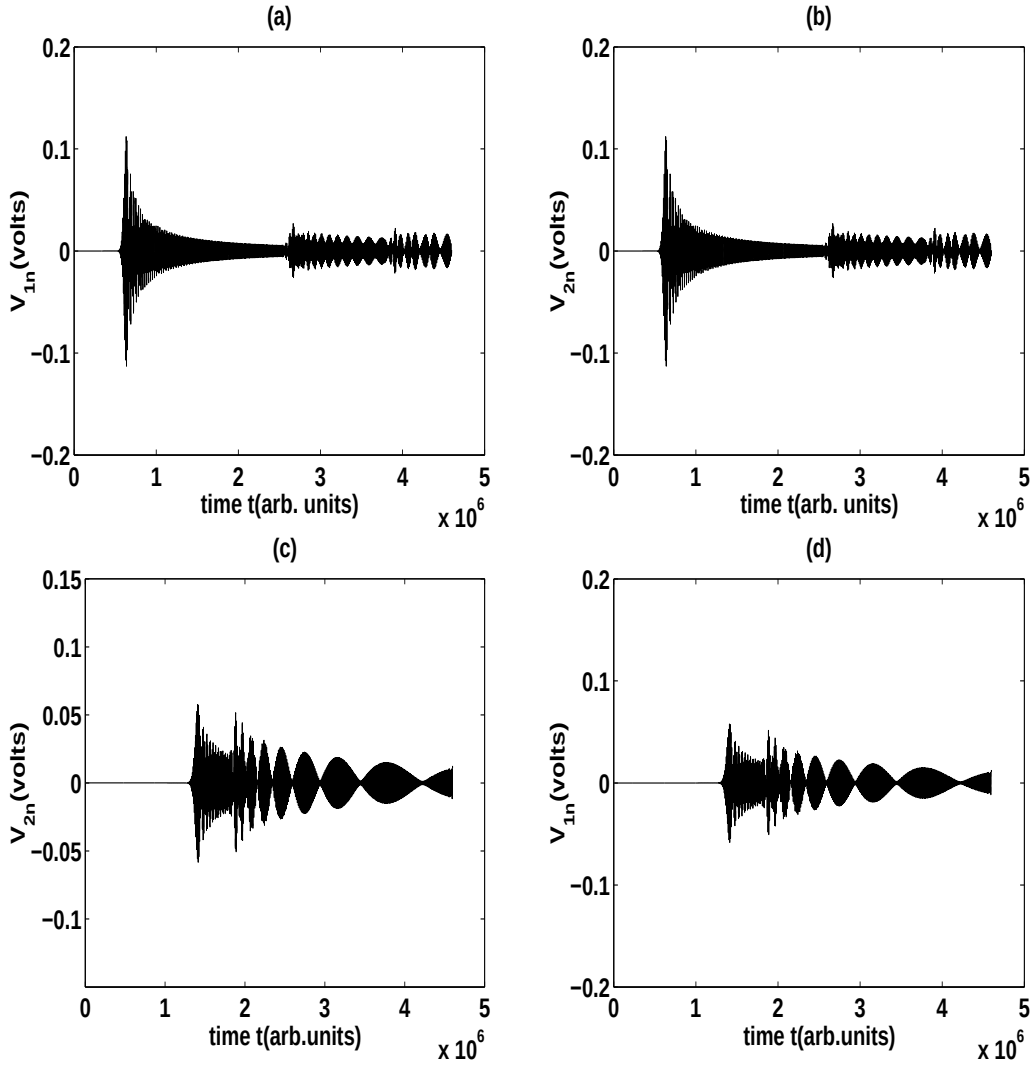

Figure 3.16: *Propagation of waves through the network for the fast-mode in the absence of second-neighbor. (a) and (c) For line 1 respectively in the cells 400 and 500; (b) and (d) For line 2 respectively in the cells 400 and 500. The parameters of the network are:* $L_1 = 0.310mH$*;* $L_2 = 0.100mH$ $C_0 = 400pF$*;* $\beta = 0,0197V^{-2}$.

and we can observe that the amplitude of the voltage has increased; we can note that this contribution can be used to control the magnitude of waves due to the competitive effect between first and second-neighbor couplings.

On Figure 3.18, we confirm the synchronization between the waves through the two lines. This is obtained for the same cell (500) from datas collected during the evolution of the signal in the last figures case. For the slow-mode, the slope is negative while for the fast-mode, the slope is positive as predicted by Eq.(3.35).

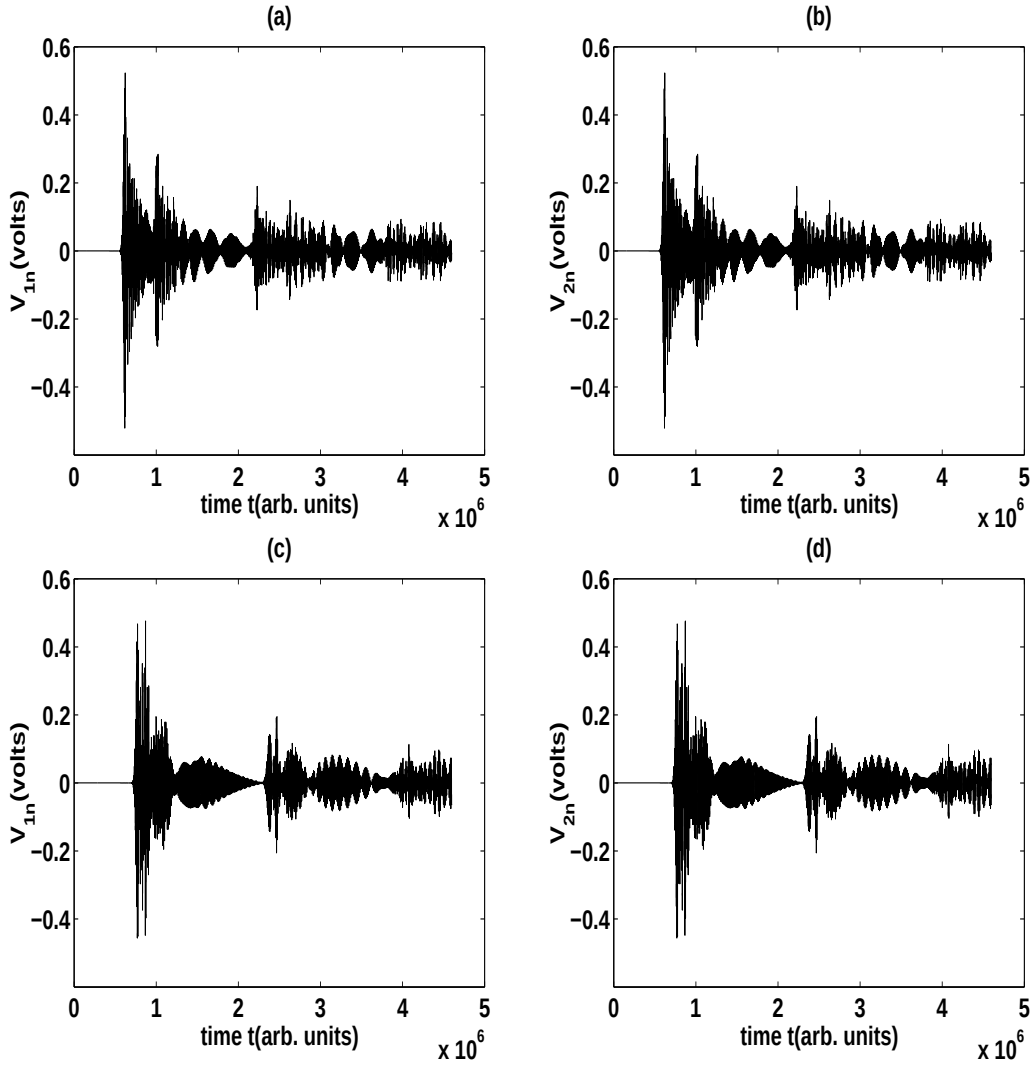

Figure 3.17: *Propagation of waves through the network for the fast-mode in presence of second-neighbor. (a) and (c) For line 1 respectively in the cells 400 and 500; (b) and (d) For line 2 respectively in the cells 400 and 500. The parameters of the network are:* $L_1 = 0.310mH$; $L_2 = L_3 = 0.100mH$ $C_0 = 400pF$; $\beta = 0,0197V^{-2}$.

3.2.4 Concluding remarks on effects of second-neighbor inductive coupling

In this part, we have studied analytically and examined the effect of modulation rate in a coupled **NETL**. Using the reductive perturbation method, we have shown that the dynamics of nonlinear waves in a coupled discrete nonlinear electrical transmission line with negative nonlinear resistance and with the contribution of the second-neighbor can

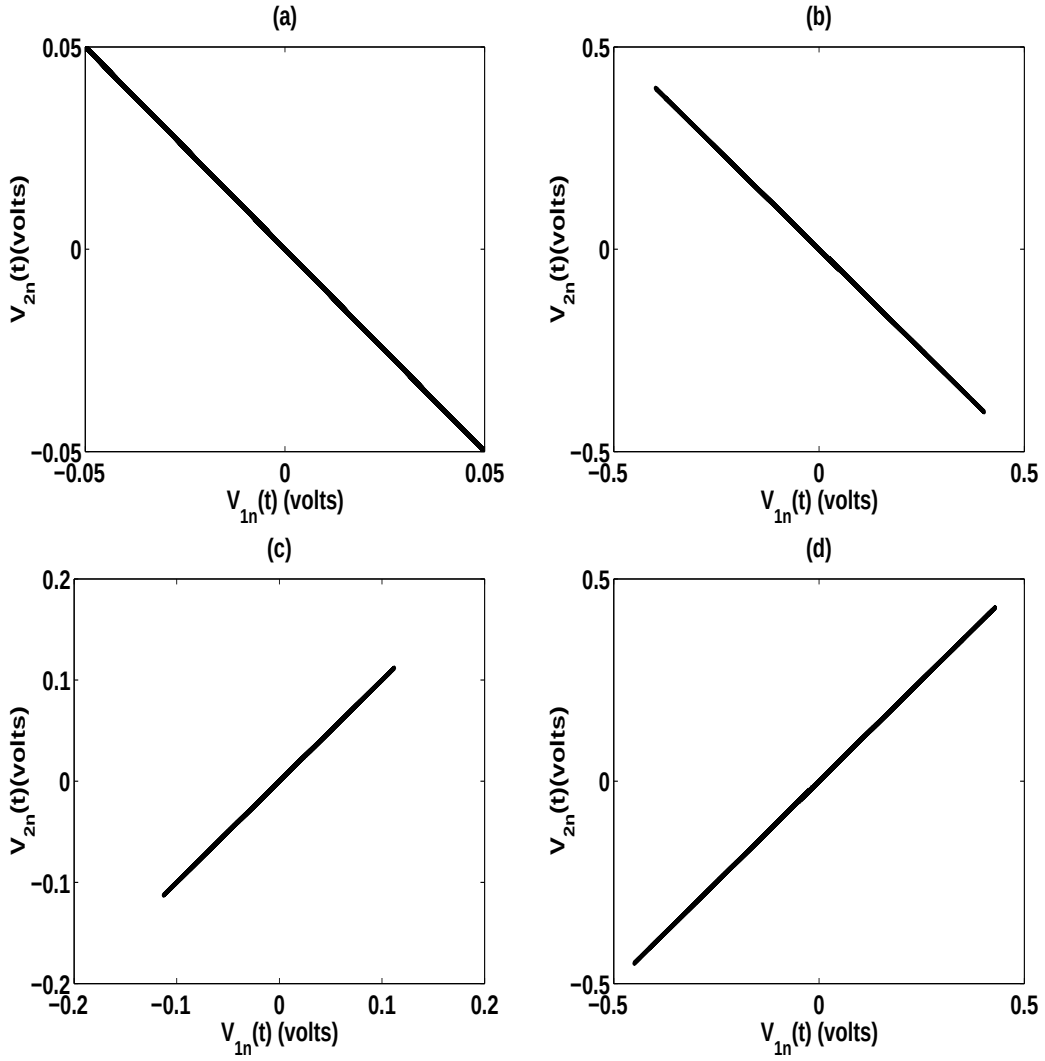

Figure 3.18: *Signal voltage at a given cell (500) in line 1 as a function of the signal voltage of the same cell (500) in line 2, (a) slow-mode without second-neighbor, (b) slow-mode with second-neighbor, (c) fast-mode without second-neighbor and (d) fast-mode with second-neighbor with the initial conditions described in figures (3.14, 3.15) and (3.16, 3.17) for the slow- and fast-mode respectively.*

be described by a set of coupled discrete complex Ginzburg-Landau equations. With some parameters, we were able to cancel the gap existing between the fast- and slow-mode by using the contribution of the second-neighbor. By employing the standard linear stability analysis, the growth rate of the instability is derived as a function of the wave numbers and system parameters. Therefore, we have analytically predicted **MI** domains by solving the fourth-order polynomial obtained from the condition of nontrivial solutions. The regions of modulational instability have been then obtained and the influence of second-neighbor

occurring via inductors in a nonlinear transmission line have been studied. As result, we found that the second-neighbor couplings add new maxima of gain; increase the group velocity, and the magnitude of the wave. Hence, the network becomes more stable to small external perturbations. The analytical studies are completed by the numerical experiments performed in the network and this lead us to show that the second-neighbor couplings can be used to control the magnitude of waves.

3.3 Suppression of modulated waves mixing in coupled nonlinear LC transmission lines

The dynamics of modulated waves in a coupled nonlinear LC transmission line is investigated. In order to solve the crucial problem of the mixing of waves of different modes and then exploit the features of the modulational instability of each of two modes through the network, we propose a different coupling type.

3.3.1 Model and equations of dynamics

We consider here the basic model usually used. This consists of a nonlinear network with two coupled nonlinear LC transmission lines. Without loss of generality, we only focus our attention in this work on two identical lines. Each line contains a finite number of cells. An elementary cell consists of two elements: a linear inductor of inductance L_1 in the series branch and a nonlinear capacitor of capacitance $C(V_{jn})$ in the shunt branch. V_{jn} represents the voltage of the line j and at the cell n. The subscript j can take the values 1 and 2. For such coupled lines, experiments and analytical studies showed that whenever the network is excited by an electrical wave, two modes of propagation (slow- and fast-modes) are generated in each line. They unavoidably enter into play with the wave-coupling behaviour. As mentioned in the previous section, Yémélé and Kofané [28] placed a linear inductor of inductance L_2 in the shunt branch and then suppress the modes mixing. We propose to use only the half of the total number of additive linear inductors. For this purpose, we modify the above described coupled **NETLs** by adding the self L_2 in parallel with the linear capacitor C which serves as the coupling element of the two lines, as shown in figure 3.19.

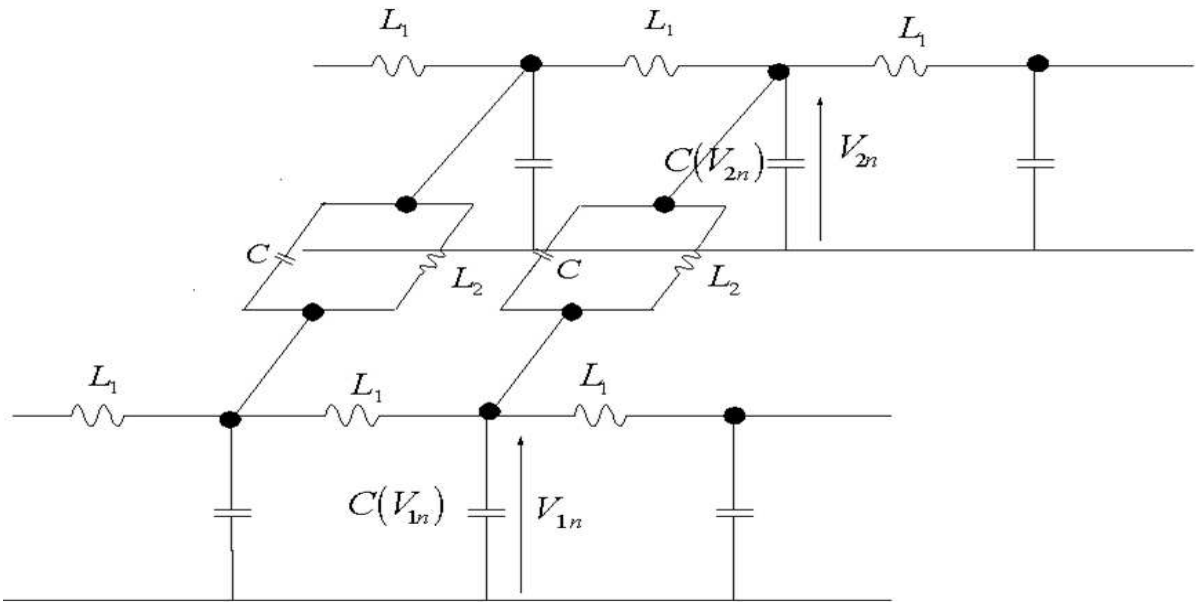

Figure 3.19: *Diagram of the coupled nonlinear electrical lines. Three unit cells are reproduced for each line.*

In the line, the nonlinearity is introduced by a varicap diode which admits that the capacitance varies with the applied voltage. The voltage dependance relation is assumed to have a polynomial form given by

$$Q(V_{jn}) = C_0(V_{jn} - \alpha V_{jn}^2 + \beta V_{jn}^3) \tag{3.49}$$

where C_0, α, β are constants. In the present work, we set $\alpha = 0.21V^{-1}$ and $\beta = 0.0197V^{-2}$.

The properties of the network can be studied by using a solution of the form

$$V_{jn}(t) = \epsilon A_j(x,t)e^{i\theta} + \epsilon^2[\Psi_j(x,t) + B_j(x,t)e^{2i\theta}] + c.c. \tag{3.50}$$

where $\theta = kn - \omega t$ is the phase and $c.c.$ stands for the complex conjugate of the preceding expression; k and ω are respectively the wave number and the angular frequency; ϵ is a small parameter.

From the Kirchhoff's laws applied to the circuit of figure 3.19, and considering the relation (3.50), we derive the following system of nonlinear equations for the voltage $V_{jn}(t)$

$$\begin{aligned}(V_{jn} - \alpha V_{jn}^2 + \beta V_{jn}^3)_{,tt} &= U_0^2(V_{j(n+1)} - 2V_{jn} + V_{j(n-1)}) \\ &\quad - a(V_{jn} - V_{(3-j)n})_{,tt} - \omega_0^2(V_{jn} - V_{(3-j)n}) \end{aligned} \tag{3.51}$$

with $U_0^2 = \frac{1}{L_1 C_0}$, $\omega_0^2 = \frac{1}{L_2 C_0}$ and $a = \frac{C}{C_0}$. For the different derivatives, we will set $T = \epsilon^2 t$ and $x = \epsilon(n - v_g t)$, where v_g is the group velocity.

3.3.2 Amplitude equations

By inserting Eq.(3.50) into Eq.(3.51), one obtains the following order equations.
i) The coefficient ϵ, proportional to $e^{i\theta}$ gives us the following system:

$$\begin{cases} (-\omega^2 - a\omega^2 + 4U_0^2 \sin^2 \frac{k}{2} + \omega_0^2)A_1 + (a\omega^2 - \omega_0^2)A_2 = 0 \\ (a\omega^2 - \omega_0^2)A_1 + (-\omega^2 - a\omega^2 + 4U_0^2 \sin^2 \frac{k}{2} + \omega_0^2)A_2 = 0 \end{cases} \tag{3.52}$$

This system leads to two modes of propagation whose angular frequency ω and wave number k are described by the dispersion relation of a typical band-pass filter for only the second-mode. The two modes are given by the relation

$$\omega_l^2 = \Gamma_l[4U_0^2 \sin^2(\frac{k}{2}) + 2\omega_0^2(l-1)] \tag{3.53}$$

where $\Gamma_l = \frac{1}{1+2a(l-1)}$, with $l = 1$ for the fast-mode, and $l = 2$ for the slow-mode. From now on, we shall use the letter l on subscript as well as on superscript to designate the fast- and slow-modes. The dispersion graph is given below on the figure 3.20.

On the figure 3.20(a), there is an overlap of fast-mode and slow-mode bandwidths. This superposition acts in favor of a mixing of frequencies during the propagation. An appropriate choice of the coupled **NETLs** parameters avoids the overlapping of these bandwidths. To clearly differentiate them, it suffices to set $L_1 = 2L_2(1 + 2a)$. Hence, the choice of L_1, C_0, and a totally determines the system of our interest. So, by using the following values ($L_1 = 0.4$ mH; $C_0 = 400$ pF; $a = 0.5$), we successfully separate the bandwidth of the fast-mode from the bandwidth of the slow-mode (see figure 3.21).

It is important to observe that the present model always provides an aggregate bandwidth greater than the one obtained from the model proposed in reference [28]. While the low frequencies are prohibited for the slow-mode in the network when working in the regime of interest, the fast-mode always admits very low frequencies as shown in figure

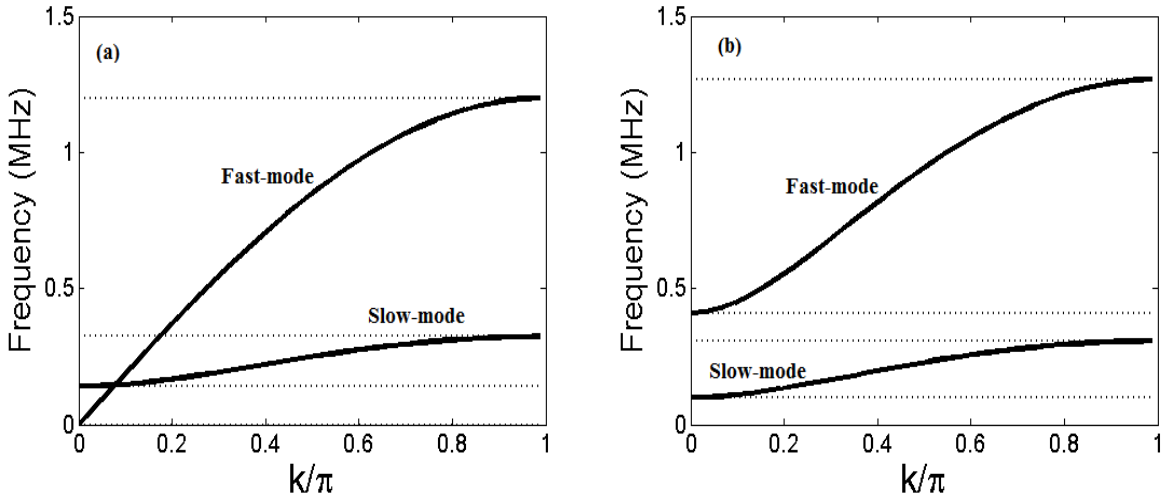

Figure 3.20: *Dispersion graph obtained with* $L_1 = 0.220\ mH$; $L_2 = 0.470\ mH$; $C_0 = 320\ pF$; $C = 2.56\ \mu F$. *(a) present model ; (b) model 2 in [28].*

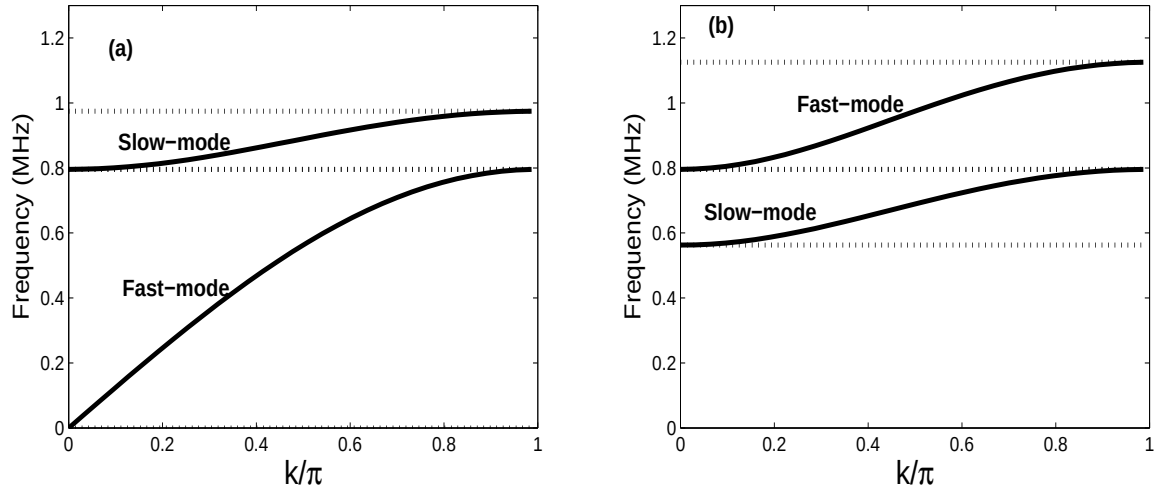

Figure 3.21: *Dispersion graph obtained with* $L_1 = 0.4\ mH$; $C_0 = 400\ pF$; $a = 0.5$. *(a) present model ; (b) model 2 in [28].*

3.21(a).

With this dispersion relation, we determine the group velocity given by

$$v_{gl} = \frac{\partial \omega_l}{\partial k} = \Gamma_l \frac{U_0^2 \sin(k)}{\omega_l} \tag{3.54}$$

On figure 3.22, we realize that the sidelining of very low frequencies signifies the loss of highest group velocities. This figure is reproduced for the same parameters as in figure

3.21.

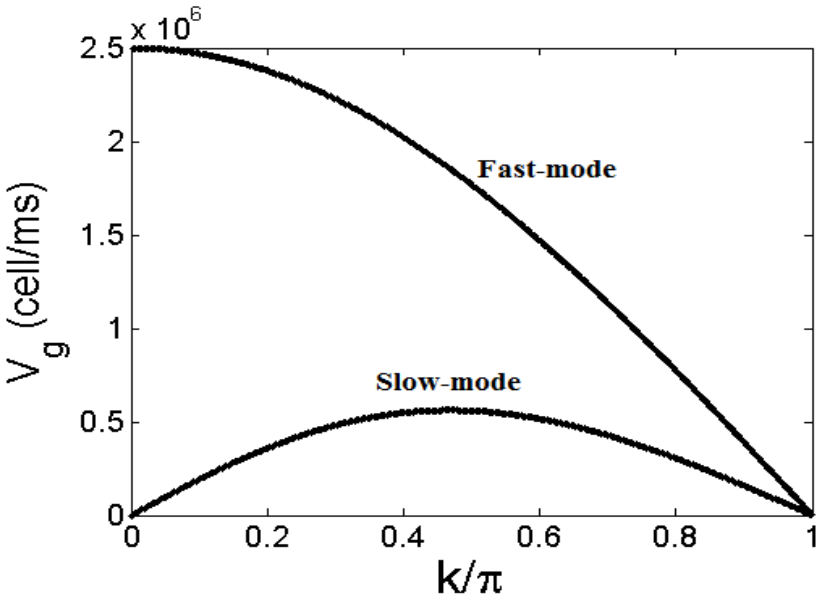

Figure 3.22: *Group velocity of the two modes obtained for the same parameters as in figure 3.21.*

The next order equation provides a relationship between the signal propagating through the two lines.

ii) The coefficient ϵ^2, proportional to $e^{i\theta}$ gives

$$A_2 = \big(1 + \frac{1}{a}(1 - \frac{U_0^2 \sin k}{\omega_l v_{gl}})\big) A_1 \tag{3.55}$$

This relation also reads as $A_2 = \lambda^l A_1$ where $\lambda^l = 1 + \frac{1}{a}(1 - 1/\Gamma_l)$ takes the value 1 for the fast-mode and -1 for the slow-mode. The equality of the absolute values of signal voltages is due to fact that we set identical linear and nonlinear components to the two lines, otherwise $|\lambda|$ will differ from 1. We might then expect to have two equivalent NLS equations.

iii) The coefficient ϵ^2, proportional to $e^{2i\theta}$ gives

$$B_j^{(l)} = \frac{\alpha \omega_l^2}{\omega_l^2 - U_0^2 \sin^2(k)} A_1^2 \tag{3.56}$$

iv) The coefficient ϵ^4, proportional to e^0 leads to

$$\Psi_j^{(l)}(x,t) = \frac{2\alpha v_{g1}^2}{v_{g1}^2 - U_0^2} |A_j|^2 \tag{3.57}$$

This equation will help us only for ω_1 when we will determine the coefficient of nonlinearity.

v) The coefficient ϵ^3, proportional to $e^{i\theta}$ leads to Eq.(3.58); this is obtained by using the Eq.(3.56) and Eq.(3.57).

$$iA^{(l)}_{,T} + P^{(l)}A^{(l)}_{,xx} + Q^{(l)}A^{(l)}|A^{(l)}|^2 = 0 \qquad (l = 1, 2) \tag{3.58}$$

The Eq.(3.58) is the **CNLS** equations describing the propagation through the network. In fact, the set of equation is written as uncounpled equations. This has been predicted since the relation (3.55) was established. Only the modes affect and differentiate the parameters. $P^{(l)}$ and $Q^{(l)}$ are respectively the dispersion and nonlinear coefficients given by the following systems:

$$\begin{cases} P^{(l)} = \frac{1}{2\omega_l(1+a-\lambda^l a)}[U_0^2\cos k - v_{gl}^2(1+a-\lambda^l a)] \\ Q^{(l)} = \frac{1}{2\omega_l(1+a-\lambda^l a)}\left[3\beta\omega_l^2 - \frac{4\alpha^2 v_{gl}^2\omega_l^2}{v_{gl}^2-U_0^2} - \frac{2\alpha^2\omega_l^4}{\omega_j^2-U_0^2\sin^2 k}\right] \end{cases} \tag{3.59}$$

$P^{(l)}$ measures the wave dispersion and $Q^{(l)}$ determines how the wave frequency is modulated in amplitude. More precisely, these coefficients are as follows.

For the fast-mode, we have:

$$\begin{cases} P^{(1)} = -\frac{\omega_1}{8} \\ Q^{(1)} = \frac{\alpha^2}{\omega_1}\left[(\eta-2)\omega_1^2 + 4U_0^2\right] \end{cases} \tag{3.60}$$

and for the slow-mode, we have:

$$\begin{cases} P^{(2)} = -\frac{1}{8\omega_2^3}\left[\omega_2^4 - 2\Gamma^2\omega_0^2(4U_0^2 + 2\omega_0^2)\right] \\ Q^{(2)} = \eta\Gamma\alpha^2\omega_2\frac{\omega_2^4 - 4\Gamma\left(\omega_0^2+\frac{U_0^2}{\eta}\right)\omega_2^2 + 4\Gamma^2\omega_0^2\left(\omega_0^2+2U_0^2\right)}{\omega_2^4 - 4\Gamma\omega_0^2\omega_2^2 + 4\Gamma^2\omega_0^2\left(\omega_0^2+2U_0^2\right)} \end{cases} \tag{3.61}$$

with $\eta = \frac{3\beta}{2\alpha^2}$.

3.3.3 Modulational instability

Up to date, the attention paid to this phenomenon still captures a lot of research works. A clear idea of this interest is given by the important number of reports found in the literature ([82–95] to cite a few).

3.3.3.1 Analytical study

In this section, we search the condition under which a uniform wave train moving along the nonlinear lines will become stable or unstable to a small perturbation. Under the frame of this instability, plane wave solution of Eq.(3.58) leads to the formation of envelope pulse solitons. For the sake of clarity, we report in the **Appendix C** the well-known details of the Benjamin-Feir instability. It then comes out that, in one hand, if $Q^{(l)}/P^{(l)} < 0$ i.e. $P^{(l)}Q^{(l)} < 0$, then $(\nu - 2P^{(l)}K\delta)^2$ is positive and plane wave solution of **NLS** equation is stable. On the other hand, if $P^{(l)}Q^{(l)} > 0$, then $(\nu - 2P^{(l)}K\delta)^2$ could be negative under certain conditions and, consequently plane wave solution of **NLS** equation is unstable; hence, it appears **MI** phenomenon. In this domain, we have (see **Appendix C**):

$$\nu = 2P^{(l)}K\delta \pm i|P^{(l)}\delta|\sqrt{\frac{2Q^{(l)}}{P^{(l)}}\Phi_{j0}^2 - \delta^2} \tag{3.62}$$

It is expected that such an instability induces the formation of small wave packets or envelope pulse solitons train, solution of the **NLS** equation (3.58). Their explicit expression are known to be on the form [96]:

$$V_{11}(x,\tau) = V_0 sech\big[\frac{1}{L_s}(x - v_e\tau)\big] exp\big[i\frac{v_e}{2P}(x - v_p\tau)\big] \tag{3.63}$$

where $L_s = \frac{1}{V_0}\sqrt{\frac{2P}{Q}}$ is the width of the soliton while v_e and v_p are respectively the envelope and the carrier speed.

By using the inequalities described above, the domains of MI are determined for each mode.

- **Domain of MI for the fast-mode**

Unequivocally for this mode, the electrical network is modulationally unstable when the carrier frequency ω belongs to the domain $[\omega_i; 2U_0]$ with $\omega_i = \frac{2U_0}{\sqrt{2-\eta}}$ and $\eta < 2$.

- **Domain of MI for the slow-mode**

In this case, the expressions of $P^{(2)}$ and $Q^{(2)}$ are more complicated and therefore render the determination of MI domains not obvious. These domains depend on many terms among which :

$\Delta_d = 4\Gamma^2\omega_0^2\big(1-\delta\big)$, $\Delta_n = 4\Gamma^2\omega_0^2\big(\delta_\eta^2 - \delta\big)$, $\omega_\pm^2 = 2\Gamma\omega_0^2\delta_\eta \pm \sqrt{\Delta_n}$, $\omega_a^2 = 2\Gamma\omega_0^2\delta_\eta$, $\gamma_{cr} = \frac{-1+\sqrt{\delta}}{U_0^2/\omega_0^2}$, where $\delta = 1 + 2\frac{U_0^2}{\omega_0^2}$, and $\delta_\eta = 1 + \frac{U_0^2}{\omega_0^2\eta}$.

One can study the variation with different parameters of interest as a the ratio of the two capacitances (C, C_0) involved in the network, or the nonlinear parameters (α, β) to cite few among other. An example is given below with respect to η:

▷ For $0 < \eta < \gamma_{cr}$, we have one domain of propagation of envelope solitons; $\omega_2 \in [\omega_s, \omega_{2max}]$

▷ For $\eta = \gamma_{cr}$, we also have one domain of propagation of envelope solitons; $\omega_2 \in [\omega_a, \omega_s]$

▷ For $\eta > \gamma_{cr}$, we still obtain one domain of propagation of envelope solitons; $\omega_2 \in [\omega_{2min}, \omega_s]$ with $\omega_{2max}^2 = (4U_0^2 + 2\omega_0^2)/(1+2a)$, $\omega_{2min}^2 = 2U_0^2/(1+2a)$ and $\omega_s^2 = \omega_{2max}\omega_{2min}$.

3.3.3.2 Numerical experiments

We now present the numerical experiments on the propagation of slowly modulated waves in the network. This is done in the scope to check the analytical results above presented. The numerical experiments are carried out in Eq.(3.51) describing the propagation of waves in the coupled **NETLs** of figure 3.19. The parameters of the network are chosen to be the same as those used above, i.e. $L_2 = 0.100\ mH$, $C = 200\ pF$, $a = 0.5$, $\alpha = 0.21\ V^{-1}$ and, $\beta = 0.0197\ V^{-2}$. The wave introduced has the form

$$V_{n=0}(t) = V_0[1 + m\cos(2\pi f_m t)]\cos(2\pi f_p t) \tag{3.64}$$

where f_m is the modulation frequency, V_0 is the amplitude of the wave and m is the modulation rate. We take $f_m = 5.4\ kHz$, $V_0 = 0.2\ V$ and $m = 1\%$. The fourth-order Runge-Kutta scheme is used with normalized integration time step $\Delta t = 5 \times 10^{-3}$. Moreover, the number of cells is chosen so that we do not encounter the wave reflection at the end of the lines. For this purpose, we consider an additive sufficiently enough number of modified cells at the end of each line. Their role is to gradually decay the voltage amplitude. This is simulated by adding a viscous damping term to Eq.(3.51), valid only for these supplementary cells; this technique is usually called absorbing boundary at the free end [97, 98].

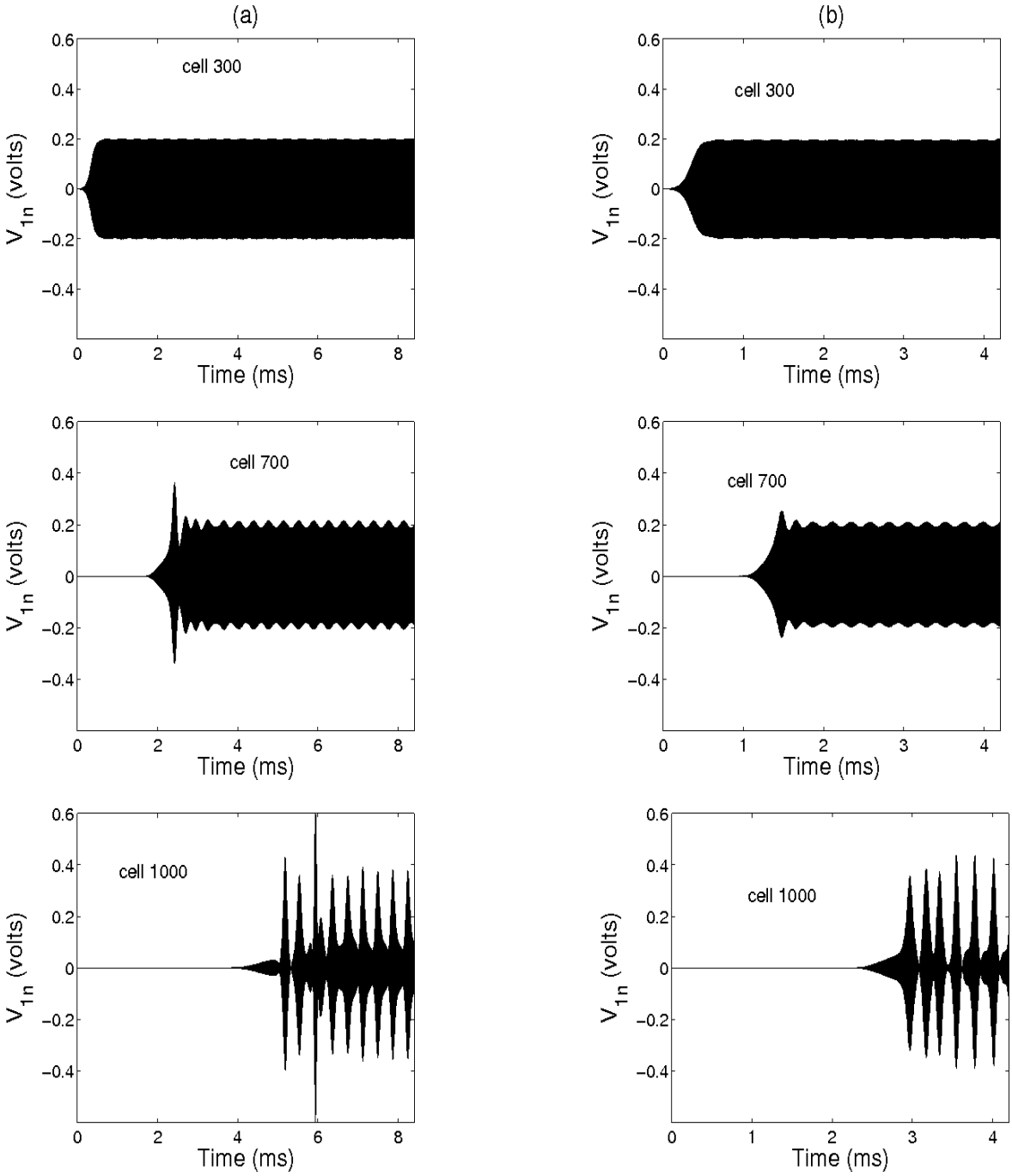

Figure 3.23: *Signal voltage as a function of time at different cells on line 1. The signal is equal in absolute value on line 2. (a) Fast-mode $f_p = 563\ kHz$, and (b) Slow-mode $f_p = 881\ kHz$. $L_1 = 0.4\ mH$; $C_0 = 400\ pF$; $a = 0.5$.*

As the sine wave applied at one end of the coupled lines is slowly modulated, we may expect modulation growth and formation of wave packets which propagates along the network. Figure 3.23 shows an example of the MI exhibited by the network for the two modes of propagation. The initial condition corresponding to the input wave is given

Domains of **IM**		
Mode	Analytical predictions (kHz)	Numerical results (kHz)
Fast-mode	69.04 - 796.18	82.96 - 789.22
Slow-mode	880.85 - 973.81	880.57 - 963.39

Table 3.2: *Analytical and numerical frequency values for which there is modulational instability.*

above by equation (3.64). We choose the carrier frequency $f_p = 563\ kHz$ for the fast-mode and $f_p = 881\ kHz$ for the slow-mode, respectively. Column (a) presents the profile for the fast-mode while column (b) is for the slow-mode. Each column shows the state of the network at three different cells (namely 300, 700 and 1000 as indicated) in function of time. As time goes on, the wave exhibits a modulation of its amplitude and phase, which leads to the formation of wave packets. When the instability occurs in the system, the amplitude of the resulting wave packet is larger than the amplitude of the input wave due to the localization of the energy. This result is in accordance with the analytical treatment for linear waves and confirm the fact that the use of the coupled **NETLs** described permits the escapement of waves mixing due to the existence of two modes of propagation in the network. Relation (3.55) permits us to present figures for only one line because the signal voltages in the two lines are always either in phase (fast-mode) or $\pi\ rad$ out of phase (slow-mode) with the same amplitudes. We recapitulate the theoretical predictions and the corresponding numerical results in the following table:

In the view to consolidate the validity of analytical results, we propagate the solution of the **NLS** equation [96] since the above observed Benjamin-Feir intability constitutes the proof that the network can support envelope solitons. For this purpose, we take as the input voltage the profile of a modulated soliton given by

$$V_{11}^{(l)} = V_m sech(\frac{v_{gl}t}{L_s^{(l)}})\cos(2\pi f_p^{(l)}t) \tag{3.65}$$

where $f_p^{(l)}$ and v_{gl} are the carrier frequency and the group velocity of the wave packet, respectively, and $L_s^{(l)}$ is the soliton width defined by $L_s^{(l)} = \frac{1}{V_m}\sqrt{\frac{2P^{(l)}}{Q^{(l)}}}$. The superscript l always stands for the two modes of propagation. The parameters of the signal voltage are the same as in figure 3.23.

Figure 3.24 shows the propagation of fast- and slow-modulated (Figs.3.24(a) and

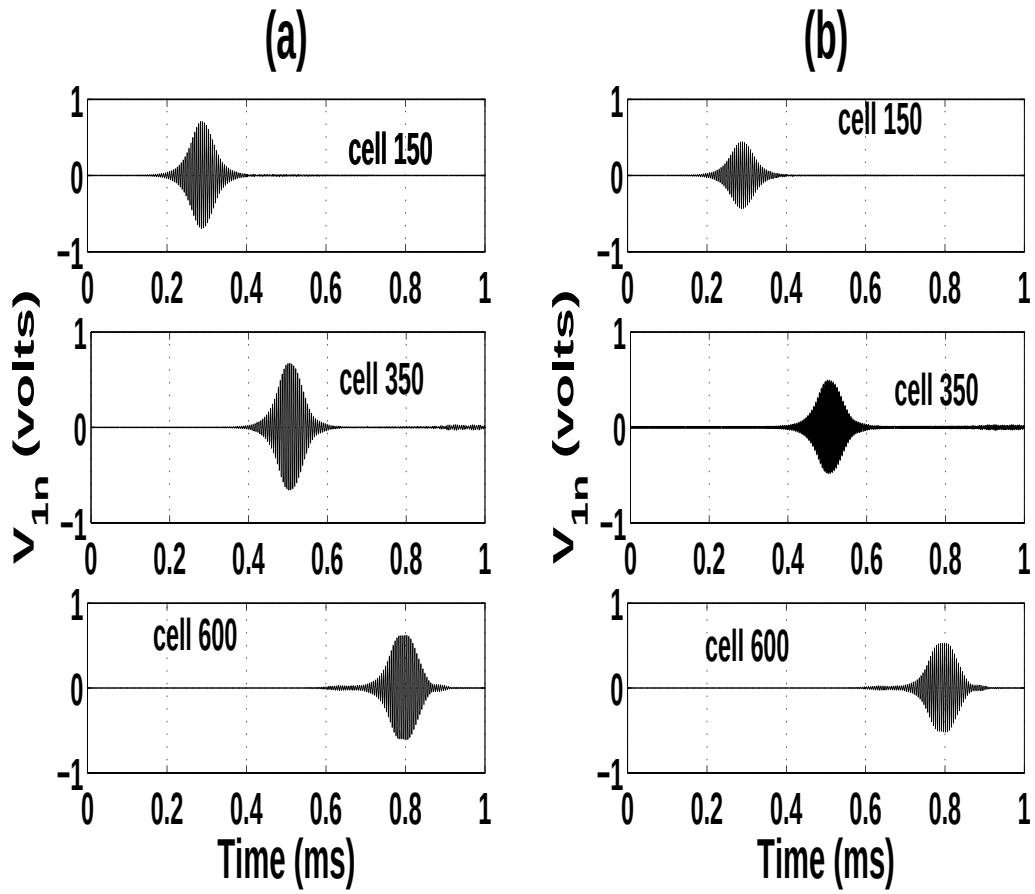

Figure 3.24: *Envelope soliton signal voltage as a function of time at different cells for the same parameters as in figure 3.23.*

3.24(b), respectively) soliton along line 1. Knowing that such envelope solitons are generally quite stable, we have numerically verified that this envelope soliton is strongly stable to small perturbation. It is well known that a large width penalizes the increase in bit rate of envelope solitons. It is then convenient to compact the width in order to increase their bit rate. As expressed in their exact profile solution [see equation (3.63)], the ratio V_g/L_s is plotted in function of the wavenumber (see figure 3.25). The dashed line corresponds to the model under investigation while the solid line corresponds to that of ref. [28]. It comes out that the present model convenes for an increase of the bit rate.

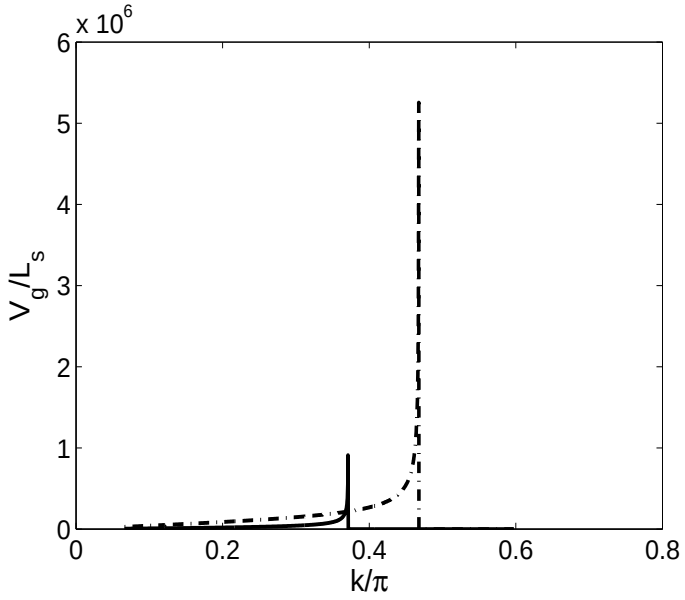

Figure 3.25: *Ratio v_g/L_s as a function of frequency for the model 2 of ref. [28] (solid line) and for the present model (dashed line). $L_1 = 0.4$ mH; $C_0 = 400$ pF; $a = 0.5$.*

3.3.4 Concluding remarks on the suppression of waves mixing

In this part, we have studied analytically and numerically the dynamics of modulated waves in two coupled **NETLs**. More precisely, the modes of propagation of these modulated solitons, i.e. the fast- and the slow-mode, have been detected. The fast-mode corresponds to the mode of propagation of a single isolated line while the slow-mode results in the coupling between the two lines. By using the reductive perturbation method, we have shown that the dynamics of nonlinear waves in this coupled discrete nonlinear electrical transmission line can be described by a set of coupled nonlinear Schrödinger equations. We have analytically predicted the domains of frequencies for which plane waves are modulationally unstable. The analytical studies have been completed by the numerical experiments. The both studies show a quite well agreement between their results. Hence from the proposed unit cell considered in this work, the waves mixing effects have been successfully suppressed. Identical results have been found for a different unit cell setup (see ref. [28]). They argue that the avoidance of wave mixing was due to the band-pass filter behavior of the unit cell they used. However, the characteristic of the unit cell considered in the present work is a low-pass filter exactly as the original unit cell before modification (refereed as model 1 in [28]); and the results of suppressing the

waves mixing effects are monitored by the coupling cell block. This suggests that the type of the unit cell is not really relevant to achieve the goal, and that only the position of the additive inductor is important. Furthermore, it is important to remark that the total number of additive linear inductors used here is the half of that required to construct the model 2 as refereed in [28]. Moreover, the overall bandwidth is larger in the present case due to the very low frequencies that are not automatically excluded. Preliminary investigations confirm all the above results [99]. A particular attention has to be paid to the fast-mode which contains these low frequencies. Besides, a more compact envelope solitons allows an increase of the bit rate.

3.4 Modulational instability in two non-identical coupled nonlinear electrical transmission lines

In this section, the dynamics of modulated waves in a non identical coupled nonlinear LC transmission lines is studied. We expect that an appropriate use of a band-pass cell through the network permits to avoid the mixing of waves of different modes in the lines; and we then exploit the features of the modulational instability of each of two modes.

3.4.1 Model and equations of dynamics

The model used in this part consists of a nonlinear network made of two different coupled lines. The first line contains a finite number of cells which consist of three elements: a linear inductor of inductance L_1 in the series branch; a nonlinear capacitor of capacitance $C(V_{jn})$ and a linear inductor of inductance L_2 in the shunt branch. This capacitor consists of a reverse-biased diode with a differential capacitance function of the voltage V_{jn}. The second line is a copy of the first one from which inductor of inductance L_2 is suppressed. Hence, the first line is an assemblage of band-pass filter while the second line is an association of low-pass filter. The two lines are connected by an intermediary linear capacitor C, as shown in Fig. 3.26. This network is an asymmetric coupled lines.

In the line, the nonlinearity is introduced by a varicap diode which admits that the capacitance varies with the applied voltage. The voltage dependance relation is assumed to have a polynomial form given by

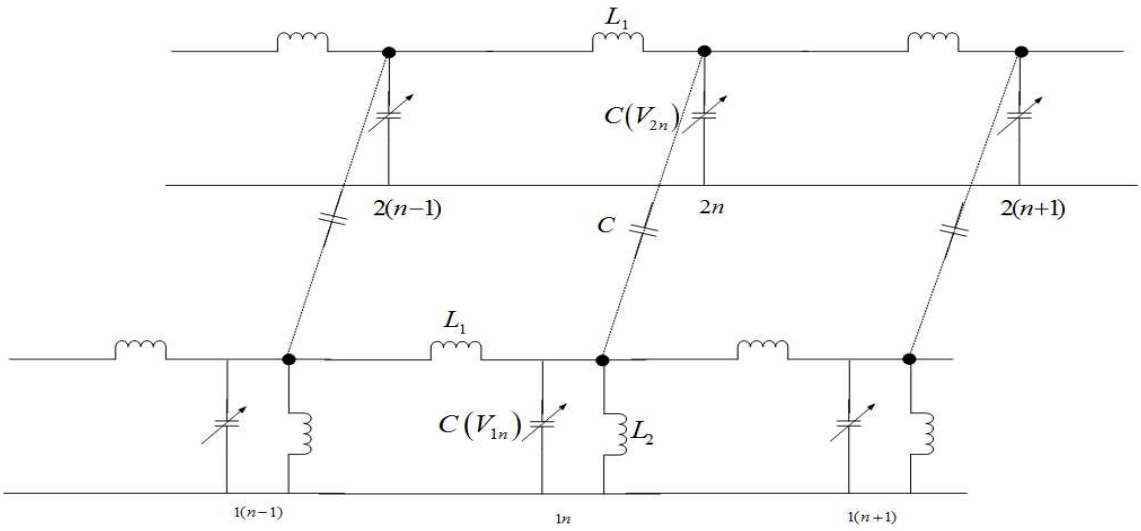

Figure 3.26: *Diagram of the network. Three unit cells are reproduced for each line. The first line, in front is different of the second line backwards because of the inductor of inductance L_2; this first line is a band-pass filter and the second line is a low-pass filter.*

$$Q(V_{jn}) = C_0(V_{jn} - \alpha V_{jn}^2 + \beta V_{jn}^3) \tag{3.66}$$

where C_0, α, β are constants.

We now focus our attention on the nonlinear behavior of the lattice. From Kirchhoff's laws, it is easy to obtain the following system by using Eq.(3.66)

$$\begin{cases} \frac{d^2V_{1n}}{dt^2} - \alpha\frac{d^2V_{1n}^2}{dt^2} + \beta\frac{d^2V_{1n}^3}{dt^2} = U_0^2(V_{1(n-1)} - 2V_{1n} + V_{1(n+1)}) - \omega_0^2 V_n - a\frac{d^2}{dt^2}(V_{1n} - V_{2n}) \\ \frac{d^2V_{2n}}{dt^2} - \alpha\frac{d^2V_{2n}^2}{dt^2} + \beta\frac{d^2V_{2n}^3}{dt^2} = U_0^2(V_{2(n-1)} - 2V_{2n} + V_{2(n+1)}) - a\frac{d^2}{dt^2}(V_{2n} - V_{1n}) \end{cases} \tag{3.67}$$

with $U_0^2 = \frac{1}{L_1C_0}$; $\omega_0^2 = \frac{1}{L_2C_0}$; $a = \frac{C}{C_0}$.

We use the semi-discrete approximation by setting $\tau = \epsilon^2 t$ and $x = \epsilon(n - v_g t)$, to obtain the short wavelength envelope solitons; v_g is the group velocity. This asymptotic approach allows us to describe the envelope in the continuum approximation and to treat properly the carrier wave with its discrete character. Then V_{jn} is given by

$$V_{jn}(t) = \epsilon A_j(x,t)e^{i\theta} + \epsilon^2[\Psi_j(x,t) + B_j(x,t)e^{2i\theta}] + \text{"}c.c\text{"}. \tag{3.68}$$

where $\theta = kn - \omega t$ is the phase and "$c.c$." stands for the complex conjugated of the

preceding expression; k is the wave number; ω is the angular frequency; ϵ is a small parameter.

3.4.2 Amplitude equations

This part is devoted to the determination of the order equations. Inserting Eq.(3.68) into Eq.(3.67), we easily find the amplitude equations.

i) The coefficient ϵ, proportional to $e^{i\theta}$ gives the following linear dispersion relations:

$$\omega_{\pm}^2 = \frac{8U_0^2(1+a)\sin^2(\frac{k}{2}) + \omega_0^2(1+a) \pm \sqrt{16U_0^2a^2\sin^2(\frac{k}{2})(4U_0^2\sin^2(\frac{k}{2}) + \omega_0^2) + \omega_0^4(1+a)^2}}{2(1+2a)} \tag{3.69}$$

where $\omega_{\pm}$ and k are respectively the angular frequency and wave number; for ω_+, the gap frequency is $\omega_{+min}^2 = \frac{\omega_0^2(1+a)}{(1+2a)}$ and the cut-off frequency

$\omega_{+max}^2 = \frac{(8U_0^2+\omega_0^2)(1+a)+\sqrt{16U_0^2a^2(4U_0^2+\omega_0^2)+\omega_0^4(1+a)^2}}{2(1+2a)}$; for ω_-, the gap frequency is $\omega_{-min}^2 = 0$ and the cut-off frequency is $\omega_{-max}^2 = \omega_{+min}^2$. The linear dispersion curve that deals with relation (3.69) is shown in Fig. (3.27).

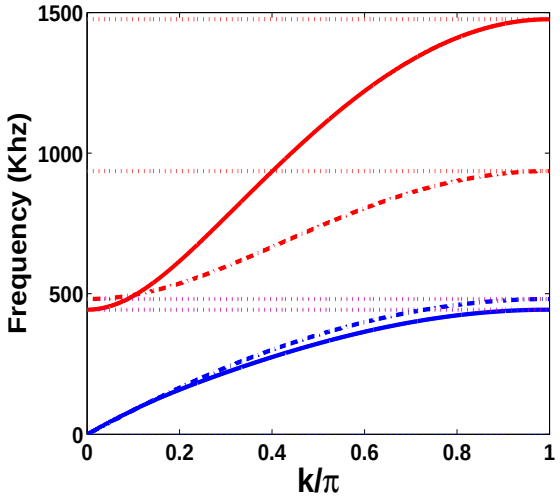

Figure 3.27: *Dispersion graph obtained with $L_1 = 0.464$ mH; $L_2 = 0.22$ mH; $C_0 = 320$ pF. The curve representing ω_+ is plotted in red color while ω_- correspond to the blue. The dashed lines correspond to $a = 1.25$ and the solid lines are represent for $a = 5.0$. The dotted lines mark the limits of different modes. The bandwidth of ω_+ increases with a.*

The blue curve line admits low frequencies and corresponds to ω_- while the red curve line is a typical band-pass filter and corresponds to ω_+. Each dispersion graph occurs on the first brillouin zone. The relation that we used to suppress the mixing frequencies is the following: $L_1 = \frac{4L_2}{1+2a^2/(1+2a)}$. Generally, when the two coupled lines have identical linear characteristic parameters, one of the two modes reduces to the standard mode of propagation of an isolated single line. In the present case, it is important to note that none of the two modes corresponds to the uncoupled network due to the difference on the two lines. The group velocity is taken to be

$$\begin{aligned} V_{g\pm}(k) &= \frac{\partial\omega_\pm(k)}{\partial k} = \frac{U_0^2(1+a)\sin(k)}{\omega_\pm(1+2a)} \\ &\pm \frac{U_0^2a^2(4U_0^2\sin^2\frac{k}{2}+\omega_0^2)\sin(k)+4a^2U_0^4\sin(k)\sin^2(\frac{k}{2})}{(1+2a)\omega_\pm\sqrt{16U_0^2a^2\sin^2(\frac{k}{2})(4U_0^2\sin^2(\frac{k}{2})+\omega_0^2)+\omega_0^4(1+a)^2}} \end{aligned} \quad (3.70)$$

Figure 3.28 shows us the group velocity of each mode.

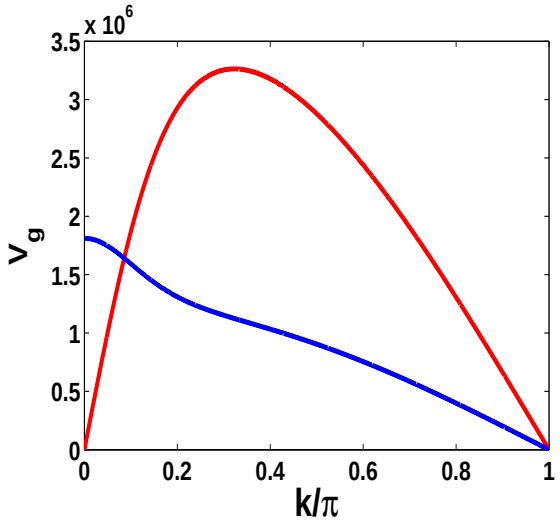

Figure 3.28: *Group velocity of the two modes obtained for the same parameters as in figure 3.27. Red and blue colors correspond to V_{g+} and V_{g-}, respectively. $V_g^* = 1.641 * 10^6$ represents the crossing point of the two curves.*

We realize that the sidelining of very low frequencies signifies the loss of highest group velocities such as we can see on figure 3.28. Usually, the coupling is made on identical type of lines; and then the group velocities are totally separated depending on the mode; the smaller group velocity remains below the higher one in the whole range of

the first brillouin zone. In figure (3.28), the group velocity of ω_- is larger than the group velocity of ω_+ for $k \in [0; 0.2690[$; for $k \in]0.2690; 3.14]$, $V_{g-} < V_{g+}$.

ii) The coefficient ϵ^2, proportional to $e^{i\theta}$ gives two relations

$$A_2 = \lambda_{(l)}^{3-2l} A_1 \qquad (l = 1, 2) \tag{3.71}$$

where $\lambda = \frac{\omega_\pm^2(1+a)-(2-l)\omega_0^2-4U_0^2\sin^2(\frac{k}{2})}{a\omega_\pm^2}$. The proportionality coefficient λ is no more equal to neither 1 nor -1 as in identical coupled lines.

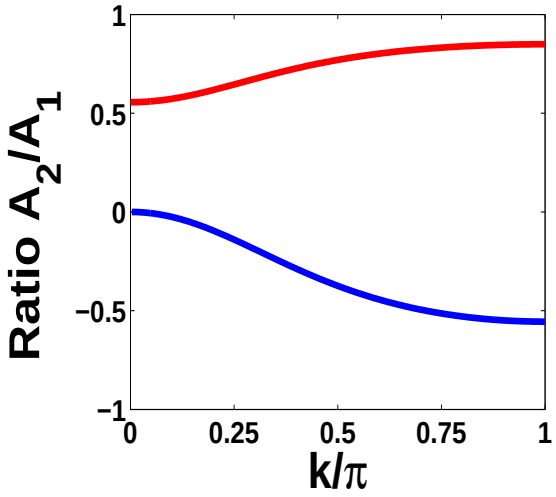

Figure 3.29: *Ratio of the amplitudes A_1 (line 1) and A_2 (line 2) for the modes corresponding to ω_+ (red curve) and ω_- (blue curve).*

iii) The coefficient ϵ^2, proportional to $e^{2i\theta}$ also leads to two relations that we can merely set as follows

$$\begin{cases} B_1 = \gamma A_1^2 \\ B_2 = \delta A_1^2 \end{cases} \tag{3.72}$$

with $\gamma = \frac{4\alpha\omega_\pm^2[\omega_\pm^2(1+a+a\lambda_l)+U_0^2(\cos^2 k-1)]}{4\omega_\pm^4(1+2a)+(1+a)(\omega_\pm^2\omega_0^2-8\omega_\pm^2U_0^2)+U_0^2(4U_0^2-\omega_0^2)+8U_0^2(-U_0^2+a\omega_\pm^2+\omega_\pm^2)\cos^2(k)+U_0^2(\omega_0^2+4U_0^2\cos^2(k))\cos^2(k)}$

and

$\delta = \frac{4\alpha\omega_\pm^2[a\omega_\pm^2+(\omega_\pm^2+a\omega_\pm^2+\frac{\omega_0^2}{4}-U_0^2+U_0^2\cos^2(k))\lambda_l]}{4\omega_\pm^4(1+2a)+(1+a)(\omega_\pm^2\omega_0^2-8\omega_\pm^2U_0^2)+U_0^2(4U_0^2-\omega_0^2)+8U_0^2(-U_0^2+a\omega_\pm^2+\omega_\pm^2)\cos^2(k)+U_0^2(\omega_0^2+4U_0^2\cos^2(k))\cos^2(k)}$.

where $l = 1$ for the first line and $l = 2$ for the second line.

iv) The coefficient ϵ^4, proportional to e^0 leads to

$$\Psi_1 = \Gamma|A_1|^2 \quad \text{and} \quad \Psi_2 = \Delta|A_1|^2 \tag{3.73}$$

where $\Gamma = \frac{2\alpha V_{g\pm}^2(2\alpha V_{g\pm}^2 + a2\alpha V_{g\pm}^2\lambda_l^2 + a2\alpha V_{g\pm}^2 - U_0^2)}{V_{g\pm}^4 + 2aV_{g\pm}^2 - 2U_0^2V_{g\pm}^2 - 2aU_0^2V_{g\pm}^2 + U_0^2}$ and $\Delta = \frac{2\alpha V_{g\pm}^2[(V_{g\pm}^2 + aV_{g\pm}^2 - U_0^2)\lambda_l^2 + aV_{g\pm}^2]}{V_{g\pm}^4 + 2aV_{g\pm}^2 - 2U_0^2V_{g\pm}^2 - 2aU_0^2V_{g\pm}^2 + U_0^2}$

v) The coefficient ϵ^3, proportional to $e^{i\theta}$ gives Eq.(3.74); this is obtained by using the Eq.(3.71), Eq.(3.72) and Eq.(3.73).

$$iA_{j,\tau} + P_j^{(\pm)}A_{j,xx} + Q_j^{(\pm)}A_j|A_j|^2 = 0 \qquad (j = 1, 2) \tag{3.74}$$

The Eq.(3.74) is the **CNLS** equations describing the propagation through the network. In fact, the set of equation is written as uncoupled equations. This has been predicted since the relations (3.71) were established. Different dispersion relations and Eq.(3.72) affect and differentiate the parameters. $P_j^{(\pm)}$ and $Q_j^{(\pm)}$ are respectively the dispersion and nonlinear coefficients given by the following relations:

$P_j^{(\pm)} = \frac{U_0^2\cos(k) + V_{g\pm}^2(a\lambda_{(l)} - a - 1)}{2\omega_\pm(1 + a - a\lambda_{(l)})}$ where the indicator j and l take the values 1 for the first line and 2 for the second line

and $Q_1^{(\pm)} = \frac{3\beta\omega_\pm^2 - 2\alpha\omega_\pm^2(\gamma + \Gamma)}{2\omega_\pm(1 + a - a\lambda_1)}$ for the first line; for the second line, $Q_2^{(\pm)} = \frac{3\beta\omega_\pm^2 - 2\alpha\omega_\pm^2(\delta + \Delta)}{2\omega_\pm(1 + a - a\lambda_2)}$.

3.4.3 Numerical study of modulational instability

We search in this section, the condition under which a uniform wave train moving along the nonlinear lines will become stable or unstable to a small perturbation. Up to date, the attention paid to this phenomenon still captures a lot of research works. A clear idea of this interest is given by the important number of reports found in the literature. Under the frame of this instability, plane wave leads to the formation of envelope pulse solitons. The fact that we can observe the formation of envelope pulse solitons in the network comes to $P_j^{(\pm)}Q_j^{(\pm)} > 0$. Under this condition wave becomes unstable. This is also call Benjamin-Feir instability. If $P_j^{(\pm)}Q_j^{(\pm)} < 0$, plane wave solution of **NLS** equation is stable. To determine the different zone where $P_j^{(\pm)}Q_j^{(\pm)} > 0$, we play on the coupling constant a; we always consider the relationship of suppression of the mixing. Then we plot the frequencies ω in function of coupling constant. Figures (3.30) and (3.31) represent the distribution of domains of MI in red for the first line (left) and for the second line (right).

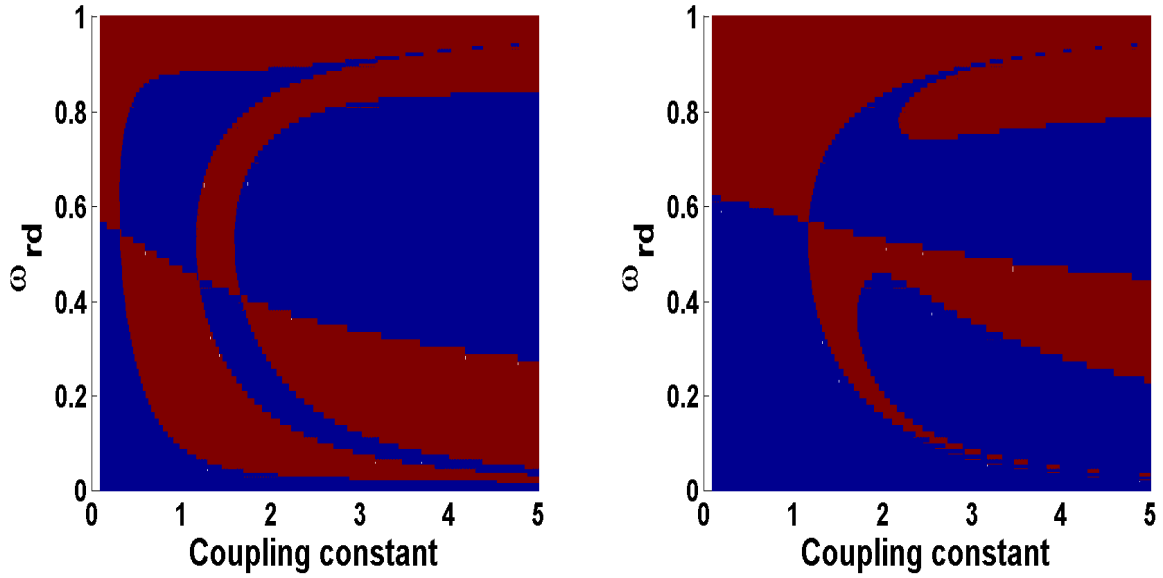

Figure 3.30: *Domains of Modulational Instability plotted for ω_+. The blue color corresponds to the case of no MI while the red color marks the MI domains. The left figure results from the first line and the right figure presents the domains of second line. $L_1 = 0.464\ mH$; $L_2 = 0.22\ mH$; $C_0 = 320\ pF$.*

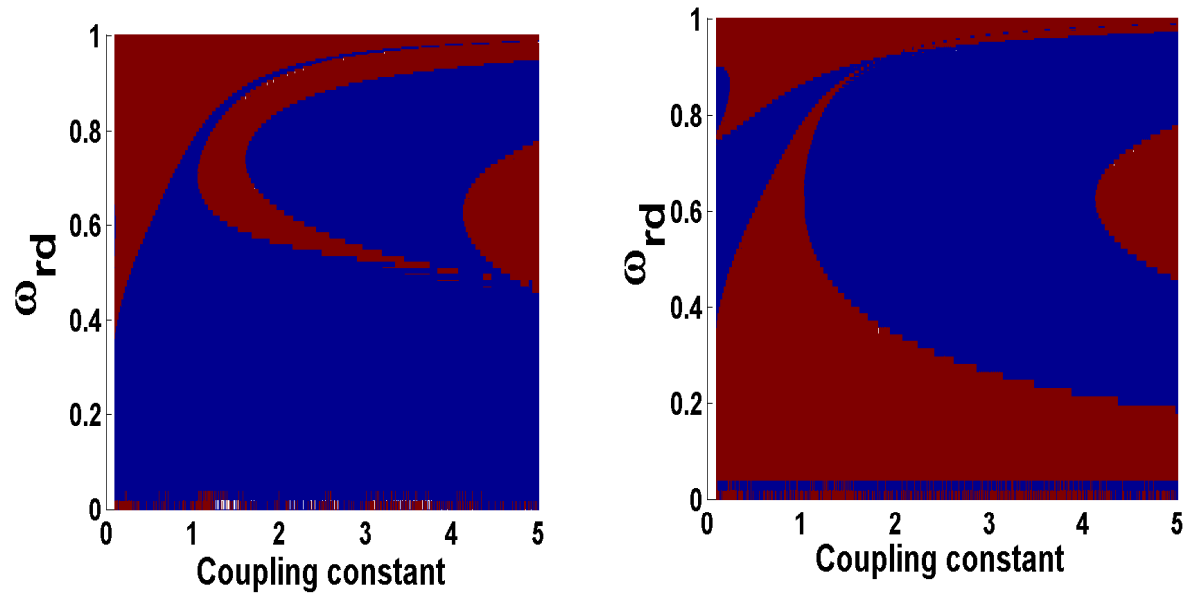

Figure 3.31: *Domains of Modulational Instability plotted for ω_-. The blue color corresponds to the case of no MI while the red color marks the MI domains. The left figure results from the first line and the right figure presents the domains of second line. $L_1 = 0.464\ mH$; $L_2 = 0.22\ mH$; $C_0 = 320\ pF$.*

In figures 3.30 and 3.31, we have considered the space of parameters a and ω_{rd} where ω_{rd} represents reduced frequency and is expressed as $\omega_{rd} = (\omega - \omega_{min})/(\omega_{max} - \omega_{min})$. ω_{max} and ω_{min} are evaluated for each new value of the coupling parameter a. We present these two figures for ω_+ (figure 3.30) and for ω_- (figure 3.31). To confirm these domains, we plot the gain for $a = 5$ only for ω_+. This is presented on figure 3.32 in which three zones of MI are obtained and then confirm the results presented on figure (3.32). δ is an arbitrary real wave number accounting for the perturbation.

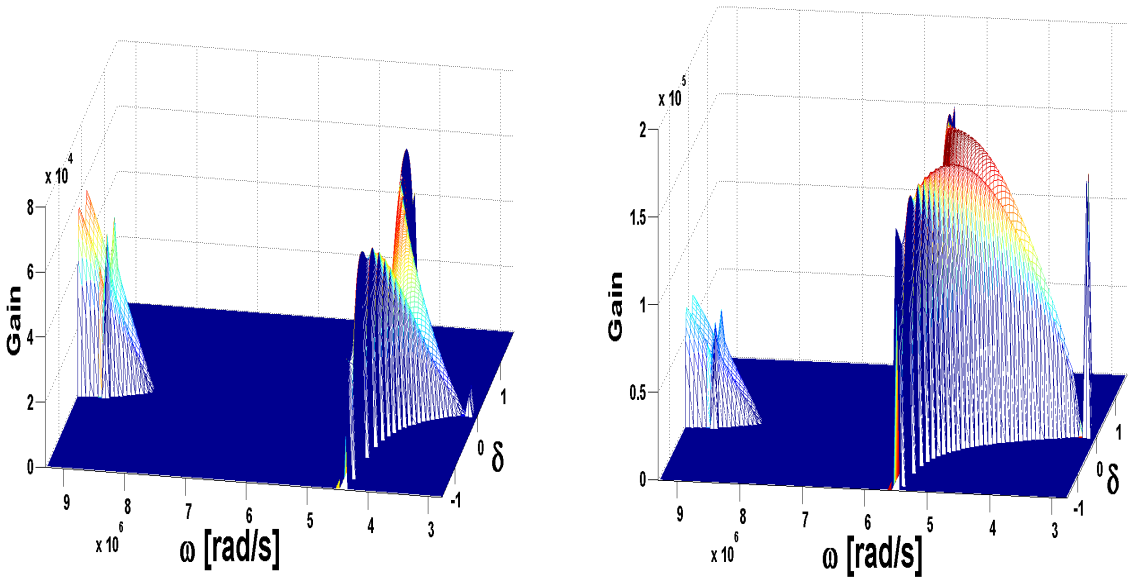

Figure 3.32: *Gain of the two lines for ω_+. At the left, line 1 and at the right line 2. On each figure, we have three areas where the gain is not equal to zero. This result confirms the observations made on figure 3.31.*

In the view to consolidate the validity of the preceding results, we propagate the solution of the **NLS** equation [100] since the above observed Benjamin-Feir intability constitutes the proof that the network can support envelope solitons. For this purpose, we take as the input voltage the profile of a modulated soliton given by

$$V_{\pm}^{(l)} = V_m sech((v_{g\pm}t)/(L_s^{(l)}))\cos(2\pi f_{p\pm}t) \tag{3.75}$$

where $f_{p\pm}$ and $v_{g\pm}$ are the carrier frequency and the group velocity of the wave packet respectively, and $L_s^{(l)}$ is the soliton width defined by $L_s^{(l)} = \frac{1}{V_m}\sqrt{\frac{2P_j^{\pm}}{Q_j^{\pm}}}$. Figures 8, 9 and

10 show the propagation of upper modulated soliton along line 1 and line 2 for different amplitudes. The numerical experiments are carried out in Eq.(3.67) describing the propagation of waves in the coupled **NETLs** of figure 3.26. The parameters of the network are chosen to be: $\alpha = 0.21\ V^{-1}$ and $\beta = 0.0197\ V^{-2}$. Variables L_1, L_2, a and C_0 have the same values as in figure 3.27. The fourth-order Runge-Kutta scheme is used with normalized integration time step $\Delta\tau = 2 \times 10^{-3}$. We choose the carrier frequency $f_{p+} = 1328.80\ kHz$ and $f_{p-} = 173.37\ kHz$; we use several amplitudes to look their influence on wave propagation. The different figures are given below where we have represented the signal to multiple cells. From the left to the right, we have the cell of rank 1, 300, 600, 900, 1200, 1500, 1800, 2100, 2400 and 2700.

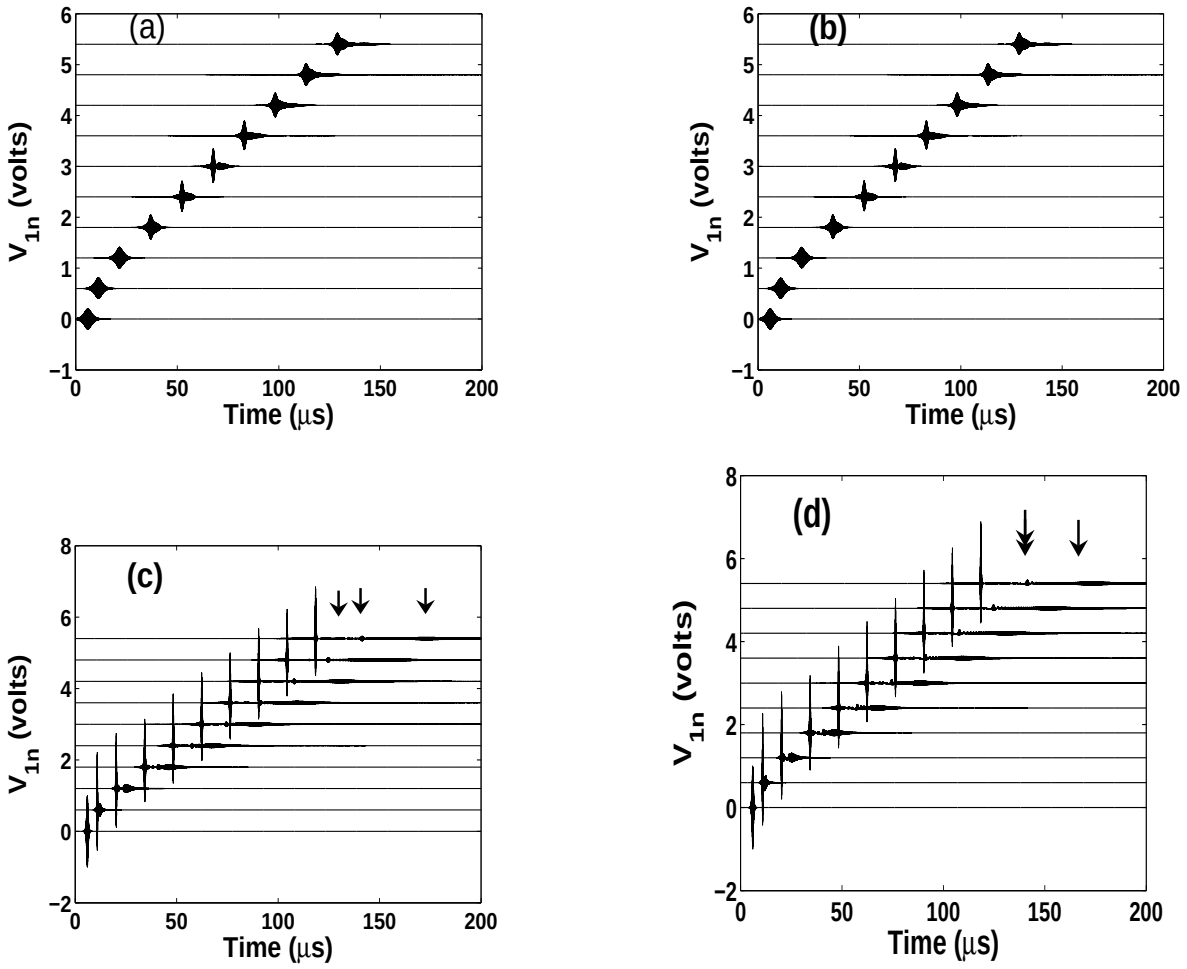

Figure 3.33: *Propagation of envelope soliton signal voltage as a function of time at different cells plotted for ω_+; left column corresponds to line 1, i.e. (a) and (c), while the right column stands for line 2 i.e. (b) and (d). The input signal is given by equation (3.75). The upper row refers to an amplitude of* 0.2 V *while the second row is obtain for signal voltage of* 1.0 V. *The fission is not obvious enough on the upper row. Variables L_1, L_2, a and C_0 have the same values as in figure 3.27.*

On figure (3.33), we realize that the non identical coupled lines support the envelope pulse solitons train. This confirms the above studies. The parameters of the envelope soliton are not always exactly the same for both lines (Fig.3.33(c) and Fig.3.33(d)). This difference has been predicted by Eq.(3.71). The phenomenon of fission has already been reported (see [96, 100]). On the upper row (Fig.3.33), the fission is very difficult to make itself visible, and to clearly split the input pulse. We are not able to tell whether the fission reduces the velocity of the secondary soliton or if it increases the velocity of the initial soliton so that the two solitons remain bounded. However, Yemele et *al.* have

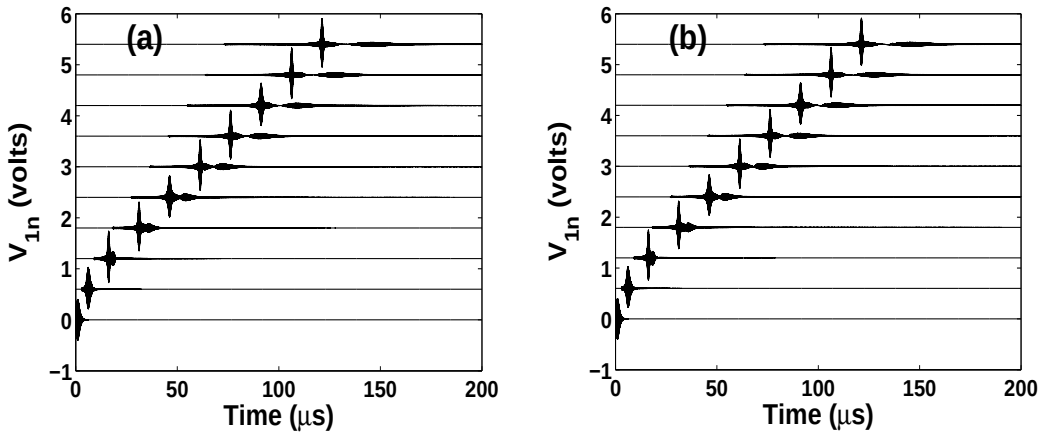

Figure 3.34: *Propagation of envelope soliton signal voltage (amplitude equal to* 0.4 *V) as a function of time at different cells always plotted for* ω_+*; (a) corresponds to line 1 and (b) corresponds to line 2. Here, we have not introduced all the energy corresponding to the chosen amplitude at the initial time; this influence the fission. Variables* L_1*,* L_2*, a and* C_0 *have the same values as in figure 3.27.*

suggested that the Raman effect is more manifested since it gives a constant deceleration inducing the increase of the soliton velocity with respect to the propagation distance. This could be verified for next figures on the second row in which the fission appears clearly. The arrows on figure 3.33 (c and d) represent the secondary solitons produced by fission. The double arrow shows the difference between the secondary soliton of the first line and the one of second line due to the difference between the two lines. The induced very low amplitude secondary solitary waves have a greater width and a higher velocity compared to the initial solitary wave. For this reason, we can consider them as a part of the input energy which is spreading along the network and therefore can be seen as a perturbation. We have numerically study the stability of the system and it comes out that the pulse is extremly stable to small perturbations. On figure 3.34, we show how the amount of input energy corresponding to a given amplitude of the signal voltage may influence the process of fission. This figure presents only one secondary soliton while figure 3.33 (c and d) presents more than two generated solitons. We conclude that fixing the amplitude and acting on the corresponding energy introduced through the line, the more the input energy is close to the full corresponding one, the better the fission occurs. The width of the main soliton is then compressed; this is good for the transmission of waves packet since the bit rate could be increased. As final result of this work, the solitary wave propagating

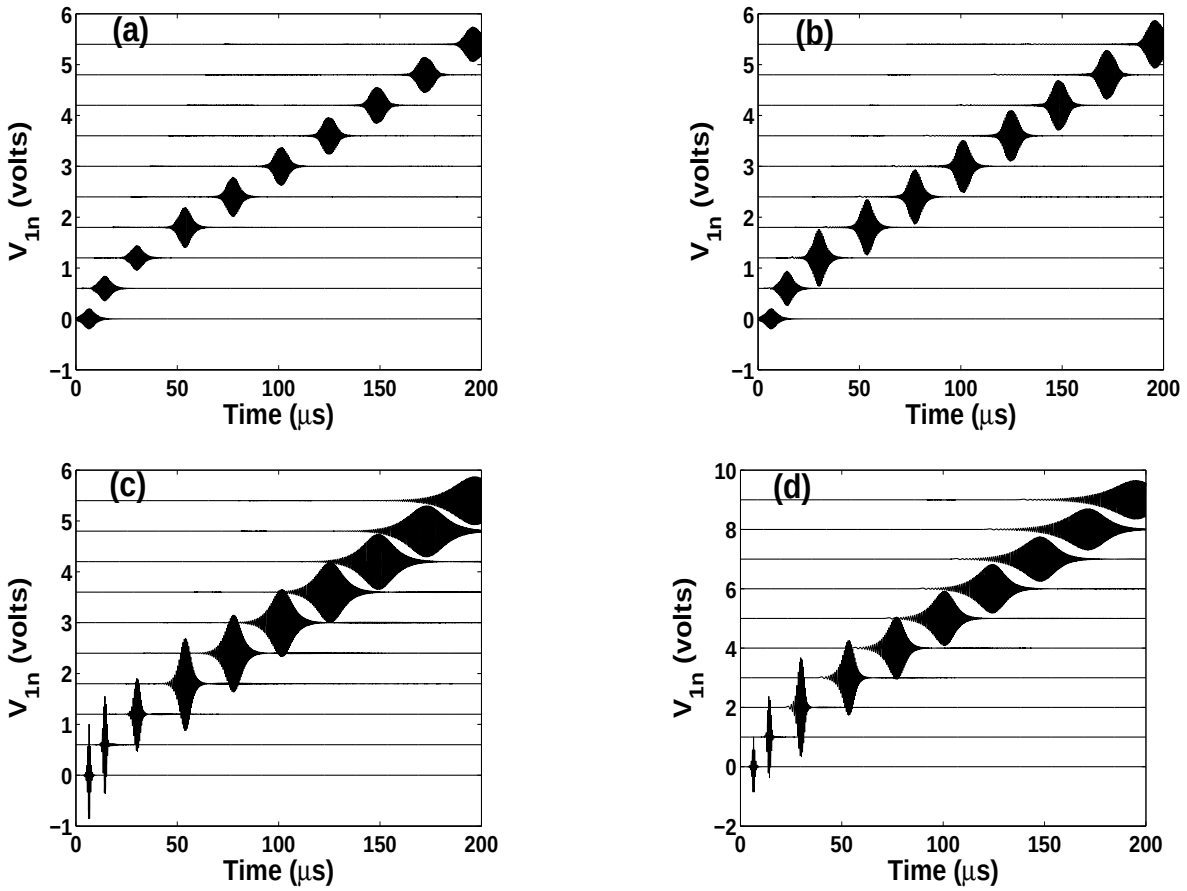

Figure 3.35: *Propagation of envelope soliton signal voltage as a function of time at different cells plotted for ω_-; left column corresponds to line 1, i.e. (a) and (c), while the right column stands for line 2 i.e. (b) and (d). The upper row refers to an amplitude of* 0.2 V *while the row below is obtain for signal voltage of* 1.0 V. *The signal voltage suffers from an effect of dispersion when the time grows. Variables L_1, L_2, a and C_0 have the same values as in figure 3.27.*

through the two lines for ω_- (see Fig. 3.35) suffers from an effect of dispersion after a long distance of propagation during which the amplitude of the signal voltage grows with the time. Hence, the network acts for these low frequencies regime as an amplifier.

3.4.4 Concluding remarks on a pair of non-identical coupled NETLs

In this section, we have studied the dynamics of modulated waves in two non-identical coupled NETLs. Two modes of propagation of modulated solitons have been detected. Generally, when the two coupled lines have identical linear characteristic parameters, one of the two modes reduces to the standard mode of propagation of an isolated single line. In the present case, it is important to note that none of the two modes cor-

responds to the uncoupled network due to the difference on the two lines. Modulational instability has been studied and we have shown that the investigated system can support a train of envelope solitons. The importance of the coupling constant for the MI domains has been highlighted. During this work, we have confirmed that it is not mandatory to couple two lines made of band-pass filters to solve the crucial problem of the mixing of waves of different modes in the network; only the existence of the band-pass filter well-positioned help for the suppressing [100]. It results that the entire coupled cells needs only the half of the total number of additive linear inductors compared to the number used to construct the line in ref. [28]. Besides, it is important to notice that for ω_{-}, the use of an appropriated width reducer could bring back the profile of the signal at its initial form. Particularly for this mode corresponding to low frequencies, the system acts as an amplifier. Another important thing is the fission which appears in the two lines during propagation for only ω_{+}. This fission is influenced by the amplitude of the signal voltage introduced at initial time as well as by the amount of the input energy.

3.5 Transverse stability in the discrete inductance capacitance electrical network

In this section, we derive the two-dimensional NLS equation governing the propagation of slowly modulated waves in the network by a means of a method based on the semi-discrete limit and in suitably scaled coordinates. The exact transverse solution is found and the analytical criteria of stability of this solution is derived.

3.5.1 Main characteristics of the coupled NETLs and dynamic equation

The standard nonlinear discrete LC line is a structure made of elementary cells which consist of an inductance L and a nonlinear capacitor $C(V)$ [70]. Many schematic electrical lattices have already been considered in the literature [47]. The model used in this work consists of a nonlinear network with many coupled nonlinear LC dispersive transmission lines. We imagine that there are many identical dispersive lines which are coupled by means of inductance L_3 at each node, as shown in figure 3.36. Each section of line consists of a constant inductor L_1 in the series branch and a nonlinear capacitor

of capacitance $C(V_{n,m})$ in parallel with a constant inductor L_2 in the shunt branch. The nodes in the system are labeled with two discrete coordinates n and m, where n specifies the nodes in the direction of propagation of the pulse, and m labels the lines in the transverse direction.

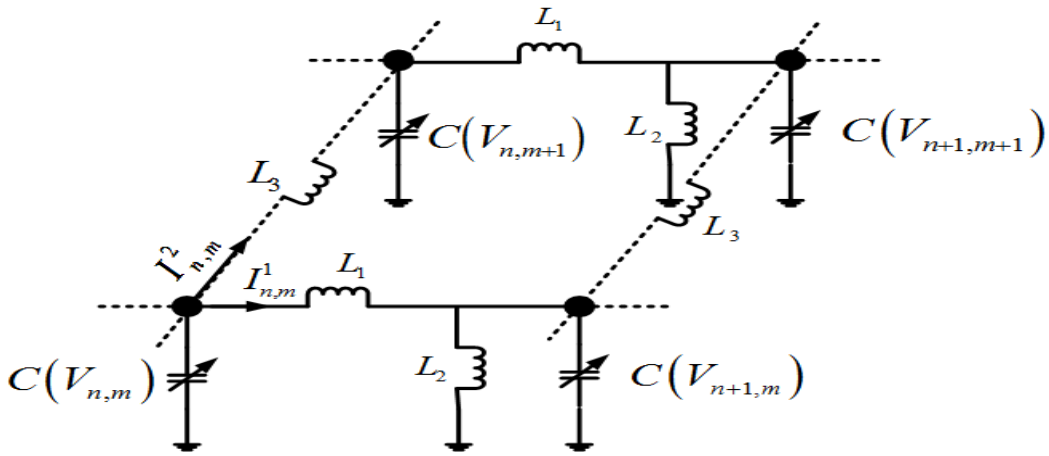

Figure 3.36: *Schematic representation of the NETL.*

In the network, nonlinearity is introduced by a varicap diode which admits that the capacitance varies with the applied voltage. The voltage dependance relation is assumed to have a polynomial form given by

$$Q\left(V_{n,m}\right) = C_0\left(V_{n,m} - \alpha V_{n,m}^2 + \beta V_{n,m}^3\right) \tag{3.76}$$

where C_0, α and β are constants. In the present work, we set $\alpha = 0.21\ V^{-1}$ and $\beta = 0.0197\ V^{-2}$. Applying Kirchoff's laws to this system leads to the following set of propagation equations:

$$\frac{d^2}{dt^2}(V_{n,m}-\alpha V_{n,m}^2+\beta V_{n,m}^3)-U_0^2(V_{n+1,m}-2V_{n,m}+V_{n-1,m})+\omega_0^2 V_{n,m}-\Omega_0^2(V_{n,m+1}-2V_{n,m}+V_{n,m-1}) = 0 \tag{3.77}$$

with $U_0^2 = 1/(C_0L_1)$, $\omega_0^2 = 1/(C_0L_2)$ and $\Omega_0^2 = 1/(C_0L_3)$. Equation (3.77) is the differential equation governing the wave propagation in the network under consideration. As one can see, all of the lines have the same characteristic frequency. This is due to the fact that all of the lines are identical. Ω_0 is the coupling frequency. The properties of the network can be studied by using a solution of the form

$$V_{n,m}(t) = \varepsilon A(x,y,t)e^{i\theta} + \varepsilon^2[\psi(x,y,t) + B(x,y,t)e^{2i\theta}] + cc \tag{3.78}$$

where $\theta = kn + qm - \omega t$ is the phase and $"cc"$ stands for the complex conjugated of the preceding expression; k and q are the wave numbers respectively in the n and m direction; ω is the angular frequency; ε is a small parameter. For the semi-discrete approximation, we set

$$\begin{cases} \tau = \varepsilon^2 t \\ x = \varepsilon(n - v_g t) \\ y = \varepsilon(m - u_g t \end{cases} \tag{3.79}$$

to obtain the short wavelength envelope solitons; v_g and u_g are the group velocities respectively in the n and m direction. Substituting Eq.(3.78) into Eq.(3.77), we obtain different equations as power series of.

↬ The coefficient of ε, proportional to $exp(i\theta)$, gives the dispersion relation

$$\omega^2 = 4U_0^2 \sin^2\left(\frac{k}{2}\right) + 4\Omega_0^2 \sin^2\left(\frac{q}{2}\right) + \omega_0^2 \tag{3.80}$$

This dispersion relation shows that our network is a band-pass filter. Figure 3.37 represents the evolution of the angular frequency in the first brillouin zone for the n direction. To plot Eq.(3.80), we fix $q = \pi$.

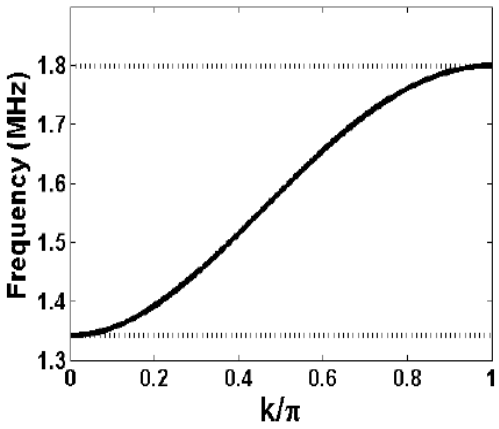

Figure 3.37: *Dispersion graph obtained with $L_1 = L_2 = L_3 = 0.22\ mH$; $C_0 = 320\ pF$.*

The group velocity is taken to be

$$v_g = \frac{U_0^2 \sin(k)}{\omega} \tag{3.81}$$

This group velocity is represented in Fig. 3.38.

↬ The coefficient of ε^2, proportional to $exp(2i\theta)$, leads to the following relation:

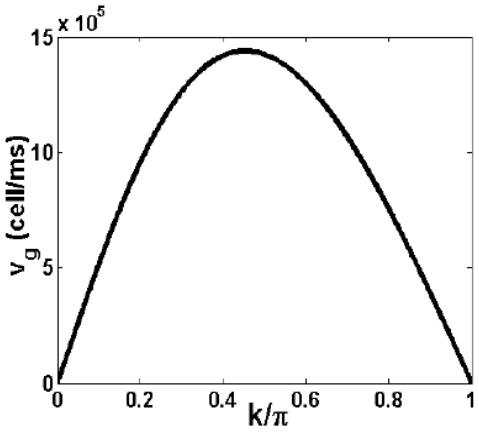

Figure 3.38: *Group velocity obtained for the same parameters as in figure 3.37*

$$B = \frac{\alpha\omega^2}{\omega^2 - U_0^2\sin^2(k) - \Omega_0^2\sin^2(q) - \omega_0^2/4}A^2 \tag{3.82}$$

↬ From the coefficient of ε^3, proportional to $exp(i\theta)$, we obtain the following two-dimensional nonlinear Schrödinger equation for A:

$$iA_\tau + P_1A_{xx} + P_2A_{yy} + P_3A_{xy} + Q|A|^2A = 0 \tag{3.83}$$

with the following definitions

$$\begin{cases} P_1 = (U_0^2\cos(k) - v_g^2)/2\omega \\ P_2 = (\Omega_0^2\cos(q) - u_g^2)/2\omega \\ P_3 = -u_gv_g/2\omega \\ Q = 3\beta/2\alpha^2 - \delta/\alpha \\ \delta = \alpha\omega^2/(\omega^4 - U_0^2\sin^2(k) - \Omega_0^2\sin^2(q) - \omega_0^2/4) \end{cases} \tag{3.84}$$

The numbers P_1, P_2 and P_3 are the dispersion coefficients, while Q is the nonlinearity coefficient of the nonlinear Schrödinger equation.

3.5.2 Solution and stability of NLS

The focal point here corresponds to the determination of the solution of Eq.(3.83). Before the discovery of solitons, mathematicians thought that nonlinear differential equations could not be solved, at least not exactly. However, solitons lead to the recognition that through a combination of such diverse subjects as quantum physics and algebraic

geometry, one can actually solve some nonlinear equations exactly. This innovation opens up a wide window in the world of nonlinearity [101]. With the development of soliton theory, many powerful methods for obtaining the exact solutions of NETLs have been presented [102–106]. In the present case, we use the variational method [107]. This method is a powerful solution method for the computation of exact traveling wave solutions. Because of the complexity of the nonlinear wave equations, there is no unified method to find all solutions of these equations. Here, we look for a propagating wave under the form:

$$A\left(x,y,\tau\right)=a\left(z\right)e^{i(g(z)+\Omega\tau)} \tag{3.85}$$

where $a(z)$ is the amplitude, $g(z)$ is the phase, Ω represents the spectral parameter of the wave and $z=x+y-v_e\tau$ the single variable for the amplitude, depending on v_e which is the velocity of the wave packet. By substituting Eq.(3.85) into the two-dimensional NLS Eq.(3.83), and equating real and imaginary parts to zero, the following two coupled ordinary differential equations are obtained:

$$\begin{cases} -v_e a'+2Pa'g'+Pg''a=0 \\ \left(v_e g'-\Omega\right)a+P\left(a''-ag'^2\right)+Qa^3=0 \end{cases} \tag{3.86}$$

where the prime stands for derivation with respect to z and $P=P_1+P_2+P_3$. By multiplying the first equation of (3.86) by $a(z)$ and integrating once, it follows that the phase g is related to the amplitude $a(z)$ through the expression:

$$\left(\frac{v_e}{2}-Pg'\right)a^2=k_1 \tag{3.87}$$

where k_1 is the constant of integration, which can naturally be taken as $k_1=0$ for all continue solution at the origin $a=0$. Taken then $k_1=0$, Eq.(3.87) yields

$$g'=\frac{v_e}{2P} \tag{3.88}$$

By substituting Eq.(3.88) into the second equation of (3.86), we arrive to the following differential equation satisfied by the amplitude $a(z)$:

$$Pa''+Qa^3+\left(\frac{v_e^2}{4P}-\Omega\right)a=0 \tag{3.89}$$

from which the first integral is obtained by multiplying Eq.(3.89) by a' and integrating the resulting equation:

$$a'^2 + \frac{Q}{2P}a^4 + \left(\frac{v_e^2}{4P^2} - \frac{\Omega}{P}\right)a^2 = \frac{2k_2}{P} \tag{3.90}$$

with k_2, another constant of integration. Let us mention that, Eq.(3.90) can be also derived from the auxiliary Hamiltonian $\widetilde{H}$ and lagrangian $\widetilde{L}$ defined as follows:

$$\begin{cases} \widetilde{H} = \frac{1}{2}m(a)\left[a'^2 + U(a)\right] \\ \widetilde{L} = \frac{1}{2}m(a)\left[a'^2 - U(a)\right] \end{cases} \tag{3.91}$$

This Hamiltonian may be viewed as the energy of a particle with an effective mass $m(a) = 1$ moving in the effective potential

$$U(a) = \frac{Q}{2P}a^4 + \frac{v_e^2 - 4P\Omega}{4P^2}a^2 - \frac{2k_2}{P} \tag{3.92}$$

It is obvious that equation (3.89) can be transformed into the following equivalent autonomous dynamic system:

$$\begin{cases} \frac{da}{dz} = a' \\ \frac{da'}{dz} = \left(-\frac{Q}{P}a^2 + \frac{\Omega}{P} - \frac{v_e^2}{4P^2}\right)a \end{cases} \tag{3.93}$$

where solutions are the fixed points of the system. The number of equilibrium points, and consequently the dynamic of this system depends on the sign of the quantity

$$F_0 = \frac{v_e^2 - 4P\Omega}{4PQ} \tag{3.94}$$

In fact, when $F_0 > 0$, the system (3.93) admits only the equilibrium point $(0, 0)$ and consequently, none nonlinear localized wave (NLW) can be obtained. However, for $F_0 < 0$, the system admits three equilibrium points: $(0, 0)$ and $(0, \pm A_{eq})$, with

$$A_{eq} = \sqrt{\frac{4\Omega_0 P - v_e^2}{4PQ}}. \tag{3.95}$$

From the linear stability analysis, it appears that the stability of these equilibrium points depend on the sign of the product PQ (the saddle point is obtained if $\lim_{a=A_{eq}} \frac{d^2U(a)}{da^2} < 0$ and the center point else). In fact, when $PQ > 0$, the equilibrium point $(0, 0)$ is a saddle while the two others, $(0, A_{eq})$, are the centers. This analysis is confirmed by the phase plane plot of the system sketched in Fig.3.39.(1) obtained for the numerical values of parameters: $P = Q = 1.0$, $v_e = 0.0$ and $\Omega = 1.0$; that is $PQ > 0$ and $4P\Omega - v_e^2 > 0$, in which closed trajectories are present. These trajectories indicate that small oscillations of

the system as well as periodic solutions are possible and are separated by the homoclinic orbit known as the separatrix characterizing the existence of pulse soliton or bright solitary waves (BSW) in the context of the NLS system. These BSW are nonlinear solutions of Eq.(3.93) with the vanishing boundary conditions

$$\lim_{z\longrightarrow\infty} a = 0, \quad \frac{da}{dz} = 0 \quad for \quad a = A_0, \quad and \quad \frac{d^n a}{dz^n} = 0 \quad for \quad a = 0, n = 1, 2, ... \quad (3.96)$$

where A_0 is the maximum amplitude of the envelope wave. The condition (3.96) leads to the following constraint to be satisfied by the integrating constant k_2 and the spectral parameter Ω

$$k_2 = 0, \quad and \quad \Omega = \frac{v_e^2}{4P} + \frac{Q}{2}A_0^2. \quad (3.97)$$

However, when $PQ < 0$, there is a changes in the properties of the above equilibrium

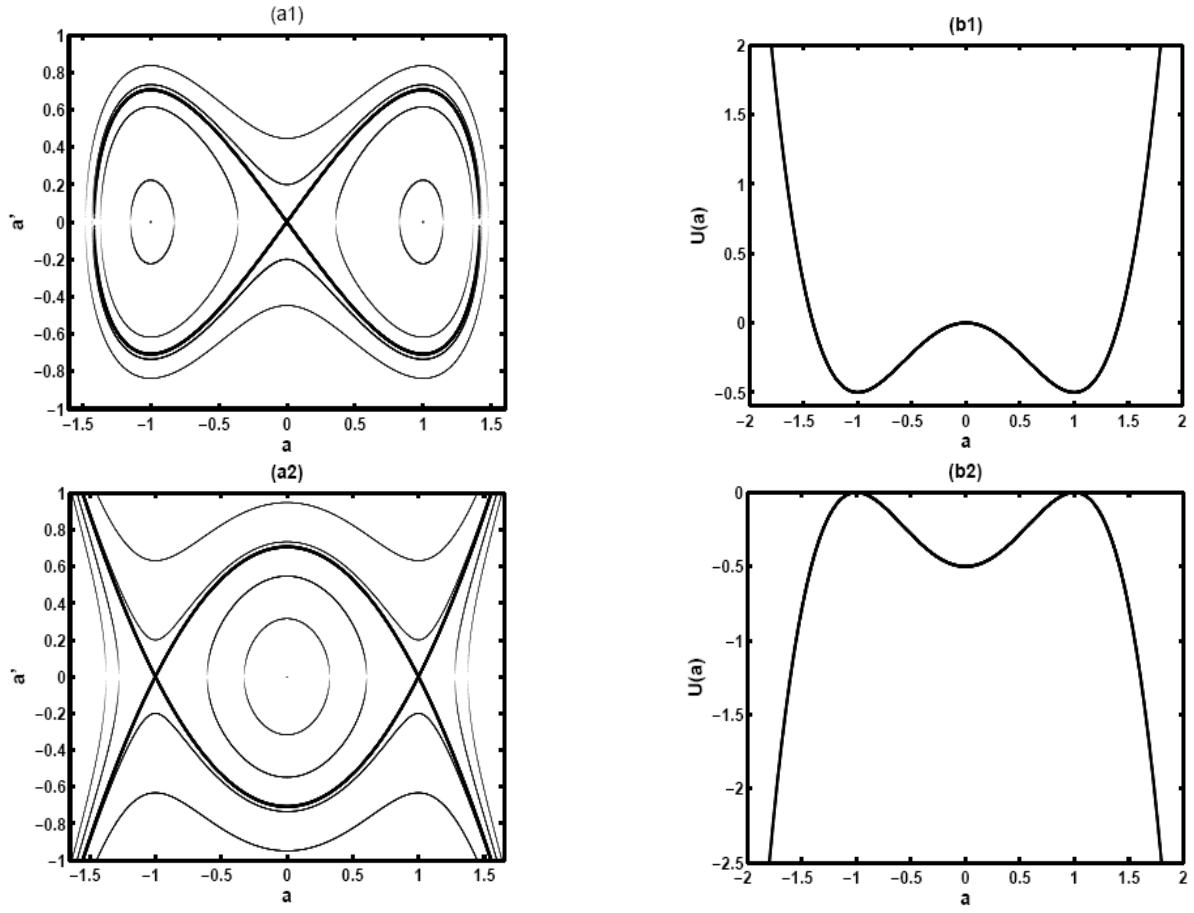

Figure 3.39: *Phase plane plot (a), and the effective potential U(a) (b) of the system described by the NLS equation. The homoclinic orbit (a1) and the heteroclinic orbit (a2) are plotted in bolt lines.*

points; $(0, 0)$ becomes a center while $(0, \pm A_{eq})$ are the saddle points. The phase plane plot

sketched in **Fig.3.39.(2)**, obtained for $P = -Q = 1$, $v_e = 0.0$ and $\Omega = -1$; that is $PQ < 0$ and $4P\Omega - v_e^2 < 0$ shows a changes in the behavior of the system. The closed and open orbits are now separated by the heteroclinic orbits which evidences the existence of dark solitary waves (DSW) which are NLW satisfying the non vanishing boundary conditions

$$\lim_{z \longrightarrow \infty} a = A_0, \quad \frac{d^n a}{dz^n} = 0 \quad for \quad a = A_0, n = 1, 2, ... \tag{3.98}$$

from which the following expressions of the spectral parameter and the integration constant are obtained:

$$\Omega = \frac{v_e^2}{4P} + QA_0^2, \quad and \quad k_2 = -\frac{Q}{4}A_0^4. \tag{3.99}$$

The plot of the effective potential $U(a)$ indicates the presence of a double wells when $PQ > 0$ and a single well for $PQ < 0$ which are in agreement with results of the phase plane plots. It is then obvious that the solutions of NLS equation depend on the sign of the product PQ.

3.5.2.1 Bright solitary waves as solution

Now we focus our attention to the derivation of bright solution (in this case $PQ > 0$) of the NLS. For this end, the integration constant $k_1 = 0$, while k_2 and the spectral parameter Ω will be taking as given in Eq.(3.97); thus, Eq.(3.90) can be rearranged as

$$\left(\frac{da}{dz}\right)^2 = \mu^2 a^2 (1 - a^2/A_0^2), \tag{3.100}$$

which admits the following well-known one bright soliton solution

$$a(z) = A_0 sech\left[\mu(z - z_0)\right], \tag{3.101}$$

with $\mu = A_0\sqrt{\frac{Q}{2P}}$; μ is a parameter describing the pulse width. From Eq.(3.88), the phase $g(z)$ is given by

$$g = \frac{v_e}{2P}(z - z_0), \tag{3.102}$$

where z_0 is the initial position of the wave which can be equal to zero. Hence the solution of the NLS equation can explicitly be rewritten as:

$$A(x, y, \tau) = A_0 sech\left[A_0\sqrt{\frac{Q}{2P}}(x + y - v_e\tau)\right] \exp\left\{i\left[\frac{v_e}{2P}(x + y - v_p\tau)\right]\right\}, \tag{3.103}$$

where v_p is the carrier velocity, with the following expression

$$v_p = v_e - \frac{2P\Omega}{v_e} \tag{3.104}$$

As for the particular case of solution with stationary phase in time ($v_p = 0$), we have:

$$v_{e\pm} = \pm A_0\sqrt{2PQ} \quad and \quad \Omega = QA_0^2 \tag{3.105}$$

3.5.2.2 Stability of solitary waves

Having found this solution, we then check its stability because an important aspect of any family of solutions is their stability properties. For conservative systems, under certain conditions, it is possible to derive an analytical criterion for linear stability of solitons, which involves only the dependence of invariants on the solution parameters. The stability of the BSW is determined here by the dependence of the norm (the power) on the velocity v_e. Solitons are stable if $\frac{dN}{dv_e} > 0$ and unstable otherwise [108]. For the model considered here, $N(v_e)$ can be found analytically as $N = \int_{-\infty}^{+\infty} a^2 dz$, leading to:

$$N = A_0^2 \int_{-\infty}^{+\infty} \frac{dz}{\cosh^2(\mu z)} = \frac{2A_0^2}{\mu} \tag{3.106}$$

Substituting the v_e obtained in Eq.(3.105) into (3.106), one obtains

$$N = \frac{v_e^2}{PQ\mu}, \tag{3.107}$$

which is an increasing function of the envelope velocity for $PQ > 0$ and then pulse soliton is stable.

3.5.2.3 Condition for possible MI

MI is a generic nonlinear phenomenon governing nonlinear wave propagation in dispersive an nonlinear media; it leads to a self-induced modulation of an input plane wave with the subsequent generation of localized pulses. To determine the conditions of instability of the modulated waves in the network, we use the plane wave solution given below:

$$A\left(x, y, \tau\right) = A_0 e^{i\left(\widetilde{k}x + \widetilde{q}y - \varpi\tau\right)} \tag{3.108}$$

By inserting equation (3.108) into equation (3.83), we have the following dispersion relation:

$$\varpi = \widetilde{k}^2 P_1 + \widetilde{q}^2 P_2 + \widetilde{k}\widetilde{q} P_3 - QA_0^2. \tag{3.109}$$

The linear stability of this continuous wave can be investigated by looking for a solution of the form

$$A\left(x, y, \tau\right) = \left(A_0 + b(x, y, \tau)\right) e^{i\left(\widetilde{k}x + \widetilde{q}y - \varpi\tau + \theta(x,y,\tau)\right)} \tag{3.110}$$

where $b(x,y,\tau)$ and $\theta(x,y,\tau)$ are small perturbations for the amplitude and for the phase respectively; they can be write as follows:

$$\begin{cases} b\,(x,y,\tau) = b_0 e^{i(\delta x+\sigma y-\nu\tau)} \\ \theta\,(x,y,\tau) = \theta_0 e^{i(\delta x+\sigma y-\nu\tau)} \end{cases} \tag{3.111}$$

Substituting (3.110) and (3.111) into Eq.(3.83), one obtains a system for the perturbations. For the nontrivial solutions of this system, we then have:

$$\left[\nu - 2\widetilde{k}\delta P_1 - 2\widetilde{q}\delta P_2 - \left(\widetilde{q}\delta + \widetilde{k}\sigma\right) P_3\right]^2 = \left(\delta^2 P_1 + \sigma^2 P_2 + \delta\sigma P_3\right)^2 \left(1 - \frac{2QA_0^2}{\delta^2 P_1+\sigma^2 P_2+\delta\sigma P_3}\right) \tag{3.112}$$

It appears that the behavior of ν depends on the quantity $\frac{Q}{\delta^2 P_1+\sigma^2 P_2+\delta\sigma P_3}$. In one hand, if this quantity is negative, the plane wave solution of NLS equation is stable. On the other hand, if this quantity is positive, $\left[\nu - 2\widetilde{k}\delta P_1 - 2\widetilde{q}\delta P_2 - \left(\widetilde{q}\delta + \widetilde{k}\sigma\right) P_3\right]^2$ could be negative under certain conditions and the consequence is that the plane wave solution of NLS equation is unstable; hence, it appears MI phenomenon in the line. This instability induces the formation of small wave packets or envelope pulse solitons train, solution of the NLS Eq.(3.83).

3.5.3 Numerical experiments

This section is intended to present the numerical experiments on the propagation of slowly modulated waves in the network, this to check the analytical calculations presented in the previous sections. The numerical experiments are carried out on Eq.(3.77) describing the propagation of waves in the NETL of figure 3.36. The wave is introduced in the following form

$$V(t) = V_0\left[1 + \widetilde{m}\cos(2\pi f_m\tau)\right]\cos(2\pi f_p\tau) \tag{3.113}$$

where f_m is the modulation frequency, V_0 is the amplitude of the wave and $\widetilde{m}$ is the modulation rate. We take $f_m = 54kHz$, $V_0 = 0.2\ V$ and $\widetilde{m} = 1\%$. A fourth-order Runge-Kutta algorithm has been used and a normalized integration time step $\Delta t = 2\times10^{-3}$ is used for numerical simulations. Similarly, the number of cells N in the n direction is chosen to be equal to 3000 and we have used periodic boundary conditions so that we do not encounter the wave reflection at the end of the line. In the m direction, we have taken $M = 18$. The parameters of the network are the same as in figure 3.37. This simulation is made in the case where $\delta = \sigma$, $\widetilde{k} = \widetilde{q}$ that is $P = P_2 + P_2 + P_3$. We take the carrier frequency $f_p = 1752\ kHz$.

Figure 3.40 shows the evolution of the plane wave in the network. On this figure, we observe examples of the MI exhibited by the network. As time goes on, the wave exhibits a modulation of its amplitude, which leads to the formation of wave packets which is in agreement with the analytical calculations. In the view to consolidate the validity

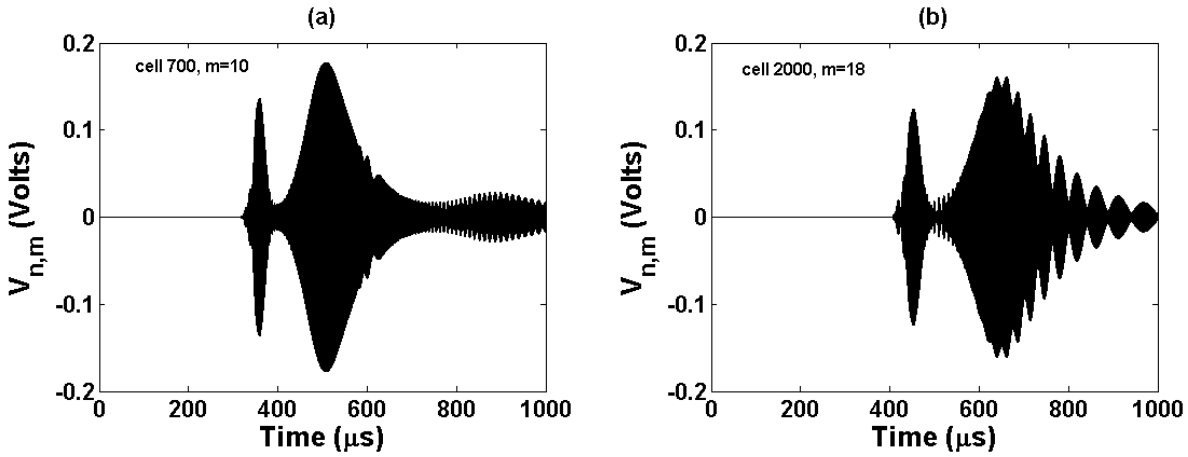

Figure 3.40: *Propagation of waves through the network at the cell* 700 *for* $m = 10$ *(a) and at the cell* 2000 *for* $m = 18$ *(b). The parameters of the network are:* $L_1 = L_2 = L_3 = 0.22\ mH$; $C_0 = 320\ pF$.

of preceding results, we propagate the solution of the NLS since the above observed Benjamin-Feir instability constitutes the proof that the network can support envelope solitons. For this purpose, we take as input voltage the profile of a modulated soliton given by Eq.(3.114)

$$V(t) = V_m \sec h\left(\mu v_g \tau\right) \cos\left(2\pi f_p \tau\right) \tag{3.114}$$

In Fig. 3.41, we depict the time evolution of relation (3.114) in the line characterized by equation (2) for the same frequency as in Fig.3.40. This result confirms the fact that our network can support the pulse soliton. On this last figure, we can observe the fission of two-bound solitons; this can be explained by the additional terms in the NLS equation. A similar phenomenon has been already obtained in the context of higher-order NLS by David Yemélé *et al.* [10].

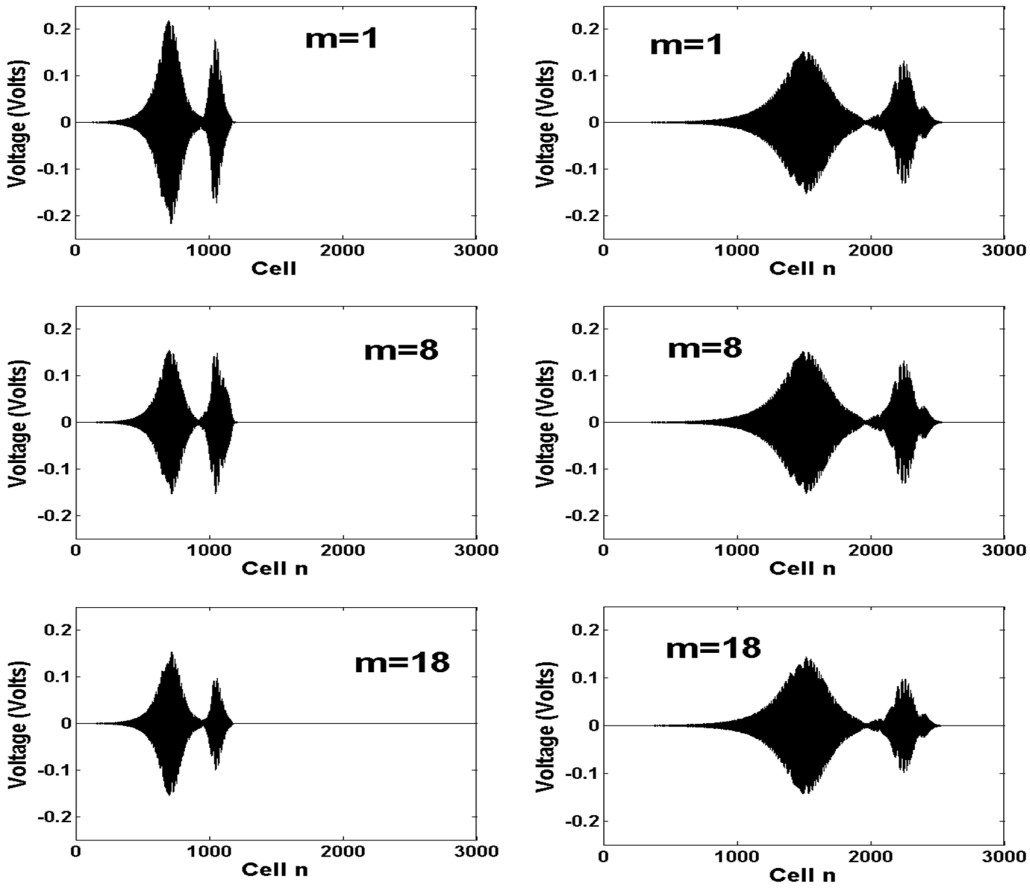

Figure 3.41: *Propagation of envelope soliton signal voltage as a function of cell number n at different times. The left column is obtained for* $t_1 = 450$ μs *while the right is obtained for* $t_2 = 850$ μs*. The parameters are the same as in figure 3.40.*

3.5.4 Concluding remarks

In this section, we have considered a system of coupled nonlinear dispersive transmission lines and we have shown that the voltage for the transmission lines is described by a two-dimensional nonlinear Schrödinger equation. The exact transverse solution has been found and its stability has been studied. The condition for which the network can exhibit modulational instability is also determined and we observe a good agreement between analytical calculations and numerical simulations.

Conclusion

The aim of this chapter is to discuss the results of our findings. We have solved four main problems namely: the study of the effect of nonlinear coupling on modulational instability, the study of the effect of second-neighbor inductive coupling on the modulational instability in a coupled line of transmission, the suppression of modulated waves mixing in coupled nonlinear LC transmission lines and the study of the transverse stability in the discrete inductance-capacitance electrical network. The main results are summarized in the different concluding remarks.

General Conclusion

$\rightsquigarrow$ **Main Results of the Thesis**

Throughout this dissertation, we have studied the nonlinear dynamics on some nonlinear electrical lines. The thesis has been organised in three parts.

In chapter 1, we made a literature review on the soliton, nonlinear electrical transmission lines and modulational instability;

The second chapter was devoted to methodology. We presented the mathematical and numerical methods used to achieve our goals;

The last chapter discussed the results of our investigations.

The main objectives of this work were:

• to study the effect of nonlinear coupling on modulational instability in nonlinear transmission lines; we show that by coupling NETLs in this way, the propagation of waves in each line can be alternatively described by two nonlinear Shrödinger equations according to the direction of the current flow through the coupling branch. We also point out that the nonlinear coupling adds the domains of modulational instability (MI) of each line. Finally, we show that a small variation of the nonlinear elements used in the coupling branch can change significantly the behavior of the network.

• to study the effect of second-neighbor inductive coupling on the modulational instability in a coupled line of transmission; as result, we found that the second-neighbor couplings add new maxima of gain; increase the group velocity, and the magnitude of the wave. Therefore, the network becomes more stable to small external perturbations.

• to study the suppression of modulated waves mixing in coupled nonlinear LC transmission lines. It results from our investigation that: the entire network needs only the half of the total number of additive linear inductors compared to that found in the literature; the overall bandwidth is wider; the new coupling type allows the suppression of some mixing of modes without excluding very low frequencies; hence, it becomes possible to think of using the high group velocities of low frequencies of the first-mode. With another

model, we confirm that for the suppression of modulated waves mixing in coupled nonlinear LC transmission lines, the entire network needs only the half of the total number of additive linear inductors compared to that found in the literature. It also results from this work that: On one hand, the difference between the two lines induced the fission for only one mode of propagation. This fission is influenced by the amplitude of the signal and the amount of the input energy as well; it also narrows the width of the input pulse soliton, leading to a possible increasing of the bit rate. On the other hand, the dissymmetry of the two lines converts the network into a good amplifier for the ω_{-} mode which corresponds to the regime admitting low frequencies.

$\rightsquigarrow$ Open problems and future directions

Despite the results that were found in this thesis, other points of interest may be solved in the future.

• In this thesis we have derived only one type of soliton (envelope solution) of the NLS equation. It would also be interesting to derive other types of soliton such as dark soliton which can describe other physical properties of the network.

• We have used for numerical investigations on the full equation of the NETL the exact analytical solution for the NLS equation instead of real NETL analytical solution. We propose to look for these kinds of solution both in the case of continuous approximation and its discrete fundamental form.

• The NLS equation derived in this thesis may be also used to describe the same phenomena in many nonlinear systems. It is important to mention that, the NLS equation obtained here has been derived under the Tanuiti reductive method; it would be also interesting to know the effect of higher harmonics contribution generated by the NETL on this equation.

• Our study also focused on the analytical and numerical study of modulated waves. To complete our knowledge in such subjects, experimental studies through dissipative nonlinear electrical transmission lines should be carried out.

Bibliography

[1] P. Rosenau and J. M. Hyman, Phys. Rev. Lett. 70, (1993) 564; P. Rosenau, Phys. Rev. Lett. 73, (1994) 1737.

[2] F. Cooper, J. M. Hyman, and A. Khare, Phys. Rev. E 64, 026608 (2001).

[3] A. C. Scott and L. Macheil, Phys. Lett. A 98, 87 (1983).

[4] A. Nogochi, Electron. Commun Japan A 57 9 (1974).

[5] A. J. Sievers and S. Takeno, Phys. Rev. Lett. 61, 970 (1988).

[6] J. A Kolosick, D. K. Landt, H. C. S. Suan, and K. E. Lonngren, Proc. IEEE 62 578.

[7] W. P. Su, J. R. Schrieffer and A. J. Heeger, Phys. Rev. Lett. 42, 1698 (1979).

[8] D. Jäger Appl. Phys 16 35 (1978);

[9] D. Jäger, J. Phys. Soc. Japan 51 1686 (1982).

[10] S. Watanabe, M. Miyakaya and K. Muroya, J. Phys. Soc. Japan. 48, 1029 (1980).

[11] R. Hirota and K. Suziki, 28, 1366 (1970).

[12] K. Fukushima, J. Phys. Soc. Japan 52, 376 (1983).

[13] P. Marquie, J. M. Bilbault and M. Remoissnet, Phys. Rev. E 49, 828 (1994).

[14] P. Marquie, J. M. Bilbault and M. Remoissnet, Phys. Rev. E 51, 6127 (1995).

[15] F. B. Pelap and M. M. Faye, J. Math. Phys. 46, 033502 (2005).

[16] K. Tse Ve Koon, J. Leon, P. Marquié, and P. Tchofo-Dinda, Phys. Rev. E 75, 066604 (2007).

[17] E. Kengne, R. Vaillancourt, Can. J. Phys. 87, 1191 (2009).

[18] Saïdou Abdoulkary, Tibi Beda, S. Y. Doka, Fabien II Ndzana, Louis Kavitha, and Alidou Mohamadou, J. Mod. Phys. 3, 438 (2012).

[19] Fabien Kenmogne and David Yemélé, Phys. Rev. E, 88, 043204 (2013).

[20] G. B. Whitham, Linear and Nonlinear Waves (Wiley, New York) (1974).

[21] G. L. Lamb, Elements of Soliton Theory (Wiley, New York) (1980).

[22] R. K. Dodd, Eilbeck J C, Gibbon J D and Morris H C, Solitons and Nonlinear Wave Equations (Academic Press, London) (1982).

[23] J. N. Dinkel, Setzer C, Rawal S and Lonngren K E, Chaos, Solitons Fractals, 12, 91 (2001).

[24] R. M. Nguimdo, S. Noubissié, and P. Woafo, J. Phys. Soc. Jpn. 77, 124006 (2008).

[25] P. K. Shukla, Phys. Plasmas, 10, 1619 (2003).

[26] T. Yoshinaga and Kakutani T J. Phys. Soc. Japan 49, 2072 (1980).

[27] T. Kakutani and N. Yamasaki: J. Phys. Soc. Jpn. 45, 674 (1978).

[28] D. Yemélé and T. C. Kofané: J. Phys. D 39, 4504 (2006).

[29] D. C. Hutchings and J. M. Arnold: J. Opt. Soc. Am. B 16, 513 (1999).

[30] T. Yoshinaga and T. Kakutani: J. Phys. Soc. Jpn. 56, 3447 (1987).

[31] J. S. Russell, Report of the fourteenth meeting of the British Association for the Advancement of Science, York, September 1844 (London 1845), pp 311-390, Plates XLVII-LVII.

[32] H. Helmholtz, Arch. Anat. Physiol. 57, 276 (1850).

[33] O. Lehmann, Ann. Phys. 4, 1 (1902).

[34] J. W. Rayleigh, Phil. Mag. 1, 257 (1876).

[35] J. Boussinesq, Compt. Rend. Acad. Sc. 72, 755 (1871).

[36] D. J. Korteweg and H. de Vries, Phil. Mag. 39, 422 (1895).

[37] M. Peyrard and T. Dauxois, Physique des solitons. EDP Sciences/CNRS EDITIONS, (2004).

[38] N. J. Zabusky and M. D. Kruskal, Phys. Rev. Lett. 15, 240 (1965).

[39] C. S. Gardner et al., Phys. Rev. Lett. 19, 1095 (1967).

[40] V. E. Zakharov and A. B. Shabat, Funct. Anal. Appl. 8, 226 (1974).

[41] http://pe.soliton.free.fr/solitons.htm.

[42] P. G. Drazin and R. S. Johnson, Solitons: An Introduction. Cambridge, U.K.: Cambridge Univ. Press, 1989.

[43] A. T. Filippov, The Versatile Soliton. Boston, MA: Birkhauser, 2000.

[44] M. Remoissenet, Waves Called Solitons: Concepts and Experiments. New York: Springer-Verlag, 1999.

[45] A. C. Scott, Active and Nonlinear Wave Propagation in Electronics (Wiley, New York, 1970).

[46] M. Remoissenet, Waves Called Solitons(Springer, Berlin, 1996) 2nd ed.

[47] Aurélien Kenfack-Jiotsa and Eric Tala-Tebue: J. Phys. Soc. Jpn, 80, 034003 (2011).

[48] A.B. Togueu Motcheyo, C. Tchawoua, M. Siewe Siewe, J.D. Tchinang Tchameu, Commun. Non. Sci. Numer. Simulat., 18, 946 (2013).

[49] B. Z. Essimbi, T. C. Kofane, and J. M. Ngundam, Physica Scripta, 67, 157 (2003).

[50] F. Ndzana II, A. Mohamadou, and T. C. Kofané: Phys. Rev. E 79, 047201 (2009).

[51] F. Ndzana II, A. Mohamadou, and T. C. Kofané: Phys. Rev. E 78, 016606 (2008).

[52] E. N.Economou. Green's Functions in Quantum Physics. Springer- Verlag, Berlin, 2nd edition, 1990.

[53] A. Bezryadina, D. N. Neshev, A. S. Desyatnikov, J. Young, Z. Chen, and Yu. S. Kivshar, Opt. Express, 14, 8317 (2006).

[54] J. C. Eilbeck and M. Johansson. The discrete nonlinear Schrödinger equation - 20years on. In L. Vázquez, R.S. MacKay, and M. P. Zorzano, editors, Proceeding of the Third Conference on Localization and Energy Transfer in Nonlinear Systems, pp 44. World Scientific, Singapore, 2003.

[55] Michael Garth Case, Nonlinear Transmission Lines for Picosecond Pulse, Impulse and Millimeter-Wave Harmonic Generation . PhD. dissertation, University of California Santa Barbara, July 2, 1993.

[56] D.S. Ricketts, X. Li, and D. Ham, IEEE Trans., Micrw. Theory Tech. 54, 373 (2006).

[57] T.B. Benjamin, Proc. Roy. Soc. A., 299 (1967) 59U75.

[58] M. I. Carvalho, S. R. Singh, and D. N. Christodoulides, Phys. Rev. Lett., 82, 394 (1999).

[59] Benjamin, T. Brooke, Feir, J.E., Journal of Fluid Mechanics 27 (3), 417 (1967).

[60] V. I. Bespalov and V. I. Talanov, Pis'ma Zh. Eksp. Teor. Fiz. 3, 471 (1966) [JETP Lett. 3, 307 (1966)].

[61] Agrawal, Govind P.. Nonlinear fiber optics (2nd ed.). San Diego (California): Academic Press. ISBN 0-12-045142-5 (1995).

[62] Yuen, H.C.; Lake, B.M., 12, 303 (1980).

[63] Janssen, Peter A.E.M., Journal of Physical Oceanography 33 (4), 63 (2003).

[64] Dysthe, Kristian; Krogstad, Harald E.; Müller, Peter, Annual Review of Fluid Mechanics 40, 287 (2008).

[65] M. Soljacic, M. Segev, T. Coskun, D. N. Christodoulides, and A. Vishwanath, Phys. Rev.Lett., 84, 467 (2000).

[66] D. Kip, M. Soljacic, M. Segev, E. Eugenieva, and D. N. Christodoulides, Science 290, 495 (2000).

[67] J. Klinger, H. Martin, and Z. Chen, Opt. Lett., 26, 271 (2000).

[68] http://archaero.com/Vayres-Mascaret-6382.jpg.

[69] D. Yemélé, F. Kenmogné , Phys. Lett. A 373, 3801 (2009).

[70] D. Yemélé, P. Marquié, J.M. Bilbault, Phys. Rev. E 68, 016605 (2003).

[71] T. Taniuti, N. Yajima, J. Math. Phys. 10, 1369 (1969).

[72] Aurelien Kenfack-Jiotsa, Eric Tala-Tebue, Serge Bruno Yamgoué, Marius Hervé Tatchou-Ntemfack, and Timoléon Crépin Kofané, work submitted.

[73] F. Ndzana, A. Mohamadou and T. C. Kofané, J. Phys. D: Appl. Phys. 40, 3254 (2007).

[74] A. C Scott. Nonlinear Science, second edition. Oxford University Press, Oxford, (1999).

[75] S. Takeno, J. Phys. Soc. Japan, 61, 2821 (1992).

[76] S. Takeno, J. Phys. Soc. Japan, 59, 3861 (1990).

[77] S. Takeno, and K Hori. J. Phys. Soc. Japan, 60, 947 (1991).

[78] S. Takeno, K. Kisoda, and A. J. Sievers Prog. Theor. Phys. Suppl. 94, 242 (1988).

[79] S. Wang, Phys. Lett. A, 182, 105 (1993).

[80] H. Willaime, O. Cardoso, and P. Tabeling, Phys. Rev. Lett. 67, 3247 (1991); A. Mohamadou, A. K. Jiotsa, and T. C. Kofane, Phys. Rev. E 72, 036220 (2005).

[81] N. K. Efremidis and D. N. Christodoulides: Phys. Rev. E 65, 056607 (2000).

[82] Yang X. S., Liu S. Q., and Li X. Q. Gravitation & Cosmology, 16 316 (2010).

[83] Kharif C., Kraenkel R. A., Manna M. A., and Homas R., J. Fluid Mech., 664 138 (2010).

[84] Sarma A. K., Eur. Phys. Lett., 92, 24004 (2010).

[85] Raja R. V. J., Porsezian K., and Nithyanandan K., Phys. Rev. A, 82 013825 (2010).

[86] Masood W., Shah H. A., Tsintsadze N. L., and Qureshi M. N. S., Eur. Phys. Journal D, 59 413 (2010).

[87] Nimje N., Dubey S., and Ghosh S. K., Eur. Phys. Journal D, 59, 223 (2010).

[88] Mohamadou A., Latchio-Tiofack C. G., and Kofané T. C., Phys. Rev. E, 82 016601 (2010).

[89] Kengné E., Vaillancourt R., and Malomed B. A., Int. J. Mod. Phys. B, 24 2211 (2010).

[90] Bronski J. C. and Johnson M. A., Archive for Rational Mechanics and Analysis, 197, 357 (2010).

[91] Dinda P. T. and Porsezian K., J. Opt. Soc. Am B, 27 1143 (2010).

[92] Kalithasan B., Porsezian K., Senthilnathan K., and Dinda P. T., Phys. Rev. A, 81, 053802 (2010).

[93] Tabi C. B., Mohamadou A., and Kofané T. C., Eur. Phys. Journal B, 74, 151 (2010).

[94] Alcaraz-Pelegrina J. M. and Rodriguez-Garcia P., Phys. Lett. A, 374 1591 (2010).

[95] Murali R., Porsezian K., Kofané T. C., and Mohamadou A., J. Phys A: Math. Theor., 43, 165001 (2010).

[96] Hasegawa A., Optical Solitons in Fibers, Second Enlarged Edition (Berlin: Springer) (1989).

[97] Geniet F. and Leon J., J. Phys.: Condens. Matter, 15 2933 (2003).

[98] Yamgoué S. B., Morfu S. and Marquié P., Phys. Rev. E, 75, 036211 (2007)).

[99] Tala-Tebue E., Kenfack-Jiotsa A., Tatchou-Temfack M. H. and Kofané T. C., Commun. Theor. Phys., (2013).

[100] Kenfack-Jiotsa A, Tala-Tebue E and Yamgoué, work submited.

[101] M. Antonova, A. Biswas, Commun Nonlinear Sci Numer Simulat. 14, 734 (2009).

[102] S. A. El-Wakiland M.A. Abdou, Chaos, Solitons and Fractals, 31, 840 (2007).

[103] W. Malfliet and W. Hereman, Phys. Script. 54, 568 (1996).

[104] M. Yaghobi Moghaddam, A.Asgari and H.Yazdani, Appl. Math. Comput. 210, 422 (2009).

[105] E. Fan, H. Zhang, Phys. Lett.A, 246, 403 (1998).

[106] R. Hirota. The direct method in soliton theory. Cambridge University Press, Cambridge, 2004.

[107] M. T. Darvishi and M. Naja, International Journal of Applied Mathematical Research, 1, 1 (2012).

[108] W. Krolikowski, O. Bang, Phys. Rev. E 63, 016610 (2000).

Appendix A

Derivation of equation (3.3)

We consider the NETL with the schematic diagram of Fig.3.1. By applying the Kirchhoff's laws at node n for the first line, it follows that:

$$i_n^1 = I_{1,n-1} - I_{1,n} - i_n^2 - j_n \qquad (A1)$$

which can rewrite as follows after one derivative:

$$\frac{di_n^1}{dt} = \frac{d}{dt}\left(I_{1,n-1} - I_{1,n}\right) - \frac{di_n^2}{dt} - \frac{dj_n}{dt}, \qquad (A2)$$

where

$$\begin{cases} j_n = \frac{dQ_{2,n}}{dt} \\ i_n^1 = \frac{dQ_{1,n}}{dt} \\ \frac{dI_{1,n-1}}{dt} = \frac{1}{L_s}\left(V_{1,n-1} - V_{1,n}\right) \\ \frac{dI_{1,n}}{dt} = \frac{1}{L_s}\left(V_{1,n} - V_{1,n+1}\right) \\ \frac{di_n^2}{dt} = \frac{1}{L_p}V_{1,n} \end{cases} \qquad (A3)$$

$I_{1,n-1}$ is obtained between the nodes $n-1$ and n while $I_{1,n}$ is obtained between the nodes n and $n+1$. By inserting (A3) into (A2), we obtain:

$$\frac{d^2Q_{1,n}}{dt^2} = \frac{1}{L_s}\left(V_{1,n+1} - 2V_{1,n} - V_{1,n-1}\right) - \frac{1}{L_p}V_{1,n} - \frac{d^2Q_{2,n}}{dt^2}. \qquad (A4)$$

Similarly, the Kirchhoff's laws at node n for the second line give:

$$j_n^1 = I_{2,n-1} - I_{2,n} - j_n^2 + j_n \qquad (A5)$$

which can rewrite as follows after one derivative:

$$\frac{dj_n^1}{dt} = \frac{d}{dt}\left(I_{2,n-1} - I_{2,n}\right) - \frac{dj_n^2}{dt} + \frac{dj_n}{dt}, \qquad (A6)$$

where

$$\begin{cases} j_n^1 = \frac{dQ_{1,n}}{dt} \\ \frac{dI_{2,n-1}}{dt} = \frac{1}{L_s}\left(V_{2,n-1} - V_{2,n}\right) \\ \frac{dI_{2,n}}{dt} = \frac{1}{L_s}\left(V_{2,n} - V_{2,n+1}\right) \\ \frac{dj_n^2}{dt} = \frac{1}{L_p}V_{2,n} \end{cases} \qquad (A7)$$

By inserting (A7) into (A6), we obtain:

$$\frac{d^2Q_{1,n}}{dt^2} = \frac{1}{L_s}\left(V_{2,n+1} - 2V_{2,n} - V_{2,n-1}\right) - \frac{1}{L_p}V_{2,n} + \frac{d^2Q_{2,n}}{dt^2}. \qquad (A8)$$

By using Eq. (A9), that is

$$\begin{cases} Q_{1,n} = C_{01}(V_{j,n} - \eta_1 V_{j,n}^2 + \delta_1 V_{j,n}^3) \\ Q_{2,n} = C_{02}\Big[(V_{j,n} - V_{3-j,n}) - \eta_2(V_{j,n} - V_{3-j,n})^2 + \delta_2(V_{j,n} - V_{3-j,n})^3\Big] \end{cases}, \qquad (A9)$$

we obtain

$$\begin{aligned} \left(V_{j,n} - \eta_1 V_{j,n}^2 + \delta_1 V_{j,n}^3\right)_{tt} &= u_0^2\left(V_{j,n+1} + V_{j,n-1} - 2V_{j,n}\right) - \omega_0^2 V_{j,n} \\ &-a\begin{bmatrix} (V_{j,n} - V_{3-j,n}) - (-1)^{3-j}\,\eta_2\left(V_{j,n} - V_{3-j,n}\right)^2 \\ +\delta_2\left(V_{j,n} - V_{3-j,n}\right)^3 \end{bmatrix}_{tt}, \end{aligned} \qquad (A10)$$

where the subscript j can take the values 1 for the first line and 2 for the second line.

Derivation of equation (3.9)

The solution of equation (A10) is assumed to have the following general form:

$$V_{j,n}(t) = \varepsilon A_j(x,\tau)e^{i\theta} + \varepsilon^2[\phi_j(x,\tau) + B_j(x,\tau)e^{2i\theta}] + cc,$$

where $\theta = kn - \omega t$ and "cc" stands for complex conjugate. In order to use the reductive perturbation method in the semi-discrete limit, we introduce the slow-envelope variables $x = \varepsilon(n - v_g t)$ and $\tau = \varepsilon^2 t$ where ε is a small parameter and v_g is a group velocity. The terms of order ε^2 proportional to $e^{i\theta}$ allow to obtain the following relation:

$$\begin{cases} 2i\omega v_g \left(A_1\right)_x = 2iu_0^2 \sin k \left(A_1\right)_x - a\left[2i\omega v_g \left(A_1\right)_x - 2i\omega v_g \left(A_2\right)_x\right] \\ 2i\omega v_g \left(A_2\right)_x = 2iu_0^2 \sin k \left(A_2\right)_x - a\left[2i\omega v_g \left(A_2\right)_x - 2i\omega v_g \left(A_1\right)_x\right] \end{cases} \quad (A11)$$

After one integration about x and by assuming that the integration constant is equal to zero, we have:

$$\begin{cases} \left[\omega v_g \left(1+a\right) - u_0^2 \sin k\right] A_1 = a\omega v_g A_2 \\ \left[\omega v_g \left(1+a\right) - u_0^2 \sin k\right] A_2 = a\omega v_g A_1 \end{cases}. \quad (A12)$$

Now using Eq. (3.7), one obtains

$$v_g \omega = \Gamma u_0^2 \sin k, \qquad (A13)$$

with $\Gamma = 1$ for the fast-mode and $1/(1+2a)$ for the slow-mode. Inserting (A13) into (A12), we have:

$$\begin{cases} A_2 = \left[\dfrac{1}{a} + 1 - \dfrac{1}{a\Gamma}\right] A_1 \\ A_1 = \left[\dfrac{1}{a} + 1 - \dfrac{1}{a\Gamma}\right] A_2 \end{cases}. \quad (A14)$$

For the fast-mode, $A_1 = A_2$ and for the slow-mode $A_1 = -A_2$. These two relations can take the following form

$$A_j = -(-1)^l A_{3-j}, \qquad (A15)$$

where $l = 1$ for the fast-mode and 2 for the slow-mode.

Appendix B

The coefficients of the CDCGL equations (3.39) are

$Q_r = \frac{3\omega^2}{A^2U_0^2(1+a)}, Q_i = \frac{4\beta\omega}{AU_0^2(1+a)}$

$P_{1i} = \frac{2\omega}{U_0(1+a)}[\frac{\sigma_1(\omega_0^2+2U_0^2+2\Omega_0^2-\omega^2(1+a))-U_0^2(\sigma_2+2\sigma_1)}{\omega_0^2+2U_0^2+2\Omega_0^2-\omega^2(1+a)}]$

$P_{2i} = \frac{2\omega}{U_0(1+a)}[\frac{-\Omega_0^2(\sigma_2+2\sigma_1)}{\omega_0^2+2U_0^2+2\Omega_0^2-\omega^2(1+a)}]$

$P_{1r} = 1, P_{2r} = \frac{\Omega_0^2}{U_0^2}, \eta = \frac{2a\omega}{U_0^2(1+a)}$

$\gamma_i = 2(P_{1r} + P_{2r}), \gamma_r = -2(P_{1i} + P_{2i})$

$\Gamma_r = \frac{a\omega^2}{(1+a)(\omega_0^2+2U_0^2+2\Omega_0^2-\omega^2(1+a))}$

$\Gamma_i = \frac{2a\sigma_1\omega^3}{U_0^2(1+a)(\omega_0^2+2U_0^2+2\Omega_0^2-\omega^2(1+a))}$

The elements of the matrix are

This matrix form can be written as

$$\mathbf{M} = \begin{pmatrix} -\Omega + m_1 + im_2 & m_3 + im_4 & -\eta\Omega + m_5 + im_6 & 0 \\ m_3 - im_4 & \Omega + m_1 - im_2 & 0 & \eta\Omega + m_7 - im_6 \\ -\eta\Omega + m_8 + im_9 & 0 & -\Omega + m_{10} + im_{11} & m_{12} + im_{13} \\ 0 & \eta\Omega + m_{14} - im_9 & m_{12} - im_{13} & \Omega + m_{10} - im_{11} \end{pmatrix}$$

with

$$m_1 = -4P_{1r}\sin^2(\tfrac{K}{2})\cos(\nu) - 2P_{1r}\cos(K)\sin(\nu) - 4P_{2r}\sin^2(K)\cos(2\nu)$$
$$- 2P_{2r}\cos(2K)\sin(2\nu) + \Gamma_r\tfrac{A_2}{A_1} + Q_r|A_1|^2$$

$$m_2 = -4P_{1i}\sin^2(\tfrac{K}{2})\cos(\nu) - 2P_{1i}\cos(K)\sin(\nu) - 4P_{2i}\sin^2(K)\cos(2\nu)$$
$$+ 2P_{2i}\cos(2K)\sin(2\nu) + \Gamma_i\tfrac{A_2}{A_1} + Q_i|A_1|^2$$

$$m_3 = Q_r|A_1|^2,\ m_4 = Q_i|A_1|^2,\ m_5 = -\Gamma_r,\ m_6 = -\Gamma_i$$

$$m_7 = -\Gamma_r,\ m_8 = m_7,\ m_9 = m_6$$

$$m_{10} = -4P_{1r}\sin^2(\tfrac{K}{2})\cos(\nu) - 2P_{1r}\cos(K)\sin(\nu) - 4P_{2r}\sin^2(K)\cos(2\nu)$$
$$- 2P_{2r}\cos(2K)\sin(2\nu) + \Gamma_r\tfrac{A_1}{A_2} + Q_r|A_2|^2$$

$$m_{11} = -4P_{1i}\sin^2(\tfrac{K}{2})\cos(\nu) - 2P_{1i}\cos(K)\sin(\nu) - 4P_{2i}\sin^2(K)\cos(2\nu)$$
$$+ 2P_{2i}\cos(2K)\sin(2\nu) + \Gamma_i\tfrac{A_1}{A_2} + Q_i|A_2|^2$$

$$m_{12} = Q_r|A_2|^2,\ m_{13} = Q_i|A_2|^2,\ m_{14} = m_7$$

The dispersion relation which determines Ω as a function of K is obtained from the condition of the existence of nontrivial solutions of the algebraic linear homogeneous system $det(M) = 0$, that amounts to a quadratic equation for Ω. Solving Eq. (3.47), the frequency has the form

$\Omega = \Omega_r + i\Omega_i$

Hence, substituting this frequency into Eq. (3.46), one can note that the $e^{-\Omega_i\tau}$ enters inside the amplitude of the perturbation. The asymptotic behavior of the perturbation is related to the sign of the constant Ω_i. If constant Ω_i is negative, solution increases exponentially when τ goes towards the infinity and the system remains unstable under the modulation.

Appendix C

We look for plane wave solutions in the form

$\phi_{jn}(x,t) = \Phi_{j0} e^{i(Kx-\Omega t)}, (j = 1, 2) \qquad (C1)$

Inserting Eq.(*) into Eq.(3.58), we obtain the following expression describing implicitly the characteristics of the continuous-wave solution:

$$\Omega = P_j K^2 - Q_j \Phi_{j0}^2 \qquad (C2)$$

Eq. (C2) is the dispersion relation of the plane wave solution. We can see that the pulsation depend of wave number and the amplitude of the signal.
Now, we consider small perturbations $b_{jn}(x,t)$ for the amplitude and $\theta(x,t)$ for the phase; $b_{jn}(x,t)$ and $\theta(x,t)$ are real functions. We then have:

$$\phi_{jn}(x,t) = [\Phi_{j0} + b_{jn}(x,t)] e^{i[Kx-\Omega t+\theta(x,t)]} \qquad (C3)$$

Substituting this relation into Eq.(3.58), one obtains the following system for the perturbations:

$$\begin{cases} -\Phi_{j0}\theta_{,t} + P_j b_{j,xx} - 2P_j \Phi_{j0} K \theta_{,x} + 2Q_j \Phi_{j0}^2 b_j = 0 \\ b_{j,t} + P_j \Phi_{j0} \theta_{,xx} + 2P_j K b_{j,x} = 0 \end{cases} \qquad (C4)$$

We take a general solution in the form

$$\begin{cases} b_j = b_{j0} e^{i(\delta x - \nu t)} + c.c. \\ \theta = \theta_0 e^{i(\delta x - \nu t)} + c.c. \end{cases} \qquad (C5)$$

where δ and ν are an arbitrary real wave number of the perturbation and the corresponding propagation frequency respectively, which is complex in the general case, b_{j0} and

θ_0 being amplitudes' perturbation. Inserting Eq.(C5) into Eq.(C4), we arrive at a set of linear homogeneous equations for b_j and c_j. This set of homogeneous equations which are:

$$\begin{cases} (2Q_j\Phi_{j0}^2 - P_j\delta^2)b_{j0} + i\Phi_{j0}(\nu - 2P_jK\delta)\theta_0 = 0 \\ -i(\nu - 2P_jK\delta)b_{j0} - P_j\Phi_{j0}\delta^2\theta_0 = 0 \end{cases} \qquad (C6)$$

The dispersion relation given below which determines ν as a function of δ is obtained from the condition of the existence of nontrivial solutions of the algebraic linear homogeneous system Eq.(C6).

$$(\nu - 2P_jK\delta)^2 = P_j^2\delta^2(\delta^2 - \tfrac{2Q_j}{P_j}\Phi_{j0}^2) \qquad (C7)$$

It finally appears that the behavior of ν depends on the sign of Q_j/P_j;

List of Publications in International Refereed Journals

Aurelien Kenfack-Jiotsa and **Eric Tala-Tebue**, Effect of Second-Neighbor Inductive Coupling on the Modulational Instability in a Coupled Line of Transmission, *J. Phys. Soc. Jpn., 80 034003 (2011) 1-6.*

E. Tala-Tebue, A. Kenfack-Jiotsa, M. H. Tatchou-Temfack and T. C. Kofané, Modulational instability in a pair of non identical coupled nonlinear electrical transmission lines, *Commun. Theor. Phys., 60 (2013) 93-100.*

Eric Tala-Tebue, and Aurelien Kenfack-Jiotsa, Transverse stability in the discrete inductance-capacitance electrical network, *J. Mod. Phys., 4 (2013) 746-753.*

Eric Tala-Tebue, Aurelien Kenfack-Jiotsa and Timoléon Crépin Kofané , Suppression of modulated waves mixing in coupled nonlinear LC transmission lines. *(work submitted).*

Aurelien Kenfack-Jiotsa, **Eric Tala-Tebue**, Serge Bruno Yamgoué, Marius Hervé Tatchou-Ntemfack, and Timoléon Crépin Kofané, Effect of nonlinear coupling on modulational instability in nonlinear transmission lines. *(work submitted).*